Experimental and theoretical formation of Martian penitentes

Noa Schellinx



Delft University of Technology

TU Delft

Experimental and theoretical formation of Martian penitentes

by

Noa Schellinx

to obtain the degree of Master of Science
in Aerospace Engineering
at the Delft University of Technology,
to be defended publicly on Tuesday 16 December, 2025 at 10:00 AM.

Student number:	5019060	
Faculty:	Faculty of Aerospace Engineering, Delft	
Project duration:	November 2024 - December 2025	
Thesis committee:	Dr. S.J. de Vet	Thesis supervisor
	Dr. lr. B.C. Root	Examiner
	Dr. W. van der Wal	Chair

Cover: AI generated image of ice penitentes on Mars

An electronic version of this thesis is available at http://repository.tudelft.nl/.

TU Delft

Preface

This report was written for a master thesis at the faculty of Aerospace Engineering at the TU Delft. Over the period of one year research has been done to investigate penitente formation on Mars and the factors influencing penitente formation. Throughout this year it was discovered that penitente formation is more complex than first thought and that very specific conditions are required for these shapes to form in snow or ice.

In order to get a full understanding of all the contents addressed in this report a basic knowledge of physics, engineering, climate sciences and planetary sciences is required. To get a full understanding of the topic and results it is recommended to read Chapter 2 first.

Readers who have a particular interest in the design of a test setup which could be used to investigate penitente formation can read this in Chapter 3. For the readers who have more interest in the results of the laboratory experiments performed can read Chapter 4. For those interested in theoretical formation of penitentes and if penitentes are theoretically possible on Mars Chapter 5 is recommended.

I particularly would like to thank my supervisor Sebastiaan de Vet for all the support and feedback given to me during the thesis. Especially the feedback on the performed experiments and how to adjust them to get useful results was greatly appreciated. Moreover I would like to thank Yaël Bourgeois, Stéphanie Cazaux and Mascha Slingerland all the help with PISCES. Lastly I would like to thank all the personnel of the aircraft hall who helped me with set up my test set ups.

Noa Schellinx
Delft, December 1, 2025

Abstract

This research aims to investigate the possibility of penitente formation on Mars. Penitentes are blade like structures with spikes formed in snow or ice in cold dry environments with strong solar insolation due to self illumination causing differential ablation. As penitentes house life in extreme environments on Earth they are potential locations where extraterrestrial life could exist or has existed on Mars. To investigate the formation of Martian penitentes experiments have been performed that simulate the Martian temperatures, pressures and solar insolation, and a theoretical model was used to calculate the possible growth rate and penitente spacing at certain location on Mars. While no penitentes were able to form on their own during the experiments the key attributing factors for penitente formation were found: the temperature, pressure and kind of ablation material. Theoretically penitente formation on Mars is possible at Olympus Mons, Elysium Mons, Arsia Mon and Alba Mons. The growth of penitentes at these locations would take several years if the temperature and pressure remained stable. However the temperatures and pressures do not remain stable resulting is strong sublimation when temperatures rise. In the South polar region penitente formation is possible and remain stable as formation conditions are reached when the maximum temperature in that region is reached. However CO_2 snow covers the South polar region during local winter which may disrupt micro-penitentes formed during the summer. Thus while penitente formation is possible on modern Mars insufficient time is available to grow visible penitentes unless a CO_2 snow cover does not disrupt preformed penitentes.

Keywords
Penitentes, Mars, snow, ice

Nomenclature

Acronyms

EPS	Expanded Polystyrene
GN	Gastronorm
MCD	Mars Climate Database
MY	Mars Year
Nu	Nusselt number
PISCES	Plumes and Ices Simulation Chamber for Enceladus and other icy moonS
Pr	Prandtl number
Re	Reynolds number
RH	Relative humidity
TC	Thermocouple

Constants

α	velocity scale	$100 m/s$
T_{LN2}	Temperature of liquid nitrogen	$-196\,°C$
R	Perfect gas constant	$8.314 J/K/mol$

Symbols

$_\rho$	Diffusion coefficient of water vapor in the air	m^2/s
δ	Surface roughness	m
$\dot{m}$	Mass flow	kg/s
$\dot{Q}$	Heat transfer rate	J/s
κ_s	Thermal conductivity of ice or snow	$W/m/K$
Λ	Light penetration distance	m
μ	Dynamic viscosity	$Pa \cdot s$
ν	Air kinematic viscosity	m^2/s
Ω	Self illumination factor	-
ω	Albedo	-
ψ	Light volumetric power	W/m^3
ψ_a	Interfacial value of absorbed light volumetric powr	W/m^3
ρ	Density	kg/m^3
ρ'_{sat}	First derivative of saturated vapor density	$kg/m^3/K$
ρ_s	Ice density	kg/m^3
ρ_{sat}	Saturated vapor density	kg/m^3
σ	Penitente growth rate	m/s
A	Surface area	m^2
C_p	Specific heat	J/kgK
D	Diameter	m
h	Convective heat transfer coefficient	W/m^2K
h	Penitente height	m
k	Thermal conductivity	W/mK
L	Length	m
L_s	Solar longitude	$°$
m	Mass	kg
M_s	Molar weight of ice or snow	kg/mol
P_s	Saturated vapor pressure of water	hPa
p_{sat}	Saturated vapor pressure	Pa
Q	Gas load	$Pa \cdot m^3/s$

Q	Heat	J
r_i	Inner radius	m
r_o	Outer radius	m
R_{conv}	Convectional resistance	K/W
R_{conv}	Convective thermal resistance	K/w
S	Volumetric flow rate	m^3/h
t	Time	s
U	Overall heat transfer coefficient	W/m^2K
u_*	Wind shear velocity	m/s
V	Velocity	m/s
$J^{\psi}{}_0$	Light power flux due to direct Sun illumination	W/m^2
k	Wave number	-
L	Latent heat of sublimation	J/kg
l	Diffusion boundary layer thickness	m
T	Temperature	K

Contents

Preface i

Abstract ii

Nomenclature iv

1 Introduction 1

2 Scientific background 2
- 2.1 Penitente formation mechanism . . . 2
- 2.2 History of laboratory penitente experiments . . . 3
- 2.3 Influence factors on penitente formation . . . 9
- 2.4 History of penitente models . . . 14
- 2.5 Extra terrestrial penitentes . . . 15
- 2.6 Martian conditions . . . 16
- 2.7 Research proposal . . . 26

3 Experiment and Model Setup 28
- 3.1 Snow/ice mould design . . . 28
- 3.2 Ice making . . . 29
- 3.3 Snow making . . . 31
- 3.4 Setup with EPS box . . . 36
- 3.5 PISCES setup design . . . 38
- 3.6 Penitente growth model equations . . . 50

4 Experiment Descriptions and Results 54
- 4.1 Ablation material experiments . . . 55
- 4.2 Temperature effects experiments . . . 55
- 4.3 Airflow effects experiments . . . 57
- 4.4 Pressure effects experiments . . . 60
- 4.5 Discussion of experimental results . . . 62

5 Penitente Growth Model Results and Discussion 65
- 5.1 Model results for experimental conditions . . . 65
- 5.2 Model results for Martian conditions . . . 68
- 5.3 Dust influence on theoretical penitente growth and spacing . . . 74
- 5.4 Discussion of results . . . 75

6 Conclusion 79

Bibliography 85

Appendices 86
- A Experiment details and graphs . . . 86
- B Penitente Model Inputs and MCD graphs . . . 109

List of Figures

2.1 Test beds that have been used in past laboratory experiments on penitente formation . . . 5
2.2 Experimental conditions of Berisford plotted over the water vapor curve [1] . 9
2.3 Variation in the albedo for snow/ice of various grain sizes for various dust contents [2] . . . 11
2.4 The thermal conductivity of snow and ice on Mars for an atmospheric pressure of 700 Pa. The assumed grain radius for the densities 50, 400, 550 kg/m^3 are 50 μm, 800 μm, 4 mm, respectively [3] . . . 12
2.5 The phase diagram of water, including the saturated vapor pressure curve [4] 13
2.6 Observed albedo of ice at the Phoenix lander site compared to albedo spectra of 350 μm snow [2] . . . 18
2.7 Phase diagram of CO_2 [5] . . . 19
2.8 The saturation vapor pressure curve of CO_2 [6] . . . 19
2.9 Solar insolation at the surface of Mars for clear sky conditions in $\frac{cal}{cm^2 planetary day}$ [7] . . . 21
2.10 Interannual and seasonal evolution of the solar insolation and aerosol opacity measured by various rovers. The solid lines indicate the solar insolation at the top of the atmosphere, while the crosses indicate the solar insolation at the surface at each landing site. [8] . . . 22
2.11 Seasonal dependence on relative humidity on Mars during night time [9] . . . 24
2.12 Diurnal variation of surface relative humidity on various locations across Mars [9] . . . 24
2.13 The seasonal evolution of the daily mean atmospheric surface pressure as observed by various rovers [10] . . . 25
2.14 The seasonal variance in near-surface wind speed on Mars. The dark blue (minimum), green (mean) and red (maximum) lines represent the daily wind speed at the VL2 site in MY 12 and 13. The purple (minimum), cyan (mean) and orange (maximum) lines represent the daily wind speed at the VL1 site in MY 12. The light blue (minimum) and yellow (maximum) represent the daily wind speed at the PHX site in MY 29. [8] . . . 26

3.1 Ice/snow mould with thermocouple stand used for containing the snow and/or ice for the laboratory penitente experiment . . . 29
3.2 The ice made with ice making method 1 at the start and just after the end of the first experiment . . . 30
3.3 Stainless steel container in which the ice is made with the surrounding foam insulation box to ensure one directional freezing . . . 31
3.4 The ice made with ice making method 2, used for the second experiment . . . 31
3.5 Snow created by spraying water using a conventional spray bottle into a dewar vessel containing liquid nitrogen . . . 32
3.6 Lump of ice created by pouring about 100 ml of water from a measuring cup into a dewar vessel containing liquid nitrogen . . . 33
3.7 Pieces of ice created by breaking apart the lump of ice, created by dumping water into liquid nitrogen, using a spoon . . . 33
3.8 Snow/ice created by placing a sieve ontop of a dewar vessel containing liquid nitrogen and spraying water droplets using a conventional spray bottle onto the sieve . . . 34

3.9 Penitente mould designs used to create preformed 2D and 3D penitentes . . . 35
3.10 Preformed penitentes made with the 2D mould (front left shapes) and the 3D mould (front right shapes) . . . 35
3.11 Illumination profile of the Hedler Profilux 1000 [11] . . . 37
3.12 Schematic diagram (a) and picture (b) of the EPS test set-up . . . 38
3.13 Schematic diagram of the test set up when the ice temperature will be regulated using a cooling loop and liquid nitrogen . . . 41
3.14 Heat transfer model of cooling the ethanol in the cooling loop using liquid nitrogen . . . 42
3.15 The absolute pressure profile inside PISCES measured by its absolute pressure sensors (pressure sensor 1 to 3) and the average absolute pressure obtained using the readings of these three sensors . . . 47
3.16 Pressure profile of PISCES between about 500 Pa and 400 Pa, the average pressure and linear relation obtained in that pressure range . . . 48
3.17 The outside (a) and inside (b) of the PISCES setup . . . 50

4.1 Temperature progression of experiments T1.min25, T2.min25, T3.min80 and T4.min80Coldfinger with their snow sample begin temperature . . . 56
4.2 Snow surface progression of experiment A1.BlownAir with the addition of blowing wind onto the surface. The pictures were taken at the start of the experiment, at about 3 hours into the experiment just before the ventilator lost power and at the end of the experiment about 1.5 hours after the ventilator lost power . . . 58
4.3 Snow surface progression of experiment A3.BlownAir. These pictures were taken at the start, middle and end of the experiment . . . 58
4.4 Snow surface at the start, middle and end of experiment A2.SuckedAir . . . 59
4.5 Temperature readings of experiments A3.BlownAir, A2.SuckedAir and T4.min80Coldfinger (With blown airflow, sucked airflow and no airflow) . . . 60
4.6 Temperature and pressure regime of all experiments performed at Martian like pressures compared to the saturated water vapor curve in the water phase diagram and the likely penitente formation zone, as established using Berisford's results [1] . . . 61
4.7 Ice surface at start (a) and end (b) of experiment P1.variable . . . 62
4.8 Snow surface progression of experiment P6.800 into P7.200 , where the picture of surface at the middle experiment was taken just before the pressure was lowered to 200 Pa . . . 62

5.1 Pressure (from 80 to 700 Pa) and temperature (from 245 to 275 K) at Mars at $Ls = 90°$ and $t = 18h$. Actual pressure and temperatures outside of the given range could be higher or lower but were left out for analytical reasons . . . 70
5.2 Temperature and pressure conditions on Olympus, Elysium, Arsia and Alba Mons throughout one Martian year compared to the likely penitente formation zone . . . 72
5.3 Temperature and pressure conditions in the South polar regions during $L_s = 270°$ . . . 74
5.4 Temperature and pressure conditions on Olympus, Elysium, Arsia, Alba Mons and the South polar region throughout one Martian year compared to the likely penitente formation zone . . . 78

A.1 Temperature readings of experiment M1.CloudyIce . . . 86
A.2 Temperature readings of experiment M2.ClearIce . . . 87
A.3 Temperature readings of experiment M3.Snow . . . 87

A.4 Temperature and relative humidity readings of experiment T1.min25 88
A.5 Temperature and relative humidity readings of experiment T2.min25 88
A.6 Temperature and relative humidity readings of experiment T3.min80 89
A.7 Temperature readings of experiment T4.min80Coldfinger 89
A.8 Temperature and relative humidity readings of experiment A1.BlownAir . . . 90
A.9 Temperature and relative humidity readings of experiment A2.SuckedAir . . 90
A.10 Temperature and relative humidity readings of experiment A3.BlownAir . . . 91
A.11 Temperature and pressure readings of experiment P1.variable 91
A.12 Temperature, relative humidity and pressure readings of experiment P2.200 . 92
A.13 Temperature and relative humidity of experiment P3.ambient 92
A.14 Temperature, relative humidity and pressure readings of experiment P4.400 . 93
A.15 Temperature, relative humidity and pressure readings of experiment P5.600 . 94
A.16 Temperature, relative humidity and pressure readings of experiment P6.800 . 95
A.17 Temperature, relative humidity and pressure readings of experiment P7.200 . 96
A.18 Ice surface at start and end of experiment M1.CloudyIce 103
A.19 Ice surface at start and end of experiment M2.ClearIce 103
A.20 Ice surface at start and end of experiment M3.Snow 103
A.21 Snow surface of experiment T1.min25 at the start and just before the malfunction happened 104
A.22 Snow surface of experiment T1.min25 just before the malfunction happened and at the end of the experiment 104
A.23 Snow surface at start and end of experiment T2.min25 104
A.24 Snow surface at the start and end of experiment T3.min80 105
A.25 Snow surface at the start and end of experiment T4.min80Coldfinger 105
A.26 Snow surface at start, middle and end of experiment A1.BlownAir 105
A.27 Snow surface at the start and end of experiment A2.SuckedAir 106
A.28 Snow surface at the start and end of experiment A3.BlownAir 106
A.29 Ice surface at start and end of experiment P1.variable 106
A.30 Snow surface at the start and end of experiment P2.200 107
A.31 Snow surface at the start and end of experiment P3.ambient 107
A.32 Snow surface at the start and end of experiment P4.400 107
A.33 Snow surface at the start and end of experiment P5.600 108
A.34 Snow surface at the start and end of experiment P6.800 108
A.35 Snow surface at the start and end of experiment P7.200 108

B.1 Temperatures at Mars in range 245 to 275 K at $L_s = 0°$ at time 0h, 6h, 12h and 18h 115
B.2 Pressures at Mars in range 80 to 700 Pa at $L_s = 0°$ at time 0h, 6h, 12h and 18h . 116
B.3 Solar insolation at Mars at $L_s = 0°$ at time 0h, 6h, 12h and 18h 116
B.4 Temperatures at Mars in range 245 to 275 K at $L_s = 90°$ at time 0h, 6h, 12h and 18h 117
B.5 Pressures at Mars in range 80 to 700 Pa at $L_s = 90°$ at time 0h, 6h, 12h and 18h 117
B.6 Solar insolation at Mars at $L_s = 90°$ at time 0h, 6h, 12h and 18h 118
B.7 Temperatures at Mars in range 245 to 275 K at $L_s = 180°$ at time 0h, 6h, 12h and 18h 118
B.8 Pressures at Mars in range 80 to 700 Pa at $L_s = 180°$ at time 0h, 6h, 12h and 18h 119
B.9 Solar insolation at Mars at $L_s = 180°$ at time 0h, 6h, 12h and 18h 119
B.10 Temperatures at Mars in range 245 to 275 K at $L_s = 270°$ at time 0h, 6h, 12h and 18h 120
B.11 Pressures at Mars in range 80 to 700 Pa at $L_s = 270°$ at time 0h, 6h, 12h and 18h 120
B.12 Solar insolation at Mars at $L_s = 270°$ at time 0h, 6h, 12h and 18h 121

List of Tables

2.1 The key findings of the research performed by Bergeron and Berisford on penitente formation [12] [1] . . . 7
2.2 Snow/ice properties depending on their type . . . 17
2.3 CO_2 snow/ice properties in the Southern hemisphere of Mars at solar longitudes $L_s = 276°$ and $L_s = 337°$ [13] . . . 20
2.4 Maximum, minimum and average temperature seen on Mars on the course of one Mars Year . . . 23
2.5 Minimum and maximum temperatures seen on Mars throughout one sol . . . 23

3.1 Requirements for snow/ice mould . . . 28
3.2 Requirements for the EPS setup . . . 36
3.3 Requirements for the PISCES setup . . . 39
3.4 Eutectic temperatures various ice+salt mixtures can reach and the corresponding salt percentages needed to obtain the eutectic temperature [14] [15] [16] [17] 40
3.5 Influence of pipe diameter, pipe thickness and flow velocity inside the pipe on the cooling loop when cooling the ice/snow to a temperature of -70 °C . . . 45
3.6 Description of terms used in Claudin's model [18] . . . 52

4.1 All the experiments performed and their key conditions that were varied . . . 54

5.1 Theoretical dimensionless growth rate, growth rate and penitente spacing of the experimental conditions calculated with Claudin's model [18] . . . 67
5.2 Theoretical dimensionless growth rate, growth rate and penitente spacing of various Martian conditions calculated with Claudin's model [18] . . . 69
5.3 Theoretical dimensionless growth rate, growth rate and penitente spacing of Martian conditions at potential locations where penitentes could form calculated with Claudin's model [18] . . . 73
5.4 Influence of added dust to pure ice on the theoretical dimensionless growth rate, growth rate and penitente spacing . . . 75
5.5 Influence of added dust to snow on the theoretical dimensionless growth rate, growth rate and penitente spacing . . . 75

A.1 Experimental setup details of experiments performed using EPS setup . . . 97
A.2 Experimental setup details of experiments performed to investigate the temperature effects on penitente formation . . . 98
A.3 Experimental setup details of experiments performed to investigate the airflow effects on penitente formation . . . 99
A.4 Experimental setup details of experiments performed to investigate the pressure effects on penitente formation part 1 . . . 100
A.5 Experimental setup details of experiments performed to investigate the pressure effects on penitente formation part 2 . . . 101
A.6 Experimental setup details of experiments performed to investigate the pressure effects on penitente formation part 3 . . . 102

B.1 Input values used in Claudin's model. The temperature used is the temperature measurement of the snow/ice surface at time = 2 hours into the experiment 110
B.2 Input values used in Claudin's model to simulate penitente formation on Mars [19] . . . 111

B.3 Input values used in Claudin's model to simulate penitente formation on potential locations where penitentes could form on Mars [19] 112

1 Introduction

Penitentes are large spike structures with sharp peaks occurring in the snow and ice in cold, dry environments with strong solar insolation. These shapes are formed due to strong solar insolation and self reflections within the snow and ice leading to differential ablation causing the peaks to sublimate at a much lower rate than the troughs. On Earth these structures house life, algae, in the one of the most extreme and hostile environments where no other life is found within the region. Moreover these structures could obstruct movement of vehicles like rovers by blocking their path due to the penitentes sharp peaks.

The aim of this report is to document the research studying the temperature and pressure regimes in which penitentes can form on Mars and which other factors influences this penitente formation. This research is performed as locations where potential penitentes form on Mars could be locations where extraterrestrial life, past or present, is possible. Moreover penitentes could pose threats to rovers or spacecraft landings on Mars due to their sharp peaks. For this study lab experiments have been performed studying the influence of the kind of ablation material (granular snow and pure ice), temperature, airflow and pressure on penitente formation. Moreover some experiments directly simulated the pressures and temperatures found on Mars, in which penitente growth and stability at Martian conditions could be studied. Additionally a penitente growth model was used to study the influence of these mentioned factors on the theoretical growth rate and penitente spacing. The factor of adding a small amount of dust to the ice and snow was also studied with this model. Using the results of these influence factors, certain locations at Mars where pinpointed where penitente formation is thought to be possible and the theoretical growth rate at these locations were compared to the growth rate of Earth penitentes in the Andes mountain range just outside of the Chilean capital Santiago (the Santiago Andes).

The following structure is present in this report. A literature study on the topic explaining the formation physics of penitentes aswell as the climatic conditions and snow/ice properties on Mars is presented in Chapter 2. In this chapter the research proposal for the thesis which was established from the literature study is also presented. The design of the experimental setup used for the laboratory experiments on the factors influencing penitente formation and the equations of the penitente model used to simulate the theoretical penitente growth and spacing is presented in Chapter 3. The results of all of these laboratory experiments and a discussion of these results are presented in Chapter 4. In Chapter 5 the penitente model results are presented, aswell as a small discussion of these results. This chapter includes the theoretical growth rate and spacing of penitentes of the laboratory experiments performed and relates this to the results found while performing the laboratory experiments. Moreover this chapter includes the possible locations on Mars where penitente formation is thought to be possible. Lastly a conclusion of the study is presented in Chapter 6.

2 Scientific background

To gain knowledge about past research on penitentes a literature study has been performed on penitente formation physics, past research performed on penitente formation and the Martian climate. This literature study will be presented in this Chapter. The physical mechanism behind penitente formation will be explained in Section 2.1. A short history on laboratory experiments examining penitente formation is presented in Section 2.2. The factors which influence this formation will be addressed in Section 2.3. Penitente models which have already been developed are presented in Section 2.4. Current literature available on extra terrestrial penitentes will be presented in Section 2.5. The snow and ice properties which are present on Mars aswell as the modern Martian climate will be presented in Section 2.6. Lastly Section 2.7 presents the research proposal based on the literature study performed.

2.1 Penitente formation mechanism

Penitentes, blade like structures with spikes of snow or ice, form in snow or ice fields in dry and cold high alpine environments. These structures were first observed by Charles Darwin in 1835 at high altitudes in the Andes and are now known to form in snowfields at high altitudes in the Andes and Himalaya [20]. Interestingly these structures house life, namely algae, in these high mountain regions were conditions are extreme and support no other life [21]. Whilst penitentes are most commonly formed at high altitudes in the tropical regions, these structures can also occur at lower altitudes and higher latitudes if the conditions for penitentes formation are met [20].

In the past the formation of these structures has been attributed to various climatic phenomenons: the wind, thermal eddies of the air, the rain and electromagnetic orientation. But in 1942 Troll discovered that penitentes form due to differential ablation of the snow/ice due to solar insolation. Differential ablation is the phenomenon where the rate of ablation of the snow or ice is not uniform over the whole surface, but changes dependent on the location in the surface. Untill 1954 the mechanism behind the penitente formation was not explained. In 1954 Lliboutry studied penitentes in the high mountains of the Andes. Penitentes are found on all snow fields and glaciers in the Andes close to the Chilean capital Santiago, also known as the Santiago Andes, between altitudes of 4000 and 5200 m. At these locations the climate is very dry and cold and the snow fields have a prolonged radiation of the strong Solar intensity. These conditions ablate the snow, and troughs appear in the snow. Within these troughs solar rays are reflected resulting in a focus of light in the trough. Radiant heat is better absorbed in the troughs than in the peaks due to this focused light resulting in differential ablation. Due to this differential ablation sublimation occurs at the peaks while stronger sublimation or melting appears in the trough where more energy is available due to the focused light. This process in which solar rays are being reflected towards a single point by internal reflections in the snow/ice causing light focus in the trough is called self illumination. This self-illumination mechanism drives differential ablation resulting in the formation of penitentes. However besides a cold dry environment with strong solar insolation some other conditions must be satisfied in order for penitentes to form instead of other snow morphologies. [20]

According to Lliboutry five conditions must be met for penitentes to form. Firstly the dew point should be below 0 ° C. This ensures that sublimation can occur and differential ablation

is possible. Secondly there must be a strong insolation. A strong solar insolation is required as this provides energy for the ablation of the snow/ice and it enables self-illumination to take place. Thirdly the air temperature should never be too strongly positive. If this happens the formation process of the penitentes will be disrupted due to strong melting of the snow. On the otherhand, the air temperature should not be too low either since the snow will stay too powdery for penitentes to form. Fourthly the surface winds should be light, as wind is a disturbing factor that can make the humidity and temperature uniform around the penitentes preventing differential ablation to take place. The last condition is not perse necessary but speeds up the process of the formation of the penitentes. This condition is that the pressure should be lower than usual, which often is the case at higher altitudes. [20]

Moreover in 2015 Claudin discovered two other conditions that are required in order for penitentes to form. These two conditions are that vapor diffusion above the snow and heat conduction within the snow are required [18]. These two conditions are required to ensure differential sublimation in the ice, which results in the peaks sublimating at a lower rate than the troughs [22]. Both of these two conditions are only met when an atmosphere is present. If pressures are too low, as in a vacuum, a free-molecular flow regime is present. In this regime no vapor diffusion boundary layer forms on the ice and vapor diffusion is nonexistent [22] [23].

For a brief period of time misinterpretations had been made on the formation mechanism on penitentes due to various laboratory experiments and formation models [24]. This misinterpretation was that only sublimation conditions are required for penitentes to form. Laboratory experiments by Bergeron [12] and Berisford [23] researched the begin stages of penitente formation, also known as micro-penitentes, in sublimation conditions only. These micropenitentes are in the scale of mm to cm in height. Micro-penitentes can form in a snow and ice field where only sublimation occurs. Besides these laboratoy experiments a penitente model made by Claudin, were only sublimation was taken into account while omitting melt, had also been made [18]. This model gave similar results for penitente spacing and growth as was seen for the laboratory made micro-penitentes amplifying the misinterpretation regarding penitente formation. Large penitentes, just like on Earth, form from these micropenitentes. First self-illumination takes place in impurities within the snow/ice surface starting the differential ablation process creating micropenitentes. Troughs and peaks are created in the snow/ice surface due to the higher sublimation rate in the impurities caused by the self-illumination. Once these troughs are deep enough (a few centimeters) compared to the peaks water vapor cannot escape the troughs easily anymore making the air in the troughs saturated and preventing sublimation to take place in the troughs. Instead of sublimation melting occurs in these troughs. At the peaks water vapor can easily escape and sublimation is still occurring keeping them dry and cold. At this stage the large difference in the latent heat of melting and the latent heat of sublimation results that the troughs ablate even more quickly in comparison to the peaks as compared to the micropenitentes when only sublimation took place in the troughs and peaks [24]. This results that large sized penitentes can form. Thus for large penitentes to form both sublimation and melting must take place.

2.2 History of laboratory penitente experiments

Laboratory experiments on the formation of penitentes have been preformed by Bergeron and Berisford in order to research the influence of the formation conditions required to form penitentes, as adressed by Lliboutry and Claudin. Bergeron researched the influence of the

type of ablation material, the temperature, humidity and surface debris on penitente formation with his experiments. Berisford mainly researched the effect of atmospheric pressure influences on penitente formation. To perform their experiments three main aspects were required: a snow/ice sample for the penitentes to form in, a test bed to simulate the atmospheric conditions and test instrumentation to take measurements during the experiments. The execution of these three aspects by Bergeron and Berisford will be discussed in this section aswell as the results obtained by their research.

Snow/ice production

In order to perform the experiments snow or ice is required as ablation material for penitentes to form in. Bergeron used granular snow as ablation material during his experiments. This granular snow was produced by freezing water droplets with a certain particle radius, which produced snow grains of radius between 25 μm and 2.5 mm [12]. A similar method has been used by Berisford for experimenting with penitente formation in low pressure conditions [23]. For his experiments snow was made by feeding water through an atomizing nozzle, which was placed inside a walk-in freezer ($-20°C$). This nozzle was mounted to a feedthrough port at 2 m above the ground and beneath this a tarp was placed. The nozzle produced small water droplets, which would freeze inside the freezer while in the air and which were than collected by the tarp. The collected snow was than placed into a mould, where it was laid to rest to sinter for 2 weeks inside the freezer. With this method Berisford managed to produce snow with a density between 300 and 500 kg/m^3 with grain diameters between 0.02 and 1 mm.

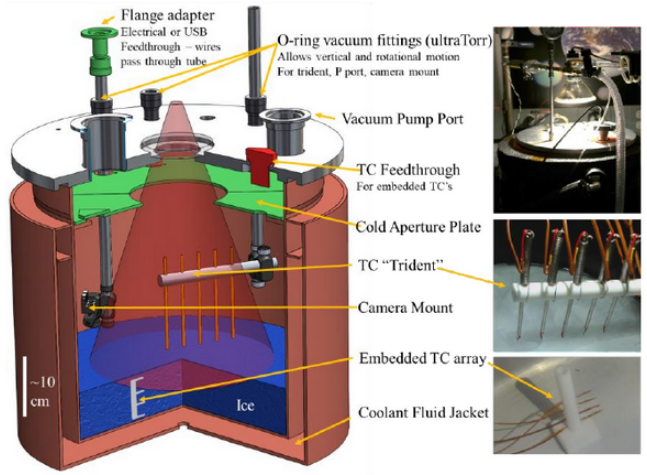
Besides granular snow, Bergeron and Berisford have also performed experiments in which the ablation material used was solid ice [12][1] [25]. This solid ice could be produced in two ways. First, ice could be produced by placing liquid water inside the vacuum chamber and freezing it in place. Second, the ice could be made elsewhere and than transferred into the chamber once it was already produced. With this second method the chamber has to be pre-chilled before the transfer and has to be purged with dry nitrogen while open to minimize ice melt and frost buildup [1]. In one of his tests the solid ice was formed by freezing degassed deionized water in place [25].

For their experiments Bergeron and Berisford each produced a set amount of snow or ice. Bergeron used a snow/ice sample of 80 by 50 cm [12]. Berisford used a smaller snow/ice sample of a diameter of 30 cm and an snow/ice thickness of 8 to 10 cm [1].

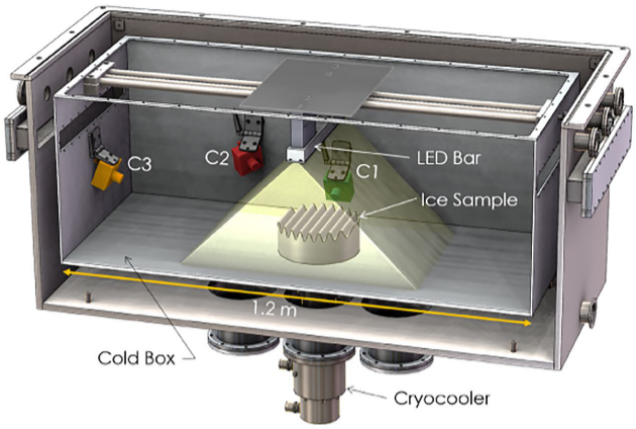
Artificial snow has also been created for experiments on the sintering rate of snow on extraterrestrial planets by Molaro [26]. This production process of these experiments can also be an inspiration for future snow and ice production for penitente experiments and will thus briefly be discussed. For Molaro's experiments the snow was created by spraying water droplets, using an atomizing nozzle and AutoJet controller, into a bath of liquid nitrogen. The bath of liquid nitrogen was placed in a plastic bucket inside a cold room with a temperature of -20 ° C. After the snow had been deposited inside this plastic bucket the liquid nitrogen was boiled off at this temperature in about one hour. This kind of system was used by Molaro to create bulk snow. To create small snow samples Molaro used only a bath of liquid nitrogen, a conventional spray bottle and a sieve. With the conventional spray bottle water was sprayed into the liquid nitrogen bath, which contained a sieve with which the snow could be collected. [26]

Test bed

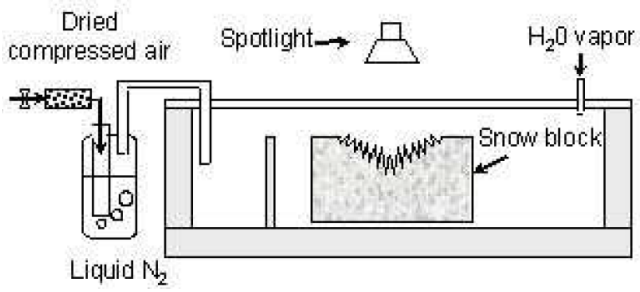
As penitentes can only form under certain conditions and to research the effects of these conditions a test bed which can simulate these conditions is required for laboratory experiments. As these test beds are required to simulate these conditions in order for penitentes to form the test beds previously used by Bergeon and Berisford will be discussed in this subsection. The three test beds that have previously been used in laboratory experiments by Bergeron and Berisford on the formation of penitentes can be seen in Figure 2.1. These figures show the environmental chamber aswell as the total test setup for experiments on penitentes. All three of these chambers could achieve set sub-zero temperatures and a low relative humidity and simulate solar insolation. Additionally the two test beds by Berisford could regulate the pressure inside the chamber.



(a) Static test bed by Berisford [25]



(b) Diurnal test bed by Berisford [1]



(c) Test bed by Bergeron [12]

Figure 2.1 Test beds that have been used in past laboratory experiments on penitente formation

Solar simulation

One of most important aspects of a test bed is an illumination source, as penitentes form due to solar radiation. In Bergeron's test bed and in Berisford static test bed the illumination source is placed outside the environmental chamber and light shines through a window into the chamber [12] [25]. Bergeron used a flood lamp with a conical irradiation pattern that could achieve a solar insolation of 300 W/m^2. Berisford used a halogen lamp with unknown flux. It is unsure if the floodlamp used by Bergeron was a LED or halogen lamp. These types of lamps differ in the wavelengths they emit. LED lights have a narrow spectral band compared to halogen lamps [25]. The static test bed of Berisford included an aperture limit, placed inside the environmental chamber, which made sure the light only directly illumi-

nates the ice surface and not the chamber walls.

In order to minimize internal reflections in the environmental chamber, the chambers walls were anodized black in the static test bed of Berisford [1]. Minimizing internal reflections inside the chamber is important as stray reflections which influence the morphology formation in the ablation material are undesired.

In the diurnal test bed the illumination source is placed inside the chamber. As it is placed inside the chamber some thermal aspects of the illumination source must be considered. To prevent the influence of additional heat emitted by the light source on the ablation surface a radiator is required to emit this additional heat away from the ablation surface. This radiator plate can be seen above the light source in Figure 2.1b. The upper surface of this plate is covered in high emissivity black paint and the bottom surface is covered with Single-Layer aluminized Kapton Insulation (SLI). The illumination source in this test bed is an array of alternating visible and Near Infrared LED's. This array of LED's is mounted to a mechanical linear stage which is driven by a stepper drive motor and is used to move the LED's across the chamber. With this a day and night cycle can be simulated inside the chamber. [25]

Temperature simulation

These three testbed could simulate subzero temperatures each using different methods. Bergeron's testbed consist of an old freezer with plexiglass on top of it where the door used to be. The walls of this freezer act as insulation from the outside but did not have a cooling feature. Subzero temperatures to -50 °C could be achieved in this chamber by introducing dry air cooled by liquid nitrogen [12]. In Berisford static testbed the walls of the chambers were cooled using a liquid cooling jacket and recirculating chiller [1]. Using this method temperatures to -73 °C could be achieved. Berisford diurnal testbed used a crycooler capable of achieving temperatures to -193 °C [25].

Humidity simulation

The relative humidity in these experiments were also controlled using various methods. Bergeron achieved low relative humidity as low as 5% by introducing dried compressed air. Additionally he could control and increase this relative humidity by introducing water vapor to the chamber [12]. Berisford did not have a system to control the relative humidity in the chamber but sometimes added dry nitrogen gas to the chamber to control the pressure resulting in a decrease of the relative humidity in the chamber [1]. Without this added nitrogen gas the relative humidity in the chamber would reach close to 100% due to the sublimating snow/ice surface [1].

Pressure and wind simulation

Unlike Bergeron Berisford's testbeds could control the pressure within the chamber using a vacuum pump and added nitrogen gas. With this method the static testbed could achieve pressures from 10 Pa to ambient pressure. The diurnal test bed could achieve pressures as low as 0.0001 Pa [25]. While Berisford was able to control the pressure in the chambers no wind could be introduced. Bergeron's testbed was capable of introducing wind using a fan that could produce a breeze of 2.5 m/s [12].

Test instrumentation

To gather usefull data during experiments, measuring instruments are required. Common measuring instruments that have been used in past penitente experiments are: thermocou-

ples, pressure sensors and cameras.

In the static testbed of Berisford, four thermocouples were embedded inside the ice at different vertical locations to measure the vertical temperature gradient inside the ice. An additional five thermocouples were used to measure the horizontal temperature gradient at the ice surface. To ensure contact is kept between the surface of the ice and these five thermocouples, the thermocouples were mounted to a horizontal Teflon rod with a soft tensile spring inside. The pressure inside the chamber was measured using an analog rough vacuum gauge and a pressure transducer. To visually monitor changes in the ice surface a webcam was used. Additionally to these common measuring instruments, the static test bed also includes a laser power meter to measure the total radiated flux. [25]

In the diurnal test bed the same kind of measuring instruments were used. Again four thermocouples are vertically embedded inside the ice to obtain the vertical temperature gradient. Seven thermocouples were embedded inside the ice near the ice surface to obtain the horizontal temperature gradient. As opposed to the static testbed, these thermocouples were not mounted to a rod with a spring to keep contact with the surface, but are embedded inside the ice itself. To monitor visible changes inside the ice six cameras have been placed at various locations inside the chamber. To ensure these camera's could function within the cold environment of the chamber Adhesive Kapton film heaters were used and the housing was covered with SLI. The pressure inside the chamber has been measured using a pressure transducer and a capacitance manometer. Like the static testbed a laser power meter has been used to measure the total radiated flux. [25]

Laboratory results

Using the produced snow/ice samples, the test bed and the test instrumentation various experiments have been preformed by Bergeron and Berisford altering some of the experiment conditions to research their influence on penitentes. The key findings from these experiments by Bergeron and Berisford are summarized in Table 2.1.

Table 2.1 The key findings of the research performed by Bergeron and Berisford on penitente formation [12] [1]

Key findings	**Author**
Penitente formation rate in snow is twice the rate of formation in ice	Bergeron
At ambient pressure penitentes can form in temperatures of -20 to -10 °C	Bergeron
A thin layer of surface debris promotes penitente growth	Bergeron
Penitentes can form in relative humidities up to 70%	Bergeron
Penitentes can form in windspeeds up to 2.5 m/s	Bergeron
At non-ambient pressures penitentes only form when the temperature and pressure is close to the water vapor curve	Berisford

Bergeron results

Bergeron has preformed various experiments altering the ablation material in which penitentes can form (snow or ice), the temperature, the relative humidity and the light source wavelength. Major findings are that penitentes took twice as long to form in ice than in snow, due to the difference in albedo between the two. Secondly penitentes did only form

in temperatures from -20 to -10 °C, confirming the theory of Lliboutry that the temperatures should never be too high or too low [20]. Thirldy a thin layer of surface debris promotes penitente growth. In one of the experiments, one half of an ice block was covered in a thin layer of carbon black powder while the other half was kept clean to test the effect of a thin debris layer. In the covered half the penitentes formed earlier and had a larger peak seperation than the penitentes formed in the clean half of the ice block [12]. Fourtly penitentes did form in a relative humidities of 10% up to 70%. Lastly penitentes managed to form in windspeeds up to 2.5 m/s. [12]

The penitentes formed in his experiments were 1 to 5 cm in height with a peak separation of about 1 cm. These penitentes managed to form in several hours, in about 2 hours in snow and about 4 hours in ice. Interestingly it took several hours after penitentes first appeared before a certain peak separation pattern was established. [12]

Berisford results

Berisford research looked more closely at the pressure in which penitentes could form. Successful penitente formations in his experiments were between ice surface temperatures of -15 to -2 °C at pressures close to the water vapor curve. If the conditions strayed too far from this curve penitentes did not form showing that penitentes need very specific conditions to exist and slight alterations could already put a halt to their existence. This can also be seen in Figure 2.2 where excavation of penitentes in Berisford experiments only happened in conditions close to the water vapor curve. The penitentes excavated during these experiments where in the magnitude of several mm in height. [1]

Additionally Berisford experimented with preformed penitentes which were 2D sinusoidal ridges with an height of 2.5 cm and a width of 1.25 cm at half height. These preformed penitentes were left in the test bed for a period of a month at a temperature of -108 to -98 °C and pressure of 0.0001 Pa. Changes in these shapes were present over the course of a month were they decreased in height by 20% and slowly lost their original shape. [23]

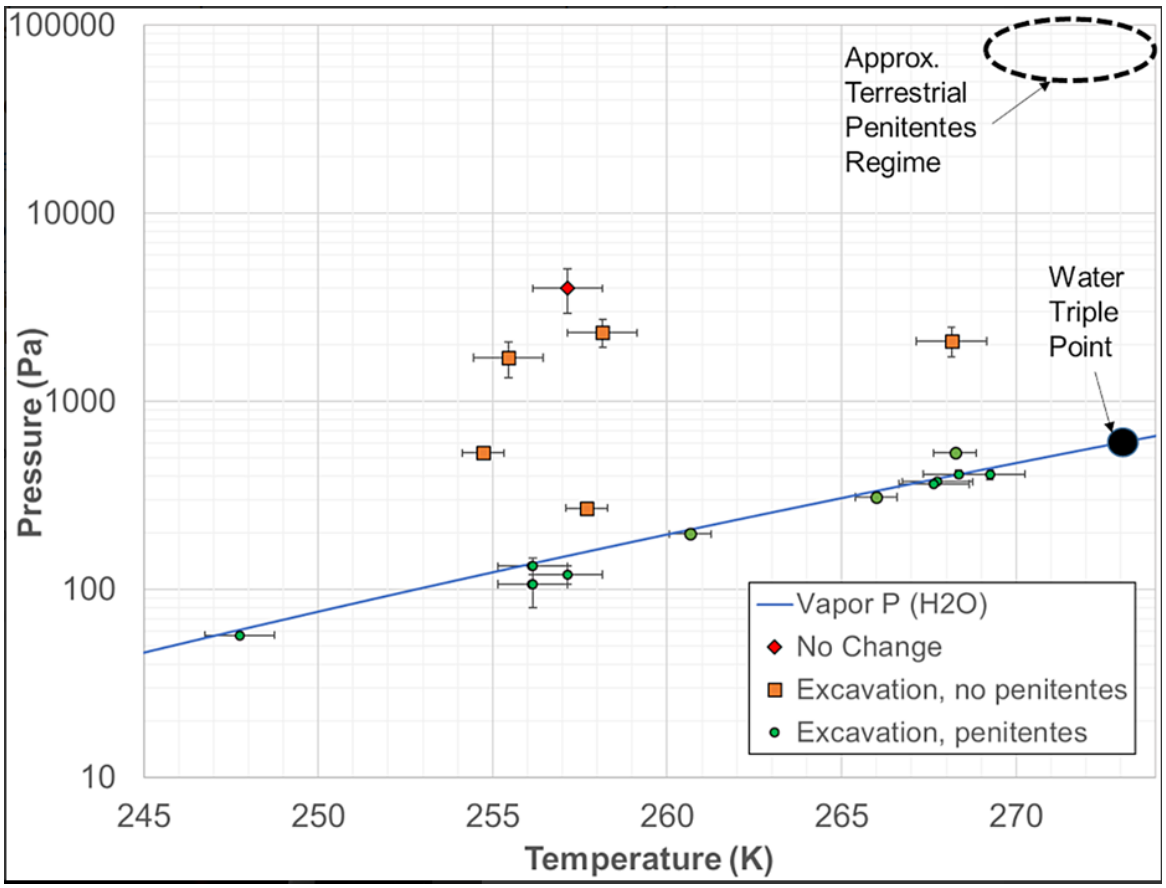


Figure 2.2 Experimental conditions of Berisford plotted over the water vapor curve [1]

2.3 Influence factors on penitente formation

As obtained by the experimental results of Bergeron and Berisford, the seven conditions that must by met for penitente formation, as established by Lliboutry and Claudin, are influenced by several factors. These factors are: the solar illumination, the snow/ice properties, the atmospheric conditions and surface debris. In this section these factors and their influence on penitente formation will more deeply be explained.

Solar illumination

The main factor that influences the formation of penitentes is solar illumination, both direct and reflected. Without solar illumination no penitentes will form, even when all the other secondary processes required to form penitentes are present [27]. The total solar illumination received by the snow, both direct and reflected, determine the insolation received by the penitentes. The strong effect of the solar illumination on penitente growth can be seen in the locations where penitentes form, their orientation, and experiments that have been preformed with penitentes.

Penitentes usually form in the tropical and subtropical regions. In these regions the Sun is almost overhead and the incidence angle is close to zero. Due to this the solar illumination is concentrated in a smaller area resulting in a stronger insolation in the tropical regions than at higher latitudes were the incidence angle is larger and the solar illumination is spread out over a larger area. This effect can also be seen in the sizes of penitentes. In the tropical zones the penitentes have a greater size due to stronger solar illumination [28]. Cathles states that

insolation strength is not the only factor inhibiting penitente growth at higher latitudes. According to him the angles of incoming solar illumination are distributed bimodally at high latitudes, which causes both sides of surface perturbations to ablate instead of only ablation in the troughs [27]. If part of this bimodal illumination would be blocked, the remainder of the solar illumination would be concentrated resulting in a stronger insolation, which would allow penitentes to form at higher latitudes [27]. Cathles also states that penitentes could form at higher latitudes if a snowfield was present on a slope pointing towards the Sun, as it decreases the incidence angle. This has later been confirmed by simulations by Nguyen. In his simulations penitentes could form at terrains with a tilt towards the equator at locations where they would not be possible to form if the terrain would be flat [19].

An interesting aspect of penitentes that shows the influence of solar illumination on penitentes is the orientation of their peaks. The peaks have a preferred orientation which aligns with average direction of the incident light, which is the Sun's local noon position. On Earth penitentes have a preferred east-west orientation [28]. In the laboratory experiments by Bergeron the peaks of the penitentes grew towards the direction of the incident light, which has a conical irradiation profile [12].

Besides the intensity of solar illumination Bergeron also suggest that the wavelength of the incoming light has an influence on penitente growth. During one of his experiments he filtered out the near-infrared and infrared wavelengths emitted by the floodlamp used in the experimental setup. When these wavelengths were filtered out the formation of penitentes was halted [12]. However, Berisford doubts the validaty of this experiment and this result. Berisford states that the lamp used in the experimental setup of Bergeron mostly emits near-infrared light, which results in a decline in the total flux reaching the ice surface when these wavelengths are filtered out and this puts a halt on the penitente formation [1]. No further research has been done on this topic, however it is known that the light penetration depth in the ice varies with wavelength which may have some effects on the ablation rate [1].

Properties of snow/ice

The properties of the snow/ice can influence the ablation rate and the self-illumination process of penitente formation. In 1958 Amstutz noticed that the formation of penitentes is different in snow than in ice [28]. This was later confirmed by experiments done by Bergeron, were penitentes took twice as long to form in ice as compared to snow, and by penitente growth simulations by Moores were a different ablation material than water snow/ice was used [12] [29]. The ablation materials used by Moores were methane ice and nitrogen ice. Penitentes were only able to form in the methane ice and not the nitrogen ice in his simulations [29]. The properties of the snow/ice that lead to these differences in formation are: albedo, grain size, density, dust content, thermal conductivity, thermal diffusivity and light penetration.

The albedo affects the self-illumination process of penitente growth and thus influences its growth rate. The growth rate of penitentes is increased in snow/ice that has a higher albedo [27] [18]. This effect in growth rate can also explain the results found in Bergeron's experiment, in which the growth rate of penitentes in granular snow was greater than in ice. Snow usually has a higher albedo than ice, resulting in a higher growth rate and earlier formation of penitentes [2]. The albedo of the snow is dependent on the density, the grain size and dust content of the snow/ice. The density does not have a direct effect on the albedo, but it is

influenced by the grain size of the snow/ice. A greater density corresponds to greater grain sizes. The grain size is the dominant factor determining the albedo of snow/ice. The smaller the grain sizes, the larger the albedo. This results that snow has a greater albedo than firn and glacier ice, which have greater densities and grain sizes than snow. [2]

Dust content in snow/ice can have a reducing or increasing effect on albedo, depending on the wavelength of the incoming light. This effect is especially pronounced at greater snow/ice grain sizes. At larger snow/ice grain sizes the reduction in albedo is larger than for snow/ice with smaller grain sizes in the visible light spectrum. At longer wavelengths this effect is however reversed for larger grain sizes, causing an increase in albedo. The effect of dust content on the albedo of snow/ice with different grain sizes can be seen in Figure 2.3. As it is unknown if near-infrared light has a stronger influence on penitente formation than other wavelength it is unknown what the effect of added dust will do to the penitente formation mechanism. As can be seen in Figure 2.3 dusty ice has a higher albedo than clear ice for the wavelengths greater than about 0.8 μm. These greater wavelengths correspond to the near-infrared and infrared spectrum. If the near-infrared and infrared wavelengths are the main contributing wavelengths to penitente formation, as thought by Bergeron [12], a larger dust content may promote penitente formation. However if Bergeron's statement is false, as believed by Berisford, a larger dust content may hinder penitente formation. [2]

Additionally to the change in albedo caused by added dust to snow/ice, dust in snow/ice may promote melting. The dust can provide extra heating leading to additional energy available for the snow/ice to melt [3]. This aspect of dusty snow/ice may promote penitente growth by promoting ablation. However it is not known if this aspect of dusty snow/ice predominates over the albedo changes in the snow/ice due to dust when it comes to penitente formation.

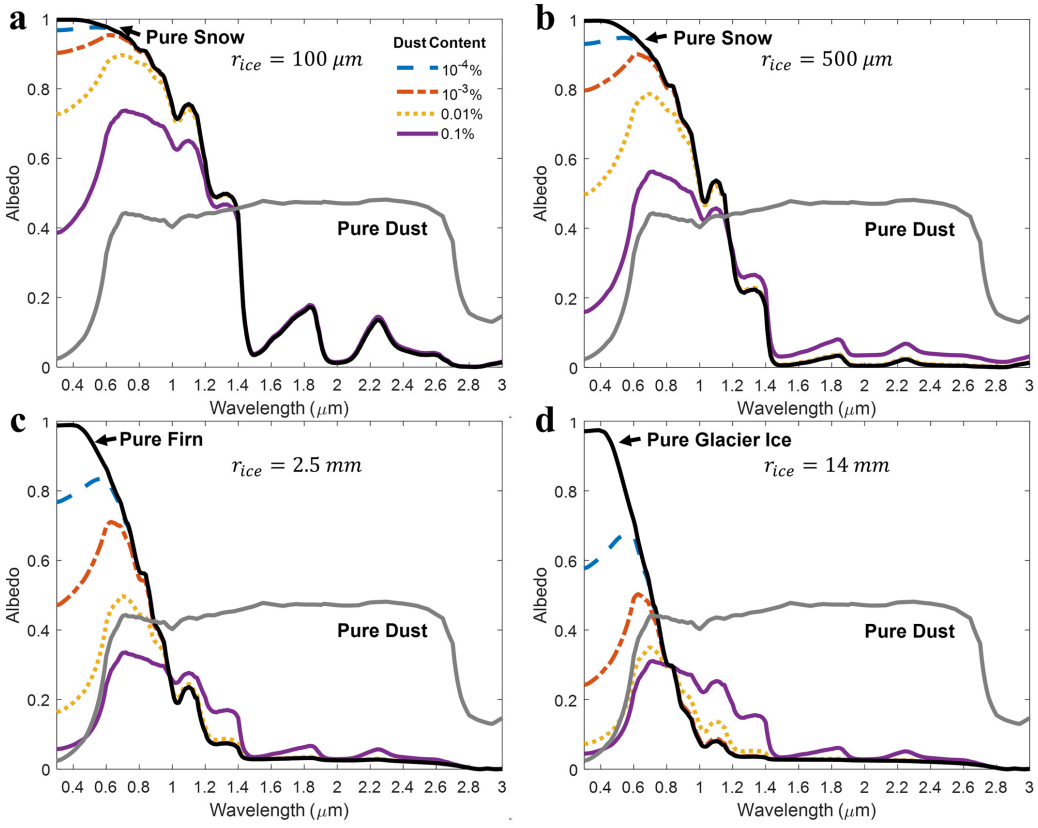


Figure 2.3 Variation in the albedo for snow/ice of various grain sizes for various dust contents [2]

Besides the albedo, the thermal conductivity of the snow/ice influences the heat conduction within the snow/ice. The distribution of the surface temperature is partly determined by the thermal conductivity of the snow/ice. Poor thermal conductivity may lead to cooler troughs than peaks, even though the insolation at the troughs is greater than in the peaks [23]. This inhibits penitente formation. A higher thermal conductivity may solve this problem [23].

The thermal conductivity of snow/ice is dependent on its morphology, its temperature and the atmospheric pressure. The difference in thermal conductivity based on the temperature and snow morphology can be seen in Figure 2.4. Granular snow has a lower thermal conductivity than ice due to the inter-particle voids in granular snow [25].

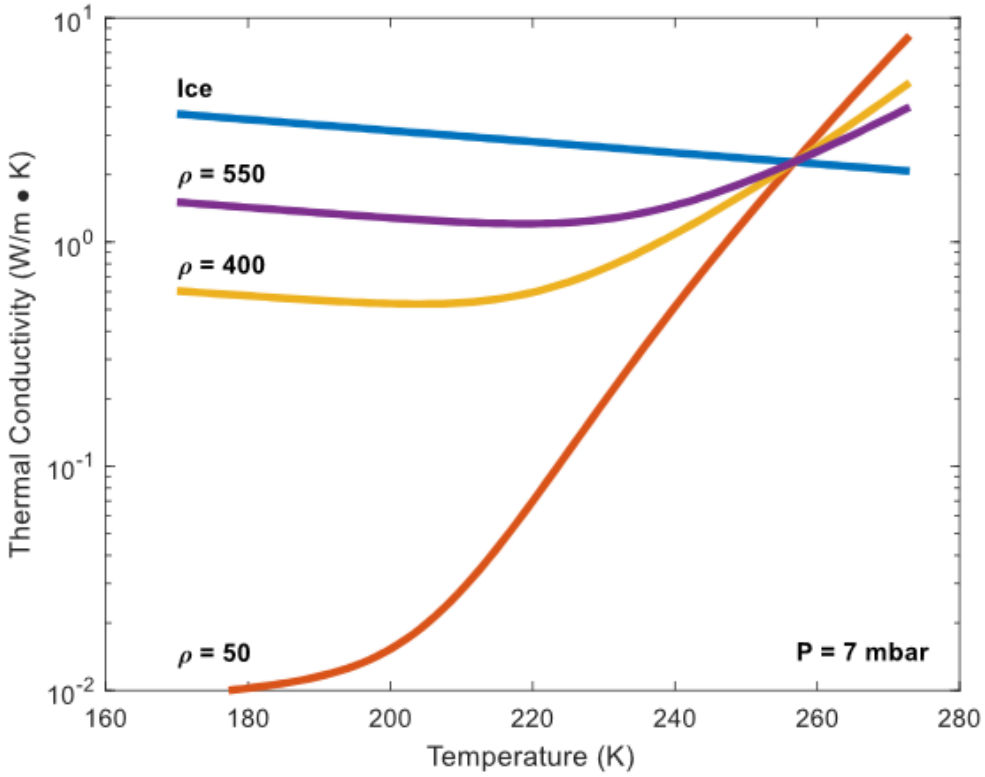


Figure 2.4 The thermal conductivity of snow and ice on Mars for an atmospheric pressure of 700 Pa. The assumed grain radius for the densities 50, 400, 550 kg/m^3 are 50 μm, 800 μm, 4 mm, respectively [3]

The thermal diffusivity of the snow/ice also affects the penitente formation. When the snow/ice has a greater thermal diffusivity the sublimation rate decreases [1].

Lastly the light penetration depth into the snow/ice influences the heat diffusion in the snow/ice and the heat absorption by the snow/ice, which affects the spacing between penitentes in a penitente field and their growth rate [19] [18]. However there is some discrepancy in literature of the effect of light penetration on the penitente formations. According to Berisford, a shorter light penetration depth leads to a decrease in the spacing between penitentes in water ice [1]. In Claudin's model however, the wavelength that dominates penitente spacing is independent of the light penetration depth [18]. Nguyen found similar results as Claudin. The penitente growth and spacing were almost unaffected by changes in the light penetration depth in his simulations [19]. It should however be noted that Nguyen used Claudin's model for the penitente simulations, so similar results are expected.

Atmospheric conditions

Most of the conditions that are necessary for penitente formation, as described by Lliboutry and Claudin, concern atmospheric conditions. These atmospheric conditions that influence the penitente growth are: the temperature, the humidity, the atmospheric pressure and the near-surface wind velocity.

A low temperature and low humidity are necessary as penitentes form in conditions that are close to the vapor pressure curve [22] [1]. If the temperature and vapor pressure conditions are too far away from this curve the penitentes do not form or cease to exist, since melting will dominate or there is a too little temperature differential across the snow surface due to little water vapor [22]. The vapor pressure of water is determined by the temperature and pressure and can be described by the Goff-Gratch equation, see Equation 2.1 [19]. The vapor pressure curve is also included in the phase diagram of water and can be seen in Figure 2.5.

$$log_{10}P_s = -9.09718(\frac{273.16}{T} - 1) - 3.56654log_{10}(\frac{273.16}{T}) + 0.876793(1 - \frac{T}{273.16}) + log_{10}(6.1071) \tag{2.1}$$

Where P_s is the saturated vapor pressure for water at temperature T in hPa .

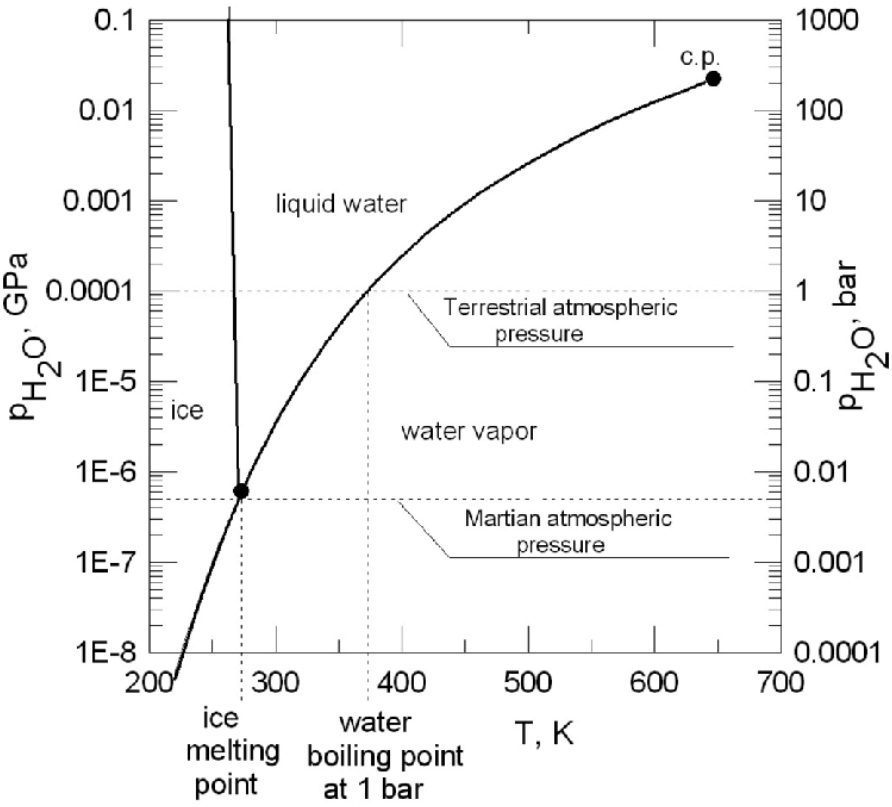


Figure 2.5 The phase diagram of water, including the saturated vapor pressure curve [4]

Besides the temperature a low humidity is universally agreed to be one of the conditions required for penitentes to form. A low humidity is required as the dew point is dependent on the relative humidity and the temperature. However at low temperatures the dew point is already quickly below 0 °C. It was found that changes in the relative humidity were found to have little effect on the formation on penitentes while changes in temperature had a large

effect [12].

Additionally the formation of penitentes is also influenced by wind velocities. High surface winds inhibit penitente formation as it makes the temperature and humidity around the penitentes uniform, obstructing the temperature gradient and thus the differential ablation necessary for penitentes to form [20]. Surface winds larger than 2.5 m/s can already eliminate the penitente formation [12]. However when penitentes increase in size the troughs are protected against the wind, which may allow them to grow with larger wind speeds present [29]. Unfortunately it is currently unknown until which precise wind speeds the troughs in larger penitentes are protected against the wind. If wind speeds are too strong penitentes cease to exist and suncups and cross-hatched terrains will form instead [29].

Surface debris

Surface debris, including dust but also coarser debris that lays on top of the snow/ice surface, can affect the ablation of snow/ice by altering its albedo. The exact effect of surface debris on albedo is dependent on the thickness of the debris on top of the snow/ice. A thin debris layer can decrease the surface albedo, increasing ablation of the snow due to more heat absorption and thus promoting penitente growth [30]. This effect of a thin layer of debris results in quicker penitente formation and in a larger peak seperation between the penitentes [12]. On the other hand a thick debris layer can form an insulation layer on top of the snow/ice, decreasing the temperature and increasing the heat required to ablate the snow [30].

2.4 History of penitente models

Previous experimental studies and field observations on penitente formation have explained which conditions are required for penitentes to form and which factors influence penitente formation and growth. However, from these studies the mechanism behind the penitente spacing pattern, which occur in penitente fields, is unclear. In 2015 Claudin has made a penitente model to research the selection of the penitente wavelengths in these patterns and to predict the penitente growth rate and associated penitente peak spacing in certain climatic conditions and snow/ice properties. This model simulates the physical principles of penitente formation to obtain these growth rates and spacings [18].

Claudin's model gives the growth on penitentes based on sublimation and self-illumination. This sublimation is governed by four processes: the diffusion of temperature, vapor and light and the conservation laws at the interface. Taking all these processes into account Claudin formulated a dispersion relation, Equation 2.2, relating the growth rate of penitentes, σ, to the wave number, k [18].

$$\frac{\rho_s L}{\psi_a}\sigma = \frac{k\Lambda}{1 + Ptanh(kl) + Rk\Lambda} \times \left[\left(1 - \frac{1}{\sqrt{1+k^2\Lambda^2}}\right) + \Omega\left(1 - \frac{k\Lambda}{\sqrt{1+k^2\Lambda^2}}\right) - \left(1 - \frac{1}{cosh(kl)}\right)P\right] \tag{2.2}$$

It should be noted that Claudin's model only takes into account sublimation conditions and does not consider melt. Due to this feature Claudin's model also assumes sublimation takes place at certain temperatures and pressures where in reality no sublimation can take place.

Thus the accuracy of the results obtained by this model is highly dependent on the input conditions given to it.

After the establishment of this model by Claudin in 2015, Moores added an additional feature with which an estimate of the change in height of penitentes over time can be made. This extra feature uses the initial height of the structures in the ice, the growth rate as modeled with Claudin's model and time duration as can be seen in Equation 2.3. [29]

$$\Delta h = h_1[exp(\sigma \Delta t) - 1] \tag{2.3}$$

Moreover this model has been used to validate the experimental results obtained by Bergeron's and Berisford's experiments. The penitente spacing and growth obtained by the model were similar to the experimental results.

In 2017 and 2019 Claudins model had been used by Moores and Nyugen, respectively, to investigate extra terrestrial penitente formation. Moores used the model to simulate the possibility of penitentes on Pluto. Nyugen used the model to simulate the possibility of penitentes on Mars.

2.5 Extra terrestrial penitentes

As climatic conditions and the influence factors on penitente formation differ throughout celestial bodies, Moores and Nguyen have investigated the possibility of penitente formation on other planets.

Moores studied the possibility of penitentes on Pluto. On Pluto the atmospheric conditions and ice conditions differ from Earth. On Pluto N_2 and CH_4 ice is present instead of water ice. Moreover the solar flux received, the temperature and the pressure are drastically lower than on Earth. Additionally the atmospheric composition differs as compared to Earth. [29]

In his research Moores obtained that penitentes can only form in the CH_4 ice and not in the N_2 ice on Pluto. This difference in formation possibility is due to the different properties of CH_4 ice compared to N_2 ice. This highlights the impact of the snow/ice chemical properties on penitente formation, as was mentioned in Section 2.3.

Nguyen studied the possibility of penitentes on Mars. Like Pluto, the solar flux received, temperature, pressure and atmospheric composition differ on Mars as compared to Earth. However water snow and ice can exists on Mars. However some inputs used by Nyugen in the model may not have been entirely correct. While Nyugen altered the atmospheric conditions in his model he failed to alter the chemical properties of the ice. Nyugen used all of the chemical properties of pure ice at Earth conditions. However it is known that the ice on Mars contains a small amount of dust, altering the bulk density and albedo of the ice [2] [31] [3]. Moreover the thermal conductivity of ice is dependent on the temperature and pressure, thus taken the value typical value of 2 W/mK for Earth conditions results in inaccurate results [18] [3]. This value of 2 W/mK is approximately consistent with the temperatures and atmospheric pressures used in the simulations of Claudin and Berisford. On

Mars the temperatures and atmospheric pressures are lower than on Earth and thus a different thermal conductivity of ice is expected. The thermal conductivity for ice and snow with different densities on Mars at an atmospheric pressure of 700 Pa can be seen in Figure 2.4. In his simulations Nguyen has directly taken the thermal conductivity value from Claudin's research, thus the value of 2 W/mK. However this value of Claudin is for Earth conditions while Nguyen uses it for Mars conditions at a temperature of 203 K and a pressure of 600 Pa. This value of 2 W/mK for ice is not correct for this temperature and pressure. At this temperature and approximate pressure the thermal conductivity of ice is about 3 W/mK, as can be seen in Figure 2.4. Eventhough this figure shows pressures at 100 Pa higher than Nguyen used in his model, the difference in pressure between the one used in this figure and the one used by Nguyen is so small that the value changes in thermal conductivity are insignificant for this small discrepancy in pressure. At Earths atmospheric pressure ($\approx$ 100,000 Pa) the thermal conductivity at about a temperature of 200 K is 3.2 W/mK [32], thus the thermal conductivity at pressures between 100 Pa and 100,000 Pa are expected to be around 3 W/mK.

In his research Nyugen concluded that penitentes are able to form on Mars, however his results have inaccuracies due to the inaccurate chemical properties of the ice used in his research. To gain better understanding of the possibility of penitentes on Mars these chemical properties must be taken into account.

Moreover Nguyen's results are only theoretical and reality may differ. Additionally Nguyen's work mainly focuses on the influence of received solar flux. During his study the pressure and temperature remained at a set value failing to take into account the great influence of these two factors. Thus to get a more comprehensive research on possible formation of penitentes on Mars all these influence factors should be taken into account and laboratory experiments should be performed.

2.6 Martian conditions

Mars is an interesting planet for research on penitente formation as water snow/ice is present on this planet and penitente formation in thought to be possible according to Nguyen. However Nguyen's study does not take into account some of the key climatic conditions and snow/ice properties on Mars which may greatly influence penitente formation. In order to asses if Mars indeed has favorable conditions for penitente formation the snow/ice properties and climate conditions on Mars will be discussed.

Martian snow/ice

As the formation of penitentes is dependent on the properties of the snow or ice medium they form in a brief explanation will be given on the snow and ice present on Mars. On Mars snow and ice exists however its physical conditions may differ compared to Earth due to the difference in environmental conditions. One main difference is that on Mars CO_2 snow and ice is present next to water snow and ice. On Mars CO_2 snow and ice can exist due to the much lower temperatures and pressures than on Earth. In this subsection the physical properties of water and CO_2 snow/ice on Mars will be discussed.

Water ice and snow

Ice and snow come in a wide variety of physical properties. On Mars the ice typically contains <1% dust, which alters the density and albedo compared to pure ice [2] [3]. Unfortunately the properties of Martian ice are poorly constrained. The only in-situ measurement of the ice have been made with the Phoenix lander, however Phoenix did not directly measure the grain size, density and dust content of the ice [2]. The indirect measurements have been compared to spectral models by Christensen to deduct the grain size (350 μm) and dust content (0.015%) of this snow/ice found by Phoenix [2]. Khuller has compared sprectral data obtained using HiRISE with spectral data of snow and ice. With his method he found that mid-latitude gullies most probably have exposed dusty water snow at its surface [3]. A spectral data comparison has also been performed by Singh using CRISM spectral reflectance measurements at the Southern hemisphere and Northern hemisphere of Mars [13]. The results of these comparisons with the spectral models can be seen in Table 2.2 together with the properties of other snow/ice types. The observed albedo of this Phoenix snow can be seen in Figure 2.6. These Martian snow properties found by Christensen, Khuller and Singh could improve the simulations of Mars penitentes by Nguyen, by providing more realistic snow properties of Mars than the current properties of pure ice used.

Table 2.2 Snow/ice properties depending on their type

Snow/ice type	**Dust content [%]**	**Density [kg/m^3]**	**Grain size**	**Study**
Pure ice	0	917	16 mm	[2]
Snow	0	50-550	50-500 μm	[2]
Firn	0	550 - 830	500 μm - 3 mm	[2]
Glacier ice	0	830-917	3 - 16 mm	[2]
Martian snow at Phoenix	0.015	-	350 μm	[2]
Martian snow in midlatitude gullies	<1	-	1 - 1.3 mm	[3]
Snow in Northern hemisphere at $L_s = 13$	0.06	-	100 μm	[13]
Snow in Northern hemisphere at $L_s = 65$	0.01	-	500 μm	[13]

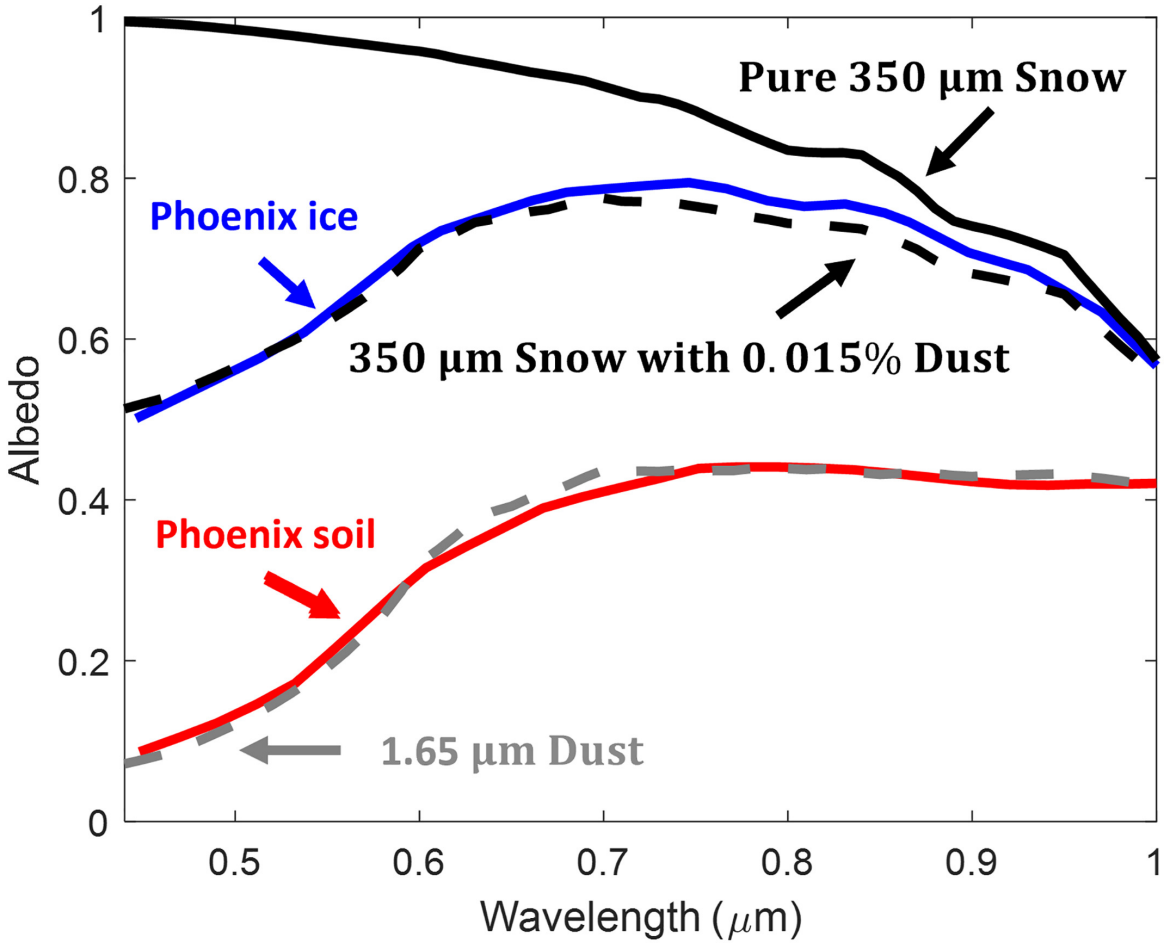


Figure 2.6 Observed albedo of ice at the Phoenix lander site compared to albedo spectra of 350 μm snow [2]

As Mars has lower temperatures and atmospheric pressures than Earth, pure water snow and ice cannot melt at the surface of Mars, but sublimates [3]. This poses a hazard to penitente formation on Mars as melting in the troughs is necessary in order to form large penitente structures. Dust in the snow and ice can provide extra heating which provides additional energy available for melting. Past models predict that a dust content of 0.1% in snow/ice on Mars is already sufficient for melting to occur [3]. Moreover denser clean snow/ice can also melt when surface temperatures are higher than 250 K, as the denser snow has a lower thermal conductivity and thus more energy is available to melt the snow/ice [3]. So large penitentes may be able to form on Mars in certain regions where the snow/ice properties allow for melting.

CO_2 ice and snow

On the surface of Mars there is a large presence of CO_2 ice and snow, especially on the South pole. On the South pole seasonal CO_2 snow is present ontop of a perennial CO_2 ice cap during the winter months. As penitentes are also thought to form in methane ice [29], CO_2 snow/ice may also be a potential ablation material for penitentes to grow in.

CO_2 ice and snow have different properties compared to H_2O ice and snow. The albedo of CO_2 ice/snow is greater and CO_2 has a different freezing and melting point compared to H_2O. The phase change diagram of CO_2 can be seen in Figure 2.7. A more zoomed-in version of this diagram at a lower temperature and including the vapor pressure curve of CO_2 can be seen in Figure 2.8. The pressure and temperature conditions on Mars allow for CO_2

to be in solid or vapor form. As conditions on Mars can be close to the pressure curve of CO_2, penitentes may be able to form in these conditions. However the pressure on Mars is usually too low to allow for melting, thus the size of penitentes in CO_2 ice on Mars could be restricted. As melting is required to form large penitentes, as mentioned in Section 2.1, only micro-penitentes are expected to be possible to form as these only need sublimation conditions.

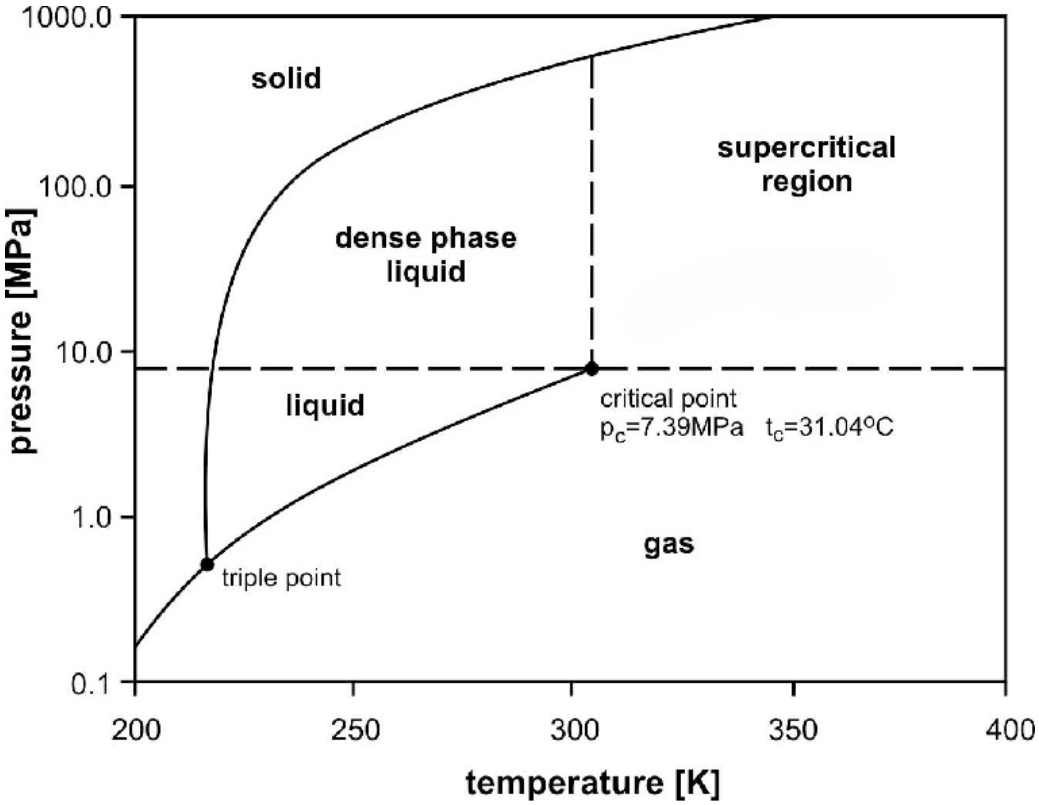


Figure 2.7 Phase diagram of CO_2 [5]

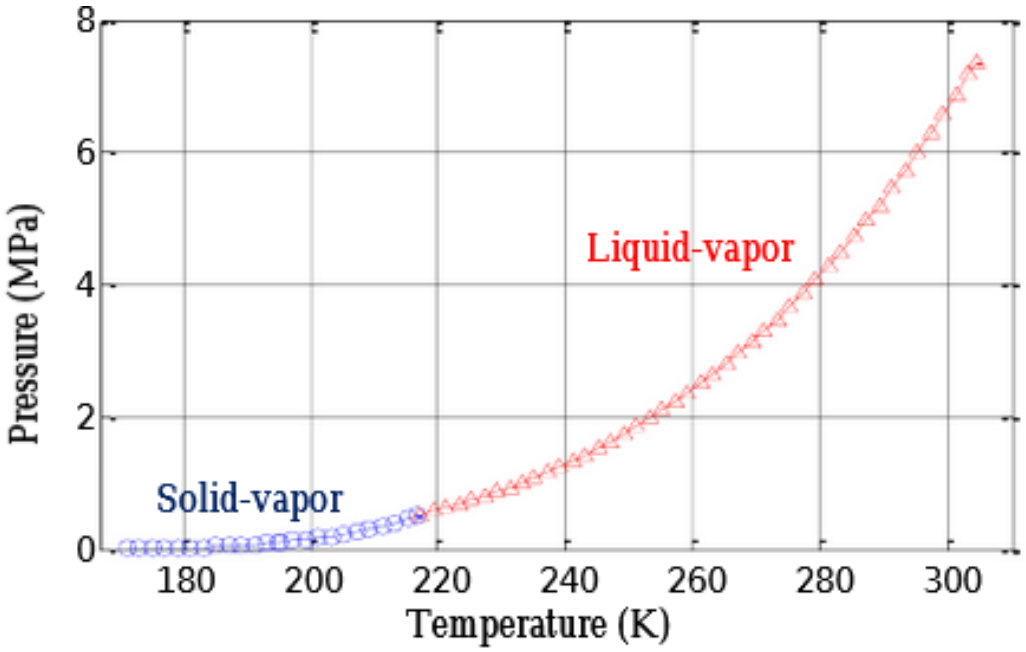


Figure 2.8 The saturation vapor pressure curve of CO_2 [6]

Compared to water snow and ice CO_2 has a greater albedo for almost all wavelengths and the albedo of CO_2 snow/ice is also less dependent on its grain size than water snow/ice [13]. This greater albedo of CO_2 snow/ice may enhance the penitente growth. While the albedo is greater in CO_2 the addition of dust to the CO_2 snow/ice has a larger affect on the albedo than in water snow/ice. Even a small amount of dust in the CO_2 ice/snow already decreases the albedo immensely and it decreases it at almost all wavelengths [13]. Due to this penitente growth may already be halted when a small amount of dust is present in the CO_2 snow/ice. No research has ever been done on penitente formation in CO_2 ice, thus the effects of a greater albedo of CO_2 and the effects of dust added to CO_2 snow/ice are still unknown.

The properties of CO_2 ice/snow on Mars have been studied by Singh using spectral data. Singh has modeled reflectance spectra for CO_2 snow on Mars and has compared this with spectral data from CRISM. The spectral data best matched CO_2 snow mixed with a tiny bit of H_2O snow. The properties of the CO_2 that matched spectral data can be seen in Table 2.3.

Table 2.3 CO_2 snow/ice properties in the Southern hemisphere of Mars at solar longitudes $L_s = 276°$ and $L_s = 337°$ [13]

Solar longitude [°]	**Dust content [%]**	H_2O **ice content [%]**	CO_2 **grain size**	H_2O **grain size**
276	0.0042	0.024	1000 μm	100 μm
337	0.003	0.07	3000 μm	200 μm

Snow/ice as surface debris

A small layer of CO_2 snow/ice on top of H_2O snow/ice may act as surface debris that can alter the albedo of the ablation medium. This alteration of albedo may occur on Mars as both snow/ice types exists simultaneously in some regions on Mars. CO_2 snow/ice has a greater albedo than water snow/ice. A small layer of CO_2 snow/ice ontop of H_2O snow/ice will increase the albedo. The opposite is true when a small layer of H_2O is deposited ontop of CO_2 snow/ice, the albedo will decrease in this case. As albedo is an important factor on the formation of penitentes, this effect may alter the growth rate of penitentes on Mars. However currently no research has been done on how this will alter penitente formation. [13]

Martian climate

Although Mars is the most Earth like place in the solar system as we see a similar large geodiversity due to complex interactions between surface and atmosphere, there are significant differences in their atmospheres and climates that could impact penitente formation. While Earth's atmosphere mainly consist out of nitrogen (78.1 %) and oxygen (20.9%) and a vast variety of trace gases, Mars atmosphere mainly consists out of carbon dioxide (95.1 %), with a little bit of nitrogen (2.59 %) and argon (1.94 %) and also a vast variety of trace gases, including water vapor (210 ppm) [33] [34]. Besides the atmospheric composition, the air temperature, received solar illumination, relative humidity, atmospheric pressure and wind speeds also differ on Mars. These conditions have been observed using various measuring instruments aboard orbiters and rovers on Mars. Moreover a proven General Circulation Model, which is in agreement with measured observations, is available which can simulate almost all atmospheric conditions on Mars. This model is the Mars Climate Database (MCD) by Laboratoire de Météorologie Dynamique [35] [36]. In this subsection various climatic factors on Mars will be presented.

Surface insolation

The solar radiation that reaches the surface of Mars varies throughout the year due to the eccentricity of Mars orbit, and dust storms. The average solar irradiance received at the top of the atmosphere of Mars is 586.2 W/m^2 [34]. However the insolation at the surface is lower due to some absorption of solar irradiance and scattering of solar radiation within the atmosphere [8]. Levine has mapped the average daily insolation across the surface of Mars over one Martian year in clear sky conditions. This map can be seen in Figure 2.9. The unit $\frac{cal}{cm^2 planetaryday}$ used in this map equals $0.4713 \frac{W}{m^2}$ for a Martian sol, which lasts 24 hours, 39 minutes and 35.244 seconds [37]. The seasonal variation of the surface insolation at various locations on Mars has also been graphed by Martínez in 2017. While Levine used calculations to map the insolation, Martínez has used rover measurements. These variations of the insolation at various rover sites can be seen in Figure 2.10. In this figure the unit $\frac{MJ}{m^2}$ equals $11.26 \frac{W}{m^2}$ for the duration of one Martian day. The insolation map by Martínez also takes into account the opacity of the atmosphere while Levine's map did not take this into account. Due to this the values by Martínez are lower and give a better overview of the actual conditions on Mars at that time. As can be seen in these two graphs the highest solar insolation happens during local summer and near the equator. As penitentes require strong solar insolation, it is likely that they form during the local summer time when insolation is strongest, if the temperature allows for this.

It should be noted that the insolation values by Martínez and Levine do not show the maximum solar insolation that can occur on Mars but shows a daily average. Due to this the values reported are not the maximum solar insolation that can reach the surface of Mars. As can be seen in Figure 2.10, about 80 to 75% of the solar insolation at the top of the atmosphere reaches the surface [8]. Thus about 20-25 % of the incoming solar radiation at top of the atmosphere is being absorbed before it reaches the surface. This means that the maximum average solar insolation that reaches the surface of Mars is about 440 to 470 W/m^2. This value is also consistent with Martian climate simulations using the Mars Climate Database [35] [36].

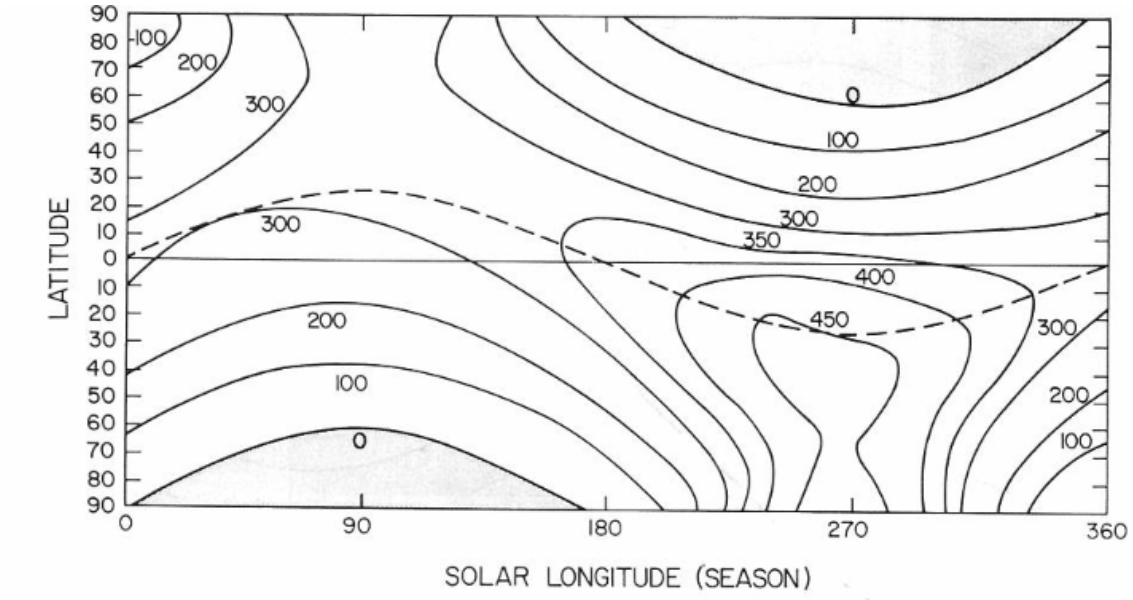


Figure 2.9 Solar insolation at the surface of Mars for clear sky conditions in $\frac{cal}{cm^2 planetaryday}$ [7]

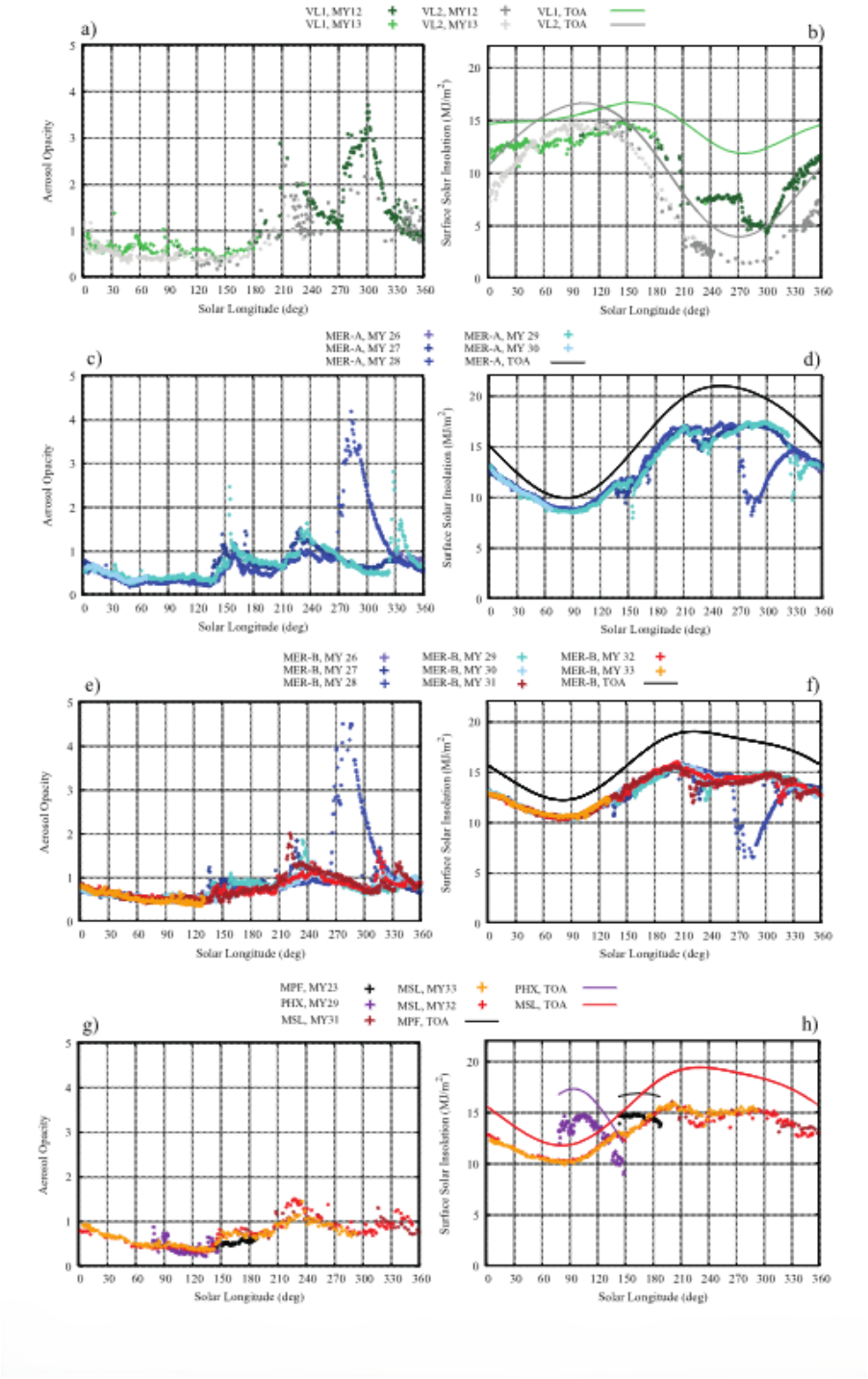


Figure 2.10 Interannual and seasonal evolution of the solar insolation and aerosol opacity measured by various rovers. The solid lines indicate the solar insolation at the top of the atmosphere, while the crosses indicate the solar insolation at the surface at each landing site. [8]

Surface temperatures

The surface temperatures on Mars are directly related to the insolation at the surface of Mars, aswell as to the surface albedo and thermal inertia of the surface layer. In the polar regions the surface temperature is however controlled by the underlying subsurface perennial ice caps [38]. The average surface temperature on Mars is about 210 K [34]. As Mars progresses along its orbit the surface temperatures vary across one Martian Year. The most recent variation in surface temperatures has been mapped out by Piqueux, based on data from the Mars Climate Sounder [38]. Piqueux did only map the minimum, maximum and average surface temperatures across Mars. While these extremes give great insight on the range of

the absolute surface temperatures possible on Mars in a year, it fails to show the progression of the temperature throughout the year. Martínez mapped out the progress of temperature throughout the year using the daily mean surface temperature measurements of the rovers Viking to Curiosity [8]. While this clearly shows how the temperature progresses throughout one year, it fails to show a complete overview of the surface temperature across Mars, since it only uses measurements at specific rover landing sites.

The maximum and minimum temperatures found by Piqueux and Martínez in a Martian year are shown in Table 2.4. The temperatures by Piqueux are shown as a range as he mapped out the temperature difference across the whole globe. Thus only the extremes found on the entire planet are shown.

Table 2.4 Maximum, minimum and average temperature seen on Mars on the course of one Mars Year

Maximum temperature [K]	**Minimum temperature [K]**	**Average temperature [K]**	**Note**	**Study**
150 - 290	130 - 190	150 - 220	Temperature range is from temperatures at the polar regions to the equator	[38]
230	150	-	These correspond to the daily mean air temperatures observed by Viking through Curiosity	[8]

In addition to seasonal variation in the surface temperatures, the surface temperatures on Mars also vary diurnally, just as on Earth. These diurnal variations have been mapped out by Atri and Martínez. Some of the minimum and maximum surface temperatures, as documented by Atri and Martínez, are presented in Table 2.5. The measurements by Atri are based on the global coverage of Mars, but are only measurements observed during a certain time period and not over a whole year. The measurements by Martínez are only at one certain location at a certain time period. Thus Atri's observation gives a better overview on the global diurnal surface temperature observations.

Table 2.5 Minimum and maximum temperatures seen on Mars throughout one sol

Minimum temperature [K]	**Maximum temperature [K]**	**Note**	**Study**
140	280	From temperatures observed during $L_s = 65.8 - 78.9$	[39]
190	240	From temperatures observed by Curiosity at $L_s \approx 60$	[8]
210	260	From temperatures observed by Curiosity at $L_s \approx 180$	[8]

Relative humidity

Large variability of relative humidity is present on Mars. This variability is due to variations in the surface temperature on Mars throughout the seasons , causing sublimation of H_2O in

the polar caps [8] [9]. At the Curiosity landing site daily relative humidity has been observed from 10%, late spring / early summer, up to 70%, in early winter [8]. At the Phoenix landing site, maximum relative humidity has been observed from about 18% to about 95% throughout the seasons [40]. The seasonal variations in relative humidity, as observed during night time, across Mars can be seen in Figure 2.11.

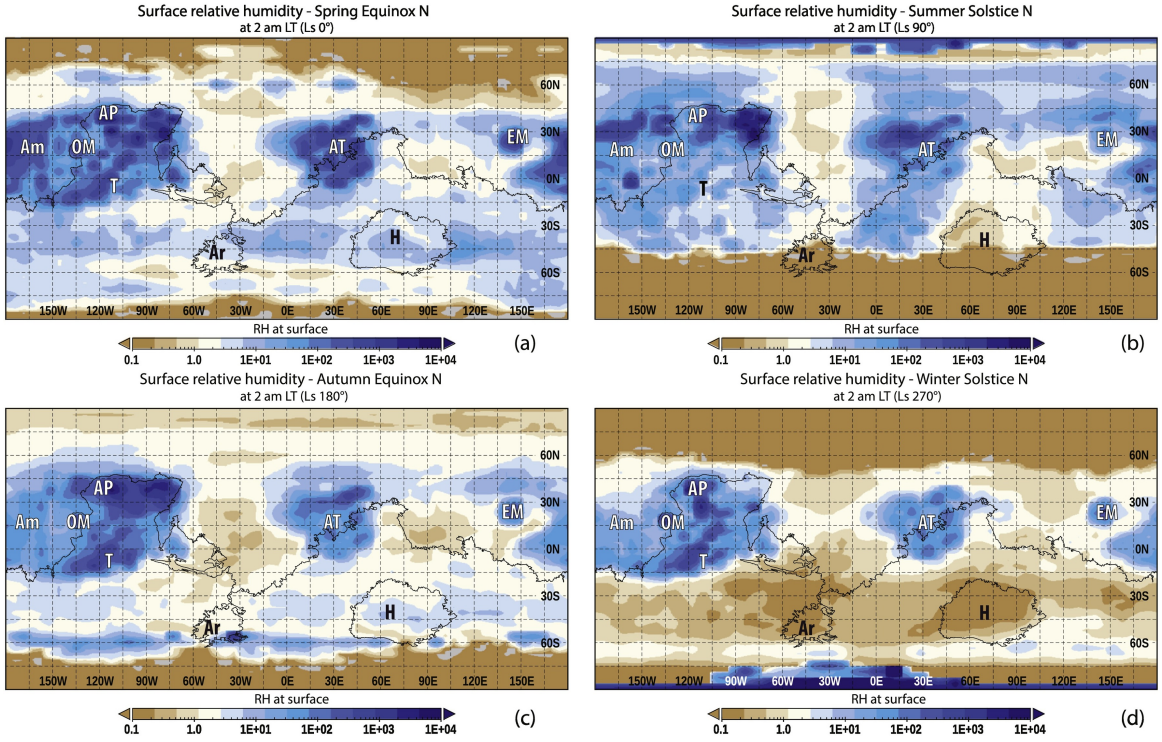


Figure 2.11 Seasonal dependence on relative humidity on Mars during night time [9]

Relative humidity also varies throughout the day due to variations in the diurnal temperature. At night, when the temperatures are lower, the relative humidity is higher than during the day when the temperatures rise. At the Curiosity rover landing site, the relative humidity varies from about 0%, during the day, to 50% at night during northern summer [41]. The diurnal variation of relative humidity in various locations on Mars can be seen in Figure 2.12.

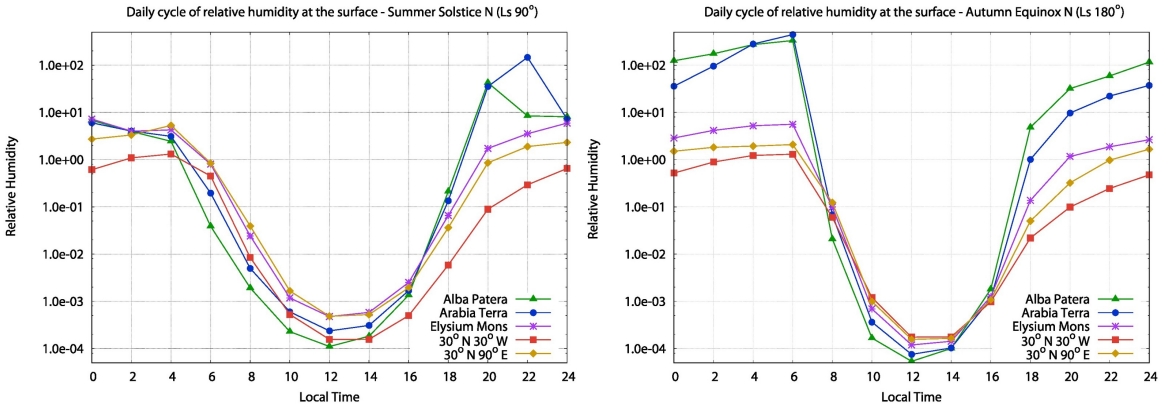


Figure 2.12 Diurnal variation of surface relative humidity on various locations across Mars [9]

Atmospheric pressure

The atmospheric pressure on Mars is dependent on the condensation and sublimation of CO_2 ice in the polar caps, causing a variation in the CO_2 content in the atmosphere. Moreover, orographic effects caused by height differences at the surface, dynamic effects caused

by the balance between mass and wind fields, and variations in atmospheric dust content, affect the atmospheric pressure on Mars, although to a lesser extent than the CO_2 content in the atmosphere [42]. These effects cause atmospheric pressure to vary up to 25% throughout a Mars Year [42]. The range of atmospheric near-surface pressures seen on Mars is 300 to 1200 Pa [10]. The variation of daily mean atmospheric pressure at various rover landing sites throughout a Martian year can be seen in Figure 2.13. In the late southern spring ($L_s \approx 260°$) temperatures rise causing CO_2 ice to sublime and release into the atmosphere, resulting in an increase in atmospheric pressure [10]. In the late southern fall atmospheric pressure decreases again due to deposition of CO_2 caused by a decrease in temperature [10]. Additionally to seasonal variations, the pressure varies depending on location and surface elevation, as can be seen in the figure. The average surface pressure on Mars is 6.36 mb at mean radius [34].

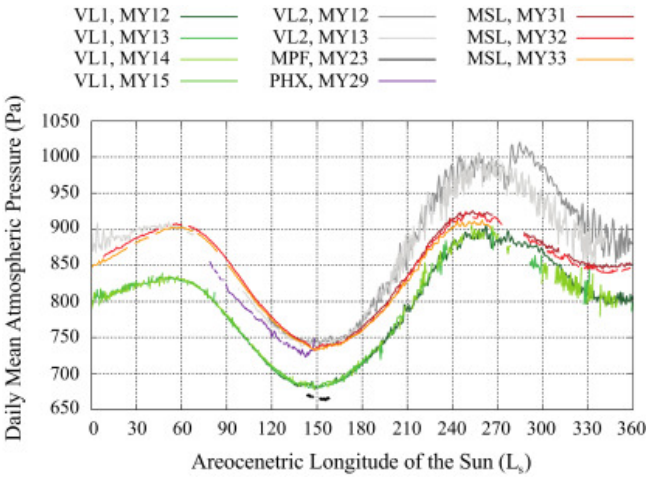


Figure 2.13 The seasonal evolution of the daily mean atmospheric surface pressure as observed by various rovers [10]

Diurnal variation in surface pressure caused by temperature variations are also present. Pressures are highest during the night when temperatures are lowest and are lowest during the day when temperatures are highest [8]. Diurnal atmospheric pressure variations up to 100 Pa (from 690 Pa during the day to 770 Pa during the night) have been observed at the Curiosity landing site [8].

Near-surface wind

Wind speeds on Mars are mostly influenced by the local and regional topography and vary largely throughout the seasons due to global circulation. This global circulation is strongest during the northern fall and winter, which causes an increase in wind speeds. This can also be seen in Figure 2.14, which shows the seasonal variation in near-surface wind speed at various rover locations. These wind speeds shown are also in rough accordance to wind speeds at the Viking 1 Lander (VL1) site reported by NASA, which range from 2-7 m/s in the summer, 5-10 m/s in the fall and 17-30 m/s when a dust storm is present [34]. Throughout one day, wind speeds generally peak during the day time [8]. This can pose threats to penitente formation, as strong winds inhibit penitente growth. The effect of wind on penitente formation on Mars has not been researched yet and is thus an interesting topic for future research.

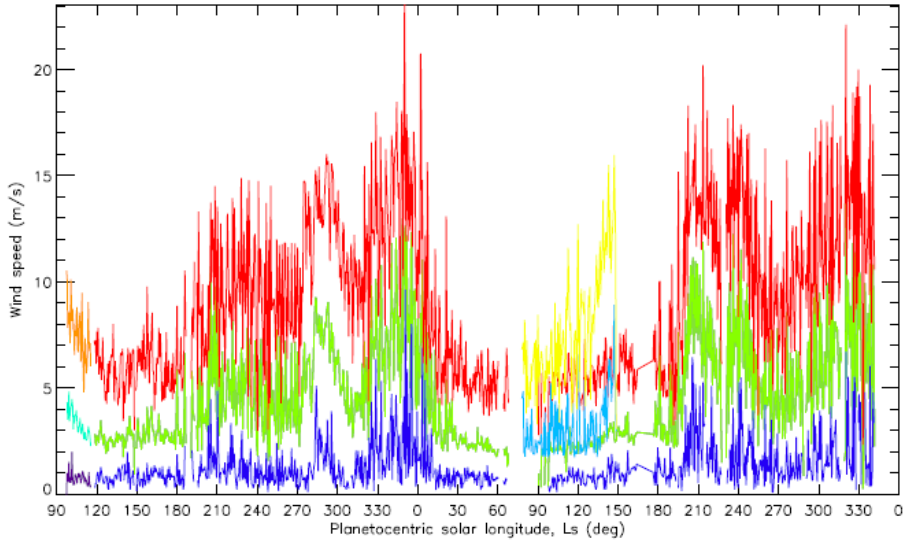


Figure 2.14 The seasonal variance in near-surface wind speed on Mars. The dark blue (minimum), green (mean) and red (maximum) lines represent the daily wind speed at the VL2 site in MY 12 and 13. The purple (minimum), cyan (mean) and orange (maximum) lines represent the daily wind speed at the VL1 site in MY 12. The light blue (minimum) and yellow (maximum) represent the daily wind speed at the PHX site in MY 29. [8]

2.7 Research proposal

As Mars has favorable atmospheric conditions: strong insolation, low relative humidity, low temperatures and low pressures close to the saturated water vapor curve, Mars is an interesting planet for further research on extraterrestrial penitentes. Moreover as terrestrial penitentes are observed to house life and penitente formation is thought to be possible on Mars, the possibility of penitentes on Mars is an interesting research area waiting to be further explored. While Nguyen already explored the idea of penitentes on Mars, his research failed to take into account some of the key snow/ice properties and ever changing climatic conditions on Mars. Moreover there is currently a lack of experimental research on the formation of penitentes at Martian conditions.

These points have led to perform the research to investigate the possibility of penitente formation on Mars, which is presented in this thesis report. In order to investigate penitentes formation on Mars and if there are locations on Mars where penitente formation is possible the following research question has been established: **In which temperature and pressure regimes are penitentes able to form on Mars?** In order to answer this research question the following sub question have been established:

- **Which factors have a key influence on penitente formation on Mars?**
- **Are penitentes able to form in known temperature and atmospheric pressure conditions on Mars?**
- **At which temperatures can penitentes form on Mars at various Martian pressures?**
- **What is the effect of the dust content on the formation duration of penitentes on Mars?**

Two methods have been used to answer these research questions. Firstly laboratory experiments have been performed in which the factors that influence penitente formation have been researched. Additionally laboratory experiments have been performed to simulate the Martian environment at different temperature and pressure conditions to research if penitentes are able to form in these conditions. Secondly Claudin's model, combined with the experimental results, has been used to simulate penitente growth at certain Martian

regions were temperature and pressure conditions are thought to support penitente formation. These Martian region were investigated using the experimental results and the Mars Climate Database general circulation model. Additionally Claudin's model has been used to further investigate the key influence factors on penitente formation and has been used to investigate the effect of the dust content in pure ice and granular snow on the growth rate of penitentes on Mars.

3 Experiment and Model Setup

To answer the research question and research the formation of penitentes in various temperature and atmospheric pressure conditions on Mars and the factors influencing this formation, various laboratory experiments have been performed, aswell as model simulations. In order to perform these experiments an experimental setup has to be made which can simulate the Martian conditions. Additionally to simulate penitente growth in a model a computer model which can simulate penitente behavior must be used.

The first penitente experiments used a small setup using an EPS box at ambient pressure to check if it was possible to form penitentes at conditions were it is known they will form and at conditions were Bergeron managed to form penitentes in his experiments. Later on experiments have been performed in PISCES, a vacuum chamber located at the aerospace faculty of the TU Delft. In this chamber the temperature, pressures and solar insolation conditions of Mars will be simulated. In this chapter the design process of the experimental setup will be discussed as well as the final design and various methods used to make the ice and snow for penitentes to form in. Additionally the model equations of the penitente growth model used to simulate the theoretical penitente growth will be discussed. In Section 3.1 the mould used to house the snow/ice sample is presented. The methods used to make the ice and snow samples for the experiments are presented in Section 3.2 and 3.3 respectively. The design of the test setup using an EPS box is presented in Section 3.4. The design of the test setup and the setup itself using PISCES is presented in Section 3.5. Lastly the equations behind the model used to calculate the theoretical penitente growth are presented in Section 3.6.

3.1 Snow/ice mould design

In order to contain and make the ice and snow for the laboratory experiments a design for a mould was made. Several requirements had been established for this mould. Some requirements are based on the snow and ice dimension used by Bergeron and Berisford, as snow and ice of their dimensions managed to form penitentes in their experiments. Moreover some requirements are based on the climatic conditions present on Mars which are desired to be simulated, as the mould should be able to withstand and operate in these conditions. These requirements are presented in Table 3.1.

Table 3.1 Requirements for snow/ice mould

Req ID	Requirement
IM.1	The mould shall be able to house snow and ice for the experiments
IM.2	The mould shall be leak tight
IM.3	The mould shall be able to house at least an ice and snow thickness of 10 cm
IM.4	The mould shall have a length and width of minimum 25 cm to maximum 75 cm, which is similar to Bergeron and/or Berisford snow dimensions
IM.5	The mould shall be able to fit within the PISCES chamber, which has dimensions 80 cm x 80 cm x 80 cm

IM.6	The mould shall not obstruct the windows and instrumentation connection points inside PISCES
IM.7	The mould shall be able to operate in temperatures between 200 K and 300 K
IM.8	The mould shall be able to withstand vacuum

A commercially available container has been selected based on these requirements. A stainless steel GN 1/2 box with a height of 15 cm has been selected. This GN box has a width of 26.5 cm and length of 32.5 cm making it close to the ice dimension of 30 cm in diameter used by Berisford. It is leak tight as it has no holes. With a height of 15 cm it is able to house at least an ice/snow thickness of 10 cm. It is able to fit within PISCES which has a length x width x height of 80 x 80 x 80 cm. It shall not obstruct windows or connection ports as the windows are located at 40 cm from the PISCES floor and the instrumentation ports are at 22.75 cm from the PISCES floor. Moreover stainless steel was selected due to its thermal properties and excellent vacuum compatibility [43] [44].

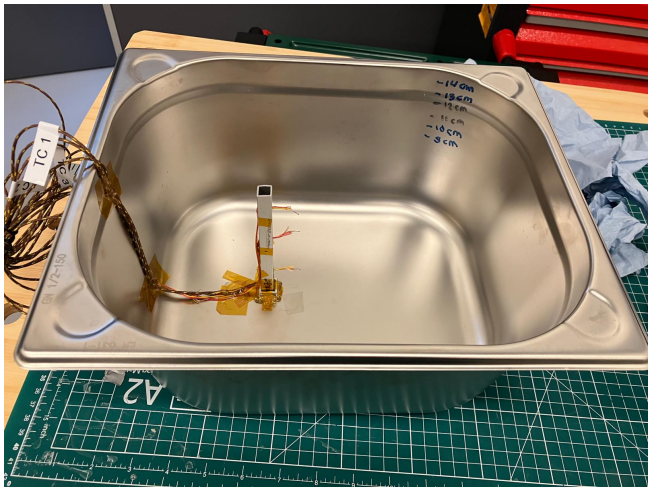


Figure 3.1 Ice/snow mould with thermocouple stand used for containing the snow and/or ice for the laboratory penitente experiment

In order to measure the temperature inside the snow/ice samples during the experiments a holder for the thermocouples has been made. This holder consist of a hollow steel tube in which three holes have been drilled. These holes have been drilled at 3.75 cm, 7.5 cm and 11.25 cm from the bottom. The measurement tips of the three thermocouples were than put through the holes and secured using tape. The holder was than glued to the bottom of the GN box at a distance of 6 cm of length and 4 cm of width. Using this holder the temperatures at 3.75 cm, 7.5 cm and 11.25 cm in ice/snow thickness could be measured during the experiments. A picture of the icemould with thermocouple stand can be seen in Figure 3.1.

3.2 Ice making

To conduct the experiments ice and snow samples have been produced which act as the ablation material for penitentes to form in. Several attempts and methods have been used to create ice that has a clear and smooth surface. For each of these attempts demi water was used that was put into the GN container and than let to freeze inside a -20 °C freezer for at least 24 hours. Demi water was specifically used as more clear ice could be achieved since

all minerals and ion are removed from this water which may cause impurities within the ice.

Method 1

For the first method water was put into the GN container layer by layer. One layer was placed inside the container which was then left to freeze for about 45 minutes to one hour after which an additional layer of water was deposited on top of it. This process was continued untill the container was almost full. The water was not poured up to the edge to allow for the expansion of the water when transitioning to ice.

This method resulted in a cloudy ice block with an elevation in the middle of the ice surface. This elevation is undesired and probably occurred due to the freezing of the water from all sides which pushed all the air in the water towards the middle. Pictures of the ice surface made using this method before and after the conduction of the experiment can be seen in Figure 3.2.



(a) Start experiment

(b) Just after end experiment

Figure 3.2 The ice made with ice making method 1 at the start and just after the end of the first experiment

Method 2

For the second experiment another method had been used to make the ice in order to get a more even leveled ice surface. For this method an insulation box had been made from styrofoam that perfectly fits around the GN container. This insolation box insulates the bottom and sides of the GN container resulting in one directional freezing from the top. This directional freezing should push all the air inside the water to the bottom while the water freezes from the top to the bottom. During this method water was also added in layers to the container, as in the previous method. The GN container with the surrounding styrofoam insulation box can be seen in Figure 3.3.



Figure 3.3 Stainless steel container in which the ice is made with the surrounding foam insulation box to ensure one directional freezing

This method resulted in an even leveled and clear ice surface. However some air entrapment in the ice was still visible, most probably due to air entrapment between the different added layers. When all layers were added but one, the water was left to freeze for an entire night. The following morning just before conducting the experiment a thin additional water layer was poured over the top ice surface to add two thermocouples to the ice surface and freeze them in place. However this addition of a small water layer resulted in an undesired large air bubble beneath the ice surface, as can be seen in Figure 3.4. Thus for the next experiments that thin additional layer shall not be added anymore and the thermocouples will just be held into place by taping them to the ice surface.



Figure 3.4 The ice made with ice making method 2, used for the second experiment

3.3 Snow making

For the other experiments snow has been made to be used, as it is believed that penitentes will form more quickly in snow as compared to ice due to their different properties. The snow made for the experiments was created by adding water to a dewar vessel filled with liquid nitrogen. Several methods of adding the water into the liquid nitrogen were tried to test which methods would create the smallest grains.

Method 1: Water spray into liquid nitrogen

In this method a conventional spray bottle filled with water is used to create the snow. Using this spray bottle, water is sprayed directly into the liquid nitrogen. The spray bottle creates a mist of fine droplets, once these droplets come into contact with the liquid nitrogen they rapidly freeze creating small ice/snow grains. After they froze the created snow grains were collected from the dewar vessel using a metal spoon. This method created fine ice/snow grains representing powder like snow as can be seen in Figure 3.5. This method is also the method that created the smallest ice/snow grains and has thus been used to make the snow for the experiments. The downside of this method is that you cannot perfectly control the size of the water droplets formed by the spray bottle, thus the grain sizes created with this method vary slightly from one another. However this can be offset by grinding the snow/ice grains through a sieve which made sure the grain size was < 2 mm.

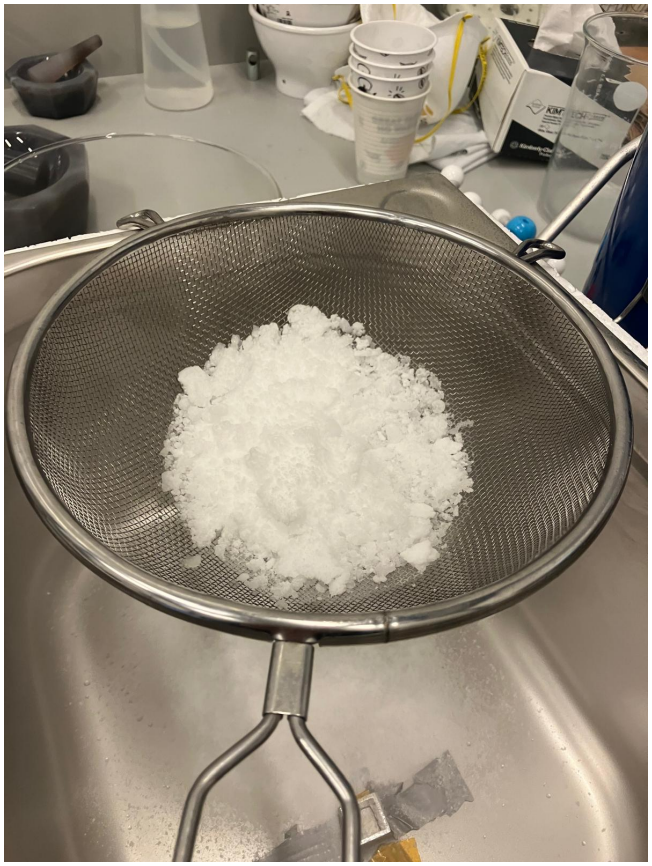


Figure 3.5 Snow created by spraying water using a conventional spray bottle into a dewar vessel containing liquid nitrogen

Method 2: Dump water into liquid nitrogen

In this method a larger volume of water is dumped directly into a dewar vessel containing liquid nitrogen. About 100 ml of water was put inside a measuring cup and than poured completely into the liquid nitrogen. Afterwards it was collected with a metal spoon. Using this method a large lump of ice was created, as can be seen in Figure 3.6. This lump of ice could easily be broken up into smaller pieces as can be seen in Figure 3.7. However even after it had been broken up into smaller pieces the ice grains were still too larger and did not represent snow.

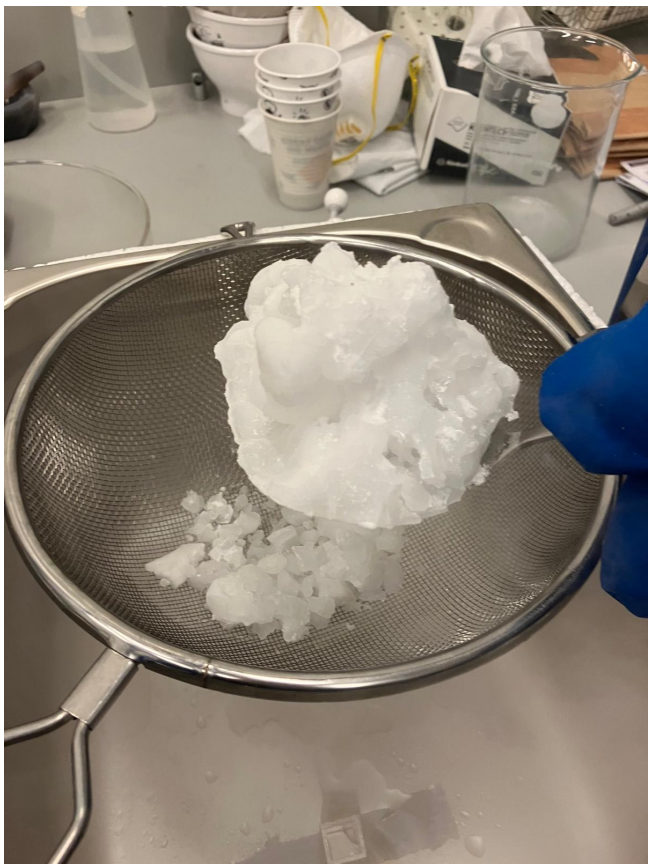


Figure 3.6 Lump of ice created by pouring about 100 ml of water from a measuring cup into a dewar vessel containing liquid nitrogen

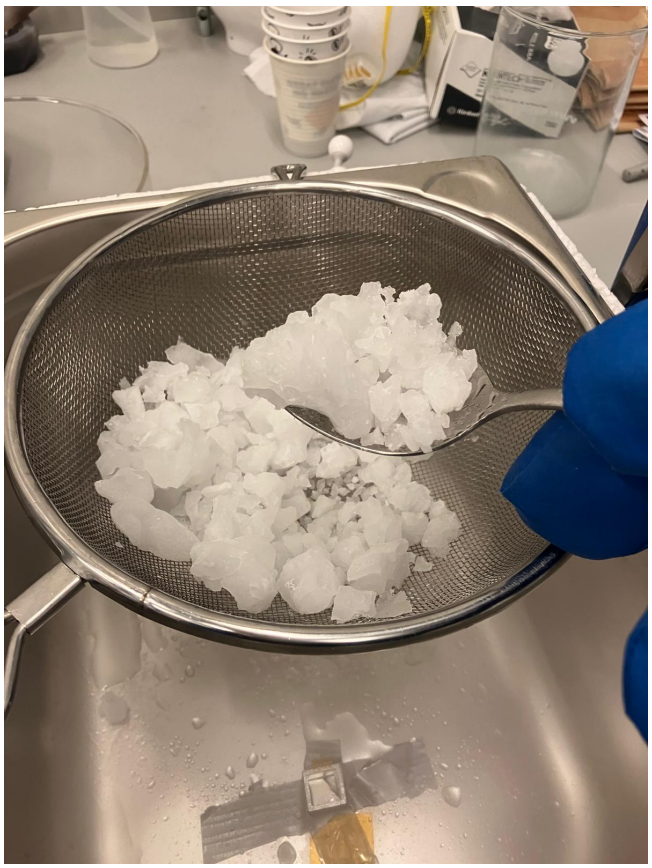


Figure 3.7 Pieces of ice created by breaking apart the lump of ice, created by dumping water into liquid nitrogen, using a spoon

Method 3: Spraying water into sieve

In this method a sieve was placed directly on top of a dewar vessel filled with liquid nitrogen and water was sprayed onto this sieve using a conventional spray bottle. The idea behind this method is that the air above the liquid nitrogen is being cooled to below the freezing point of water by the liquid nitrogen resulting in the water droplets being frozen in the air before hitting the sieve. The droplets would than be collected by the sieve. This did however not happen. The water droplets did not freeze before hitting the sieve, which resulted that water collected by the sieve flowed to its lowest point were large drops of water fell directly into the liquid nitrogen. This created a combination of larger lumps of ice and some powdery snow created by the water droplets that went directly through the sieve into the liquid nitrogen as can be seen in Figure 3.8. This method created vastly different grain sizes of snow and ice and was thus chosen not to be used to make the snow for the experiments.

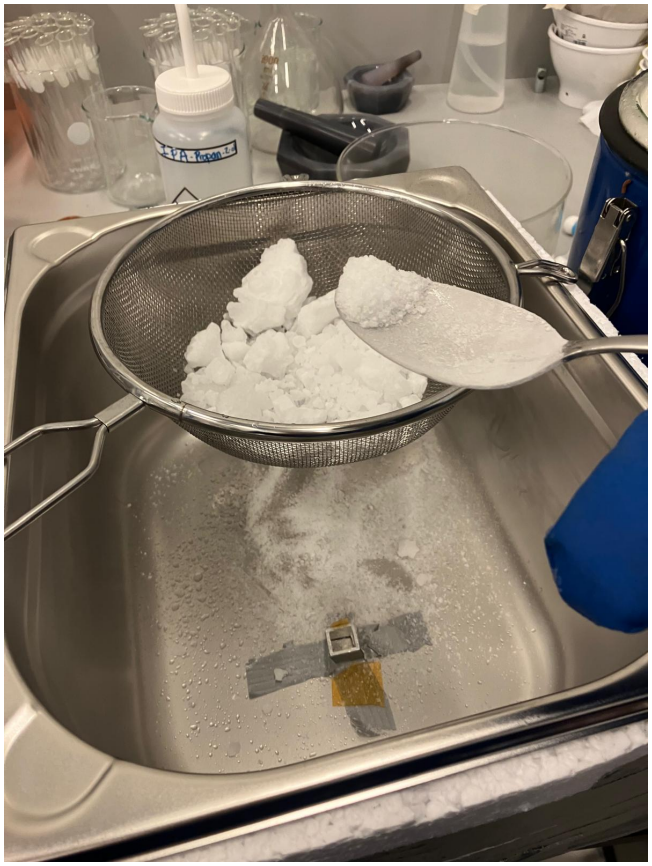


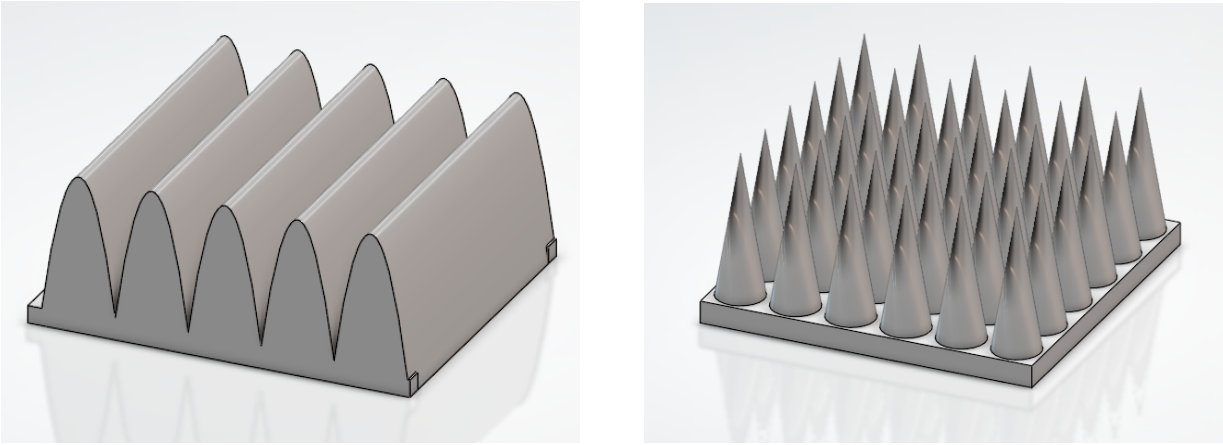
Figure 3.8 Snow/ice created by placing a sieve ontop of a dewar vessel containing liquid nitrogen and spraying water droplets using a conventional spray bottle onto the sieve

Final method used

From the three methods tested for making snow, method 1 'Water spray into liquid nitrogen' has been selected to be used to make the snow for the experiments. Method 2 was the most time efficient method but this method did not achieve small snow/ice grains that respresent snow. Thus method 2 was not selected. Method 1 and 3 took about the same amount of time to make the snow/ice grains. However method 1 achieved a much more homogeneous snow sample with less larger ice grains and more finer snow grains than method 3. Due to this method 1 was chosen to be used to make the snow for the experiments. By sieving the snow made using this method snow grains of < 2 mm were achieved.

Preformed penitentes

For the last six experiments preformed penitentes had been made to investigate their stability in Martian conditions. These preformed penitentes had been made using two different kinds of 3D printed moulds, presented in Figure 3.9. Snow made with snow making method 1, was put into these moulds and slightly pressed to form the desired penitente shapes. One mould was used to create 3D penitentes, which had peak heights of about 1 cm and a penitente peak spacing of about 1 cm. The other mould could be used to create 2D penitentes, as inspired by Berisfords preformed penitentes [23]. With this 2D mould penitentes with peak height of about 2.5 cm and a peak separation of about 1 cm could be made. The resulting penitente shapes that were made using these two moulds can be seen in Figure 3.10.



(a) 2D mould

(b) 3D mould

Figure 3.9 Penitente mould designs used to create preformed 2D and 3D penitentes



Figure 3.10 Preformed penitentes made with the 2D mould (front left shapes) and the 3D mould (front right shapes)

3.4 Setup with EPS box

To conduct the first three experiments a setup with an EPS box has been designed. This setup has been inspired by Bergeron's experimental setup to check if we could replicate his penitente formations. To design this setup the requirements presented in Table 3.2 have been established.

Table 3.2 Requirements for the EPS setup

Req ID	Requirement
EPS.1	The setup shall be able to keep the ice/snow samples in the GN container at subzero temperatures for at least 5 hours
EPS.2	The solar insolation received by the ice/snow surface shall be between 400 and 500 W/m^2, in order to represent Martian solar insolation
EPS.3	The light source shall have a light temperature between 5500 and 6000 K, in order to represent the black body radiation of the Sun
EPS.4	It shall be possible to take photo's of the ice/snow surface during the experiments

Temperature and humidity control

As the goal for this setup was to make it simple it was chosen that the ice/snow samples will be well insulated during the experiment conduction to keep the samples at subzero temperature for a couple of hours. For this an EPS box has been chosen, as these boxes are widely used for these kind of applications, for example to store dry ice. As the GN container storing the ice/snow samples has a dimension of 26.5 x 32.5 x 15 cm the EPS box shall be able to fit this GN container inside while also minimizing nonfunctional volume within the EPS box. The most suitable size EPS box for this, which is also commercially available, has an inner size of 500 x 300 x 200 mm. Thus an EPS box of this size will be used for this setup. This EPS box has a wall thickness of 50 mm. This wall thickness was chosen at it was the thickest wall thickness option available for this size of EPS box and the thicker the wall the better its insulation capacity.

To keep a cool environment within the EPS box while still being able to take pictures of the ice/snow surface during the experiments the EPS box will be covered by a see-through plexiglass sheet. A LEXAN polycarbonate plate with UV blocking properties has been used for this, which is similar to the plexiglass plate used by Bergeron during his experiments. In order to minimize unused space in this closed environment crushed ice had been added to the EPS box just before the conduction of experiments.

Originally this setup did not have any components to ensure low humidity, as addition of water vapor to Bergeron's setup to increase relative humidity did hardly influence the penitente formation in his experiments [12]. However later on for one of the experiments a moisture absorber was added inside the EPS box during the experiment.

Solar simulation

To simulate the martian solar insolation at the surface of the ice a lamp will be used. This lamp must fullfill requirements EPS.2 and EPS.3 in order to succesfully simulate the Martian solar insolation. The solar insolation stated in EPS.2 is higher than the insolation used in the

experiments by Bergeron, which used a flux of 300 W/m^2. Due to this larger solar insolation it is expected that the penitentes in this EPS setup will form more quickly than in Bergeron's experiments.

The amount of insolation that the surface receives is dependent on the lumen or lux provided by the light source, the distance between the light source and the surface, and the area which the light source illuminates. The lumen or lux provided by the light source is dependent on the lamp performance. The surface area which is illuminated is dependent on the illumination angle, also known as beam angle, and the distance between the light source and the surface.

One of the lamps available at the faculty that meets requirements EPS.2 and EPS.3 is the HEDLER Profilux 1000. This lamp produces light of color temperature 5600 K, can change its illumination angle and is dimmable. At a 1 meter distance the lamp provides a maximum of 34450 lux or 15450 lux dependent on the illumination angle, as can be seen in Figure 3.11 [11]. The first lux value corresponds to the spotlight function of the lamp and the second corresponds to the floodlight function.

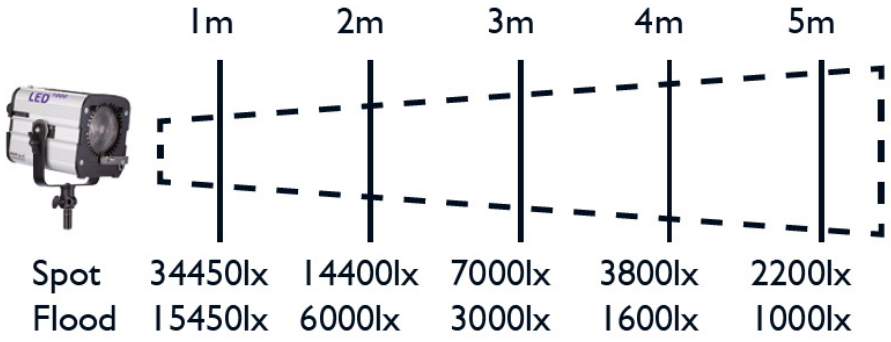


Figure 3.11 Illumination profile of the Hedler Profilux 1000 [11]

To meet EPS.2 the right settings on the lamp must be used and a correct distance from the ice/snow surface should be established. To receive an insolation between 400 and 500 W/m^2 at the ice surface a lux between 48,000 and 60,000 lux is required [45]. As the lamp will illuminate the ice surface via the polycarbonate plate on the top of the EPS box, the transmission of the plexiglass plate should be taken into account. This plate has a light transmission of 84% [46]. Using the inverse-square law for light it was calculated that the distance between the lamp and the ice surface shall be 0.78 m (when using spotlight) or 0.52 m (when using floodlight) to obtain a surface insolation of 400 W/m^2. To obtain a surface insolation of 500 W/m^2 the distance shall be 0.69 m (when using spotlight) and 0.47 m (when using floodlight). It is desired to use the spotlight function of the lamp as it has a smaller illumination area and will prevent additional undesired reflections on the ice/snow surface. At this spotlight function the whole ice/snow surface will still be illuminated. Eventually the lamp was placed at a distance of 0.7 m from the ice/snow surface using the spotlight function and a light output of 100%. Using these settings and distance the surface approximately received a lux of 58,000.

During setup for each individual experiment the solar insolation was measured using a light meter and small changes had been made to the lamp settings in order to achieve a certain desired solar insolation.

Final EPS setup architecture

The architecture of the final EPS test setup that has been used consists of the EPS box with outer dimensions of 600 x 400 x 300 mm with a wall thickness of 50 mm, the GN container to hold the ice/snow samples, A LEXAN polycarbonate plate, six type K thermocouples, a canon EOS 2000D camera and the HEDLER Profilux LED 1000 lamp. A schematic diagram of this setup can be seen in Figure 3.12a.

The six thermocouples have been placed at various locations in the setup. Three thermocouples measure the ice temperature at various vertical ice heights, one at 3.75 cm, one at 7.5 cm and one at 11.25 cm from the bottom of the container as mentioned in Section 3.1. The other three thermocouple locations were dependent on the experiment that was conducted. Usually these were used to measure the ice surface, the surrounding crushed ice and/or air temperature.

Lastly some black photo cardboard was placed on top of the edges of the GN box. This was done to prevent undesired reflections from the metal surface of the box to the ice surface. A picture of the whole setup can be seen in Figure 3.12b.

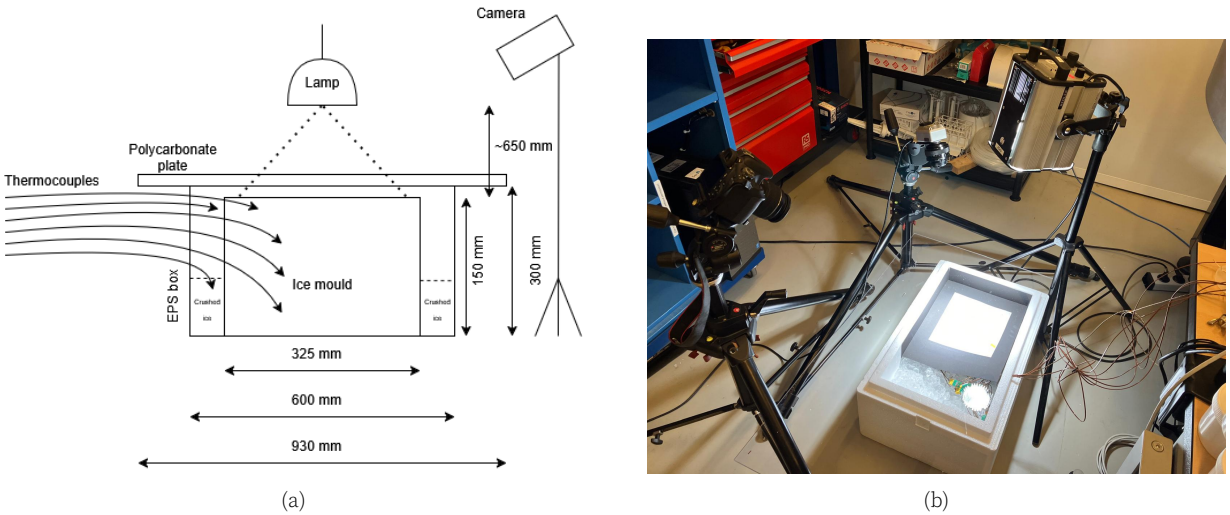


Figure 3.12 Schematic diagram (a) and picture (b) of the EPS test set-up

3.5 PISCES setup design

To perform experiments at Martian pressures and temperatures the PISCES vacuum chamber will be used. This chamber can decrease the pressure to 5E-5 Pa and can lower the temperature to 80 K at full vacuum. However this chamber cannot regulate the temperature and pressure to set a certain temperature and pressure point within the system. So additional measures should be taken to regulate the temperature of the ice and the pressure within the chamber. Various design options have been considered to regulate the temperature and pressure within the PISCES chamber and will be discussed in this section. These design options considered the established requirements presented in Table 3.3.

Table 3.3 Requirements for the PISCES setup

Req ID	Requirement
PISCES.1	The setup shall be able to keep the ice/snow samples in the GN container at Martian temperatures for at least 5 hours (200 to 273 K)
PISCES.2	The setup shall be able to achieve and maintain Martian pressures (300 to 1200 Pa)
PISCES.3.1	The dew point inside the chamber shall be kept below zero
PISCES.3.2	To keep the dew point below zero the relative humidity in the chamber shall be lower than 40%
PISCES.4	It shall be possible to take photo's of the ice/snow surface during the experiments

Temperature regulation

Four options are possible to regulate the temperature inside PISCES: option A: a recirculating chiller, option B: phase change materials, option C: a liquid nitrogen bath, option D: insulation. These four options will be discusses below.

Option A: recirculating chiller

To cool the ice inside the chamber a recirculating chiller could be used. This chiller would cool the cooling fluid inside the chiller to a desired temperature. This cooling fluid would than be transported via tubing which would be looped around the ice mould resulting in heat transfer between the cooling fluid and the ice/snow via convection in the cooling fluid and conduction between the tubing material, ice mould and ice.

This option had quickly been omitted since no suitable recirculating chillers were available at the faculty. The recirculating chiller available at the faculty can only cool to 5 °C, which is not sufficient enough for the temperatures desired to be achieved during the experiments. The other chiller that was at the faculty that could cool to -70 °C was unfortunately also not available to use as it had recently been trashed.

Option B: phase change materials

Phase change materials as cooling elements were also considered. Phase change materials can be used for cooling to keep the ice inside the chamber at a certain temperature namely the phase change temperature of the material used. With this method an additional container is required to house the phase change material in which the ice mould could than be placed so it is surrounded by the phase change material. Due to conduction the ice inside the ice mould will be cooled to the temperature of the phase change material. In order to acquire different temperatures various phase change materials have to be used to get the desired ice temperature.

One of the phase change material options is an ice and salt solution. When salt is added to ice the freezing point of the ice is lowered. Due to this the ice starts to melt. This melting draws energy from the surroundings resulting in a decrease in temperature [47]. The temperature to which the ice can be cooled using an ice and salt solution is dependent on the type of salt used and the ratio of salt to ice. The lowest possible temperature achievable with such a solution is called the eutectic temperature. Some salts that can be used are: potassium chloride, magnesium chloride, calcium chloride, table salt and lithium chloride. The eutectic temperatures that can be reached with each salt solution and the percentage of salt

needed to reach this temperature can be seen in Table 3.4. While lithium chloride would be great to reach the lower temperatures that are present on Mars it will not be considered further for this application as lithium chloride is a toxic substance and has various risks. Potassium chloride will also not be considered further as it can only lower the temperature to a minimum of - 11 °C, which could also be achieved using table salt [48]. As table salt has a lower molar mass than potassium chloride, less table salt is needed to achieve this minimum temperature than when using potassium chloride.

Table 3.4 Eutectic temperatures various ice+salt mixtures can reach and the corresponding salt percentages needed to obtain the eutectic temperature [14] [15] [16] [17]

Salt	Chemical formula	Eutectic temperature [°C]	Salt percentage [%]
Sodium chloride (table salt)	NaCl	-21	~ 23
Magnesium chloride	MgCl2	-33.6	~ 22
Calcium chloride	CaCl2	-51	~ 30
Potassium chloride	KCl	-10	-
Lithium chloride	LiCl	-79	-

While sodium chloride, magnesium chloride and calcium chloride salt/ice mixtures could be used to achieve Martian temperatures an impractical amount of salt is needed to reach and maintain these temperatures. Due to this these phase change materials will not be used to cool the ice/snow samples during the experiments.

Option C: liquid nitrogen bath

Another option to cool the ice/snow sample is to use a cooling loop using liquid ethanol and a liquid nitrogen bath. In this method liquid ethanol is cooled to a certain temperature in a liquid nitrogen bath and than looped around the ice mould through tube lines to cool the ice. This is the same kind of principle as using a circulating chiller but in this option the liquid nitrogen is used to cool the cooling liquid, ethanol. A draw back from this compared to a recirculating chiller is that liquid nitrogen always has the same temperature and thus the temperature of the ethanol is dependent on its resident time in the liquid nitrogen bath. As liquid nitrogen is very cold one risk of this system is that the liquid ethanol becomes too cold, as one completed loop through the whole system will be too short to heat up the liquid ethanol back to its initial temperature. To compensate for this and to ensure a set temperature of the liquid ethanol when leaving the nitrogen bath, an additional container may be necessary for liquid ethanol to be dumped in and heated after one loop and than be pumped back into the liquid nitrogen bath. A schematic diagram of the test setup with this cooling method can be seen in Figure 3.13.

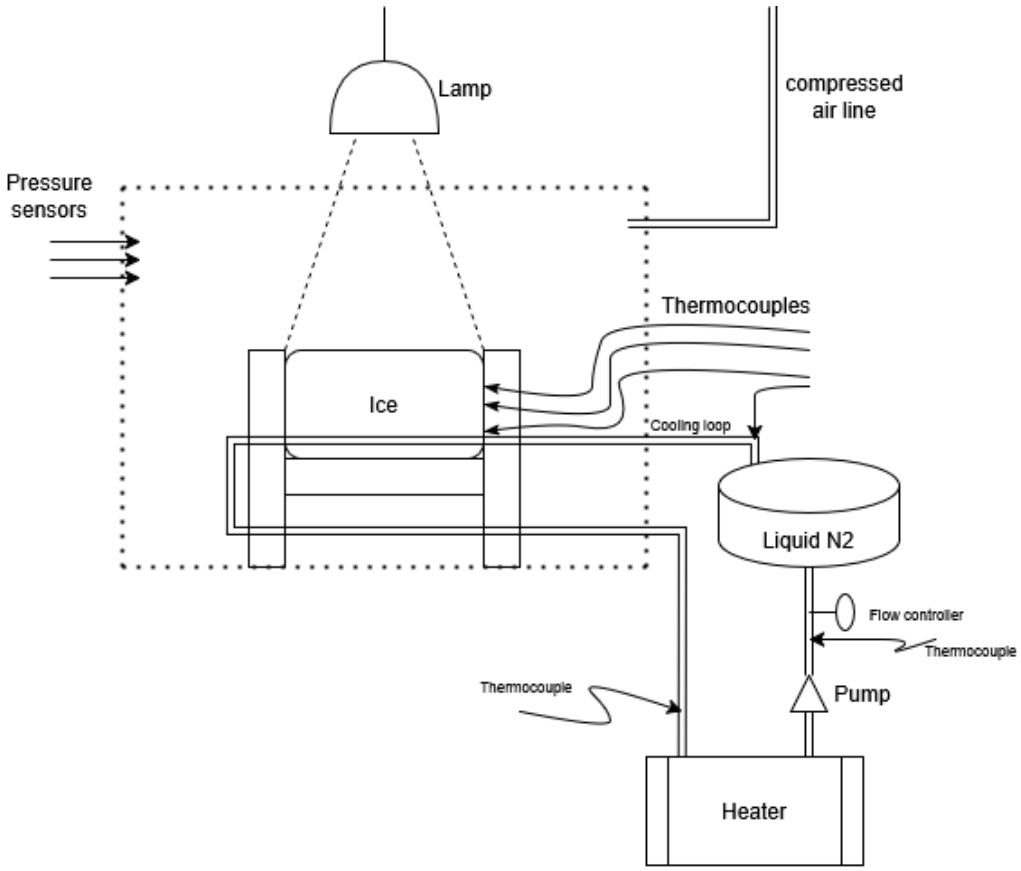


Figure 3.13 Schematic diagram of the test set up when the ice temperature will be regulated using a cooling loop and liquid nitrogen

A preliminary design of this cooling loop has been made. This design is based on the principles of heat transfer via conduction and convention. To ensure sufficient heat transfer between the various elements in the cooling loop copper piping is necessary as it has a very high thermal conductivity. This high thermal conductivity ensures realistic heating and cooling times aswell as realistic piping lengths across the system. Another benefit of copper piping is that it is flexible, which makes it easy to integrate into the system. It should however be noted that galvanic corrosion may occur where the copper pipes are in contact with the ice mould. In order to prevent this a protective coating is desired to be used at these locations.

To estimate the piping length necessary to cool the liquid ethanol, to cool the ice/snow sample and than to heat the ethanol again, the heat transfer at these various sections must be calculated. These calculations will be presented below aswell as the final preliminary design of the cooling loop.

Ethanol Cooling

A heat transfer model has been made in order to determine the length of the pipes necessary in the liquid nitrogen to reach a certain temperature of the cooling liquid (the ethanol). For this it is assumed that the outerwalls of the copper pipes are always at the temperature of the liquid nitrogen. This assumption was made as the liquid nitrogen would remain at a stable temperature, namely its phase change temperature, throughout the cooling. The heat transfer model is shown in Figure 3.14. In this model it is shown that there is heat transfer from the temperature of the ethanol inside the copper pipes to the outerwall of the copper pipes, which is in contact with the liquid nitrogen. From the ethanol to the inside wall of

the copper pipe the heat is transferred via convection while the heat from the inside wall to the outer wall of the pipes is being transferred via conduction. In the figure the thermal resistance of convection is denoted as R_{conv} and the thermal resistance of conduction is denoted as R_{cond}. The thermal resistance of conduction is dependent on the length of the path the heat takes (L), aswell as the thermal conductivity of the material (k) and the surface area (A), $R_{cond} = \frac{L}{kA}$. The thermal resistance of convection is dependent on the surface area (A), aswell as the convective heat transfer coefficient (h), $R_{conv} = \frac{1}{hA}$.

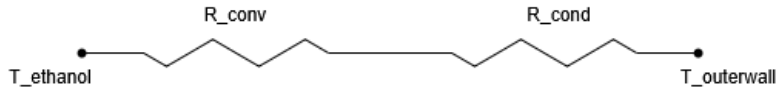


Figure 3.14 Heat transfer model of cooling the ethanol in the cooling loop using liquid nitrogen

The convective heat transfer coefficient of the medium, in this case the ethanol, is dependent on the flow properties inside the tubing. These properties can be expressed as the Reynolds number, Prandtl number and Nusselt number. By determining these three numbers an estimate of the convective heat transfer coefficient can be made. First the Reynolds number can be determined using Equation 3.1, where D is the inner diameter of the pipe, V is the fluid velocity inside the pipe and μ is the dynamic viscosity of the fluid. Second the Prandtl number can be determined using Equation 3.2, where C_p is the specific heat of the fluid and k is the thermal conductivity of the fluid. Thirdly the Nusselt number can be determined using Equation 3.3, where the value of n is dependent on whether the fluid is being heated or cooled. When heated this number is equal to 0.4 and when cooled it is equal to 0.3. As the ethanol is being cooled in this case n is taken to be equal to 0.3. Now that these numbers have been determined the convective heat transfer coefficient can be calculated using Equation 3.4. [49]

$$Re = \frac{DV\rho}{\mu} \tag{3.1}$$

$$Pr = \frac{\mu C_p}{k} \tag{3.2}$$

$$Nu = 0.023 Re^{0.8} Pr^n, Re \geq 10,000 \tag{3.3}$$

$$h = \frac{Nuk}{D} \tag{3.4}$$

Now that the convective heat transfer coefficient is known the overall heat transfer can be established using Equation 3.5, where $\dot{Q}$ is the heat transfer rate , U is the overall heat transfer coefficient , A is the surface area and ΔT is the temperature difference. In this equation $U = \frac{1}{\sum R}$, where $\sum R$ is the sum of all the thermal resistances in the model. In this heat transfer problem all of the heat transfer is in series thus the total thermal resistance is $\sum R = R_{conv} + R_{cond}$. Using these equations and keeping in mind that conduction and convection happens in a cylindrical pipe, the heat transfer can be rewritten as presented in Equation 3.6, where r_o is the outer radius of the pipe and r_i is the inner radius of the pipe. Using that the surface area on the inside of the pipe is equal to $A = 2\pi r_i L$, where L is the length of the pipe, the length of the pipe that is required to cool the ethanol to a certain temperature can be determined using Equation 3.7.

$$\dot{Q} = UA\Delta T \tag{3.5}$$

$$\dot{Q} = \frac{1}{\frac{1}{h} + \frac{ln(\frac{r_o}{r_i})}{2\pi k}} A\Delta T \tag{3.6}$$

$$L = \frac{\dot{Q}}{U2\pi r_i \Delta T} \tag{3.7}$$

Thus the length of the pipe is dependent on the fluid properties aswell as the material properties of the pipe and the temperature difference desired. As it is assumed that the outerwall temperature is equal to the temperature of the liquid ethanol the temperature difference can also be written as $\Delta T = T_{desired} - T_{LN_2}$, where $T_{desired}$ is the desired temperature to which you want the ethanol to cool to and T_{LN_2} is the temperature of liquid nitrogen equal to -196 °C. The heat flow that is required to cool the ethanol to a certain temperature is described by $\dot{Q}$ and can be obtained using Equation 3.8, where $\dot{m}$ is the mass flow of the fluid inside the pipes, C_p is the specific heat capacity of the fluid and ΔT is the difference between the initial and final temperature of the fluid. In this equation $\Delta T = T_{initial} - T_{desired}$, where $T_{initial}$ is the initial temperature at which the fluid enters the cooling system and $T_{desired}$ is the desired temperature to which you want the ethanol to cool to.

$$\dot{Q} = \dot{m} C_p \Delta T \tag{3.8}$$

Ice temperature regulation

The temperature of the ice/snow sample will be regulated with the previously cooled ethanol in the copper pipes. The ethanol in the pipes has been cooled to the desired ice/snow temperature. To get an estimate of the time it takes to cool the ice untill it reaches steady state with the ethanol some calculations have been done. The same thermal resistance model can be used as previously discussed and shown in Figure 3.14 but than swapping $T_{outerwall}$ for T_{ice}. In this problem it is assumed that the ice/snow sample is one unit with one temperature and conduction and temperature differences within this sample are ignored. This assumption has been made as it is a preliminary design of this cooling loop. The difference between this section of the cooling loop and the previous are the temperature differences and the total heat that is required to cool down the medium. In the previous section this medium was the ethanol while it is now the ice/snow sample. The total heat that is required to cool down the ice/snow sample from its initial temperature to the desired temperature is shown in Equation 3.9, where m_{ice} is the mass of the ice block, $C_{p_{ice}}$ is the specific heat capacity of ice, $T_{initial}$ is the initial temperature of the ice and $T_{desired}$ is the desired temperature of the ice/snow, which is also equal to the temperature of the ethanol after it has been cooled by the liquid nitrogen. The amount of heat flow from the ice/snow to the ethanol can be determined using Equation 3.6, where ΔT is estimated by the log mean temperature difference. In this case this log mean temperature difference was taken to be the average of the temperature of the ethanol when it enters the ice/snow sample and when it exits the ice/snow sample. The exit temperature has been assumed to be 3 °C higher than the temperature at which it enters, due to heat it gains from the ice/snow when flowing past it. This assumption should be altered when the actual temperature is known after experiments have been conducted.

$$Q_{ice} = m_{ice} C_{p_{ice}} (T_{initial} - T_{desired}) \tag{3.9}$$

The time it takes to get the ice/snow sample to the desired temperature can now be determined using Equation 3.10. Using these equations and a copper pipe length of 1 m that is in contact with the bottom of the ice block and pipe diameter and thickness of 5 mm and 0.5 mm it was found that is takes approximately 11 minutes to cool a block of ice of mass 9.23 kg from 0 °C to -70 °C.

$$t = \frac{Q_{ice}}{\dot{Q}_{ice}} \tag{3.10}$$

Ethanol heating

To ensure the ethanol will not cool too much and freeze within the pipes it has to be reheated after it has been used to cool the ice/snow and before it enters the liquid nitrogen. The ethanol will be heated up again using a warm water reservoir, in the same principle as it will be cooled down using the liquid nitrogen. Using the same calculations as used for the ethanol cooling the tube length required for the ethanol to reach a certain temperature can be estimated. For these calculations it is assumed that the water will be at 50 °C. Before the loop begins to run it is required to heat the water to this temperature. This will be done using two heating foils, each with a heating power of 100 W. These heating foils have been chosen for this design as they are currently available at the lab in the faculty. The time it takes to heat up the water to 50 °C is dependent on the total water volume and its initial temperature.

Design of ethanol cooling loop

A preliminary design of the ethanol cooling loop has been made based on the equations described above in the ethanol cooling, ice temperature regulation and ethanol heating section. First the diameter and pipe thickness have been chosen. The piping length to cool and warm the ethanol and time necessary to cool the ice block for various pipe diameters, thicknesses and flow velocities can be seen in Table 3.5. The smaller pipe diameter and smaller pipe thickness requires less pipe length for the ethanol to reach a certain temperature. However it takes a longer time to cool the ice/snow sample. Since the time it takes to cool the ice/snow sample only varies by a few minutes between the different pipe diameters and thicknesses a pipe with a small diameter and thickness is preferred as less piping length is required to heat and cool the ethanol inside the pipe. Thus a copper pipe of 4 mm and a thickness of 0.5 mm has been chosen. Besides the diameter and thickness of the pipe, the flow velocity also has a huge impact on the required length. A lower flow velocity is desired to keep the length of the pipe as small as possible. However when a different temperature is desired this flow velocity might be increased to regulate the temperature of the ethanol. The minimum length of copper pipe required for the cooling loop is chosen based on the minimum temperature it is desired to get the ethanol, which is about -70 ° and a flow velocity of 7 m/s inside the tubing. This specific flow velocity was chosen since it is the lowest safe flow velocity for liquid piping according to lecture slides of the thermal rocket propulsion course [50]. When a higher temperature is desired more of the piping can be left out of the nitrogen and heating section or the flow velocity can be increased. The best option is dependent on the desired temperature. For the ice cooling it is now assumed that a piping length of 1 m will be used. Thus a total of about 7 meters is required for the three sections. However a margin must be added to connect the three sections to one another and complete the cooling loop. To ensure the ethanol remains at a stable temperature between the sections pipe insulation might be needed in these areas.

Table 3.5 Influence of pipe diameter, pipe thickness and flow velocity inside the pipe on the cooling loop when cooling the ice/snow to a temperature of -70 °C

Pipe diameter [mm]	Pipe thickness [mm]	Pipe length to cool ethanol to -70 °C [m]	Time to cool ice/snow sample [min]	Pipe length to heat ethanol to 0 °C [m]	Flow velocity [m/s]
4	0.5	1.99	14	3.83	7
4	0.5	3.03	10	5.84	15
4	1	2.59	15	4.98	7
4	1	4.31	12	8.3	15
5	0.5	2.39	11	4.61	7
5	0.5	3.52	8	6.77	15
5	1	3.02	12	5.82	7
5	1	4.87	9	9.37	15
6	0.5	2.81	9	5.40	7
6	0.5	4.01	6	7.72	15
6	1	3.46	10	6.66	7
6	1	5.41	7	10.42	15

While this preliminary design shows good cooling capabilities it was decided not to use this method as a lot of expensive components are needed. Besides the pipes, liquid ethanol, liquid nitrogen and heaters, a pump is necessary to ensure a continuous flow of ethanol and to set a certain flow velocity a flow controller is required. This was out of budget for this project and could thus not be used.

Option D: insulation

The last option to regulate the temperature is similar to the one used in the EPS setup and is to insulate the ice/snow sample during the experiments. This method was eventually used as it is able to keep the ice/snow temperature at sub zero's temperatures for over six hours. For the insulation the EPS box is used and placed inside PISCES. However the top of the EPS box was left uncovered as the PISCES chamber is already a small enclosed space. For additional cooling aluminum pellets were used. These aluminum pellets were stored inside the -25 or -80 °C freezer before the experiments, just like the ice/snow sample.

When the Martian pressures are simulated inside PISCES the EPS box could not be used as insulation, as styrofoam loses its structure at lower pressures and to prevent styrofoam particles entering the vacuum pumps. Thus during these experiments the EPS box was omitted. Instead a plexiglass plate was placed between the GN container and the PISCES floor as insulation when the vacuum pumps were used.

Final selected temperature regulation option

From the four temperature regulation options explored finally one was selected to be used, namely option D: insulation. Option A and C have the best cooling abilities from the four explored options. However option A was quickly omitted since no recirculating chiller that could achieve sub-zero temperatures was available. Option C was the most preferred option to be used after option A was omitted. Moreover option C was the second option that was explored. It was the most preferred as it has to best cooling abilities and a wide range of temperatures could be simulated using this technique. However due to the complexity of

this system and due to the expensive price of some of the components required for this system to operate correctly this option could not be used and other options had to be explored. Option B was the third explored option. With this option various temperatures could theoretically be achieved. However this method is impractical to use as a large amount of salt is required each time to achieve a certain temperature. Thus this option was also omitted. As none of these options were available to be used option D was explored and eventually used to keep the ice/snow cool during the experiments. This method does not have the best cooling abilities, as no active cooling takes place, but this cooling method is simple and could immediately be used for the experiments, as all of the materials needed for this cooling option were already available. Thus option D was selected to be used to regulate the ice/snow temperature.

Pressure regulation

To achieve and maintain Martian pressures inside PISCES the pressure has to be regulated. PISCES has a main pump that is always on when the system is operating and cannot be turned off. This main pump is used to achieve pressure levels close to 7 Pa. In order to maintain a stable pressure inside the chamber two options are possible: additional gas can be pumped into the chamber to offset the pressure decrease in the chamber due to the PISCES main pump or one of the valves connecting the pumps to the chamber can be slightly closed to lower the amount of air being pumped out of the system once the desired pressure has been reached.

The absolute pressure profile of PISCES over time when the main pump is on can be seen in Figure 3.15. The pressure readings of the various pressure sensors do not intersect at higher pressures and some are far above the atmospheric pressure. As the pump is only used to create a vacuum the pressure inside the chamber will never be far above atmospheric pressure. These readings at the higher pressures are false readings since the pressure sensors are specifically made for low pressure readings. As can be seen the readings of the three pressure sensors almost align at lower pressures, where they measure the correct pressure inside the system.

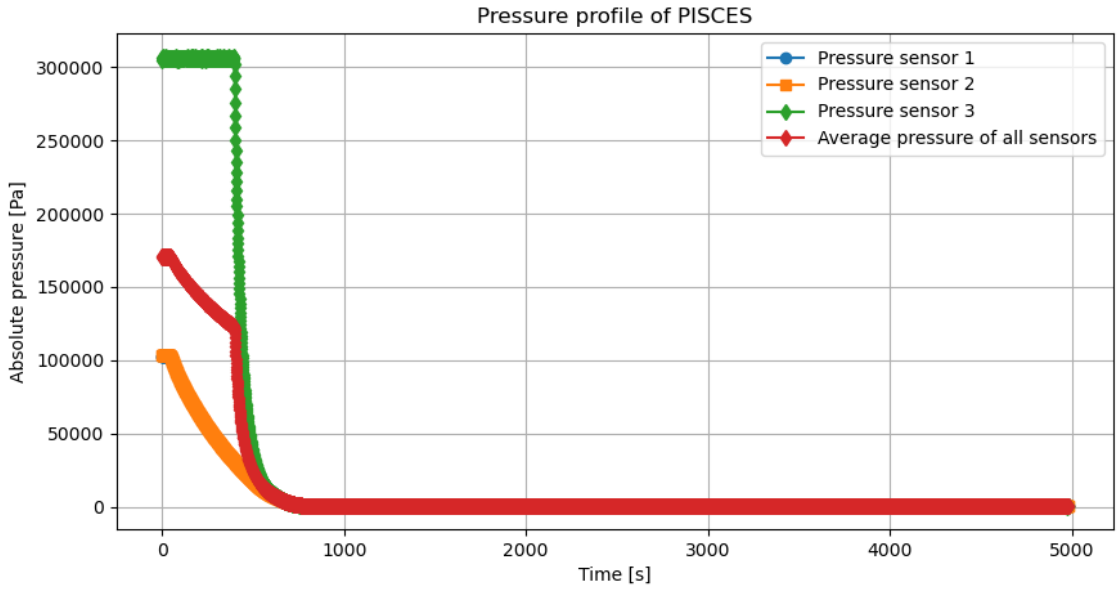


Figure 3.15 The absolute pressure profile inside PISCES measured by its absolute pressure sensors (pressure sensor 1 to 3) and the average absolute pressure obtained using the readings of these three sensors

The desired pressures in which the experiments will be done are all in the range between 200 and 1200 Pa. In order to obtain these pressures PISCES will first only use the main pump until the desired pressure is reached. Once this pressure is reached, which takes about 10 minutes, the pressure can be stabilized using the two options discussed above. These two options and their pro's and con's will be explained further.

Stabilizing pressure with added air

Once this pressure is reached additional dry air can be pumped into PISCES to stabilize and maintain the desired pressure. The amount of dry air that should be pumped into the system to stabilize the pressure was found by obtaining the linear relation of the average pressure data of the three sensors in the desired pressure range. Using this method the pressure rate lost by the system due to the main pump was found.

To maintain a stable pressure an equal amount of pressure should be pumped back into the chamber. The volumetric flow rate required to maintain a stable pressure was determined using Equation 3.11. Where S is the volumetric flow rate in m^3/h, Q is the gas load in $Pa{*}m^3/s$ and P is the pressure inside the system in Pa. The gas load was determined by multiplying the volume of the chamber with the pump rate in Pa/s found by setting up a linear relation of the pressure.

$$S = \frac{Q}{P} \tag{3.11}$$

The exact flow rate in order to maintain a pressure is dependent on the desired pressure inside this range and the pumping speed at that pressure. The pumping speed at certain pressures is calculated by zooming in on the pressure region of the desired pressure and obtaining the linear relation of the pumping speed in this region. An example of this can be seen in Figure 3.16. The linear relation obtained is almost exactly the same as the average pressure in this pressure region. The pumping rate in this pressure region was found to be

about 7.8 Pa/s which results in a required flow rate of about 32 m^3/h.

As can be seen in Figure 3.16 the pressure readings of pressure sensor 3 are far below the pressure readings of 1 and 2, which are quite similar to one another. When leaving out the pressure values of sensor 3 to obtain the average pressure value and the linear relation the pumping rate might vary from the previous obtained pumping rate including the data of sensor 3. Thus some inaccuracies might be present in the obtained pumping rate and flow rate due to slight variations in the pressure readings between the different sensors. To mitigate this, the pressure readings should be monitored when conducting the experiments and the flow rate might need to be adjusted accordingly during the experiments.

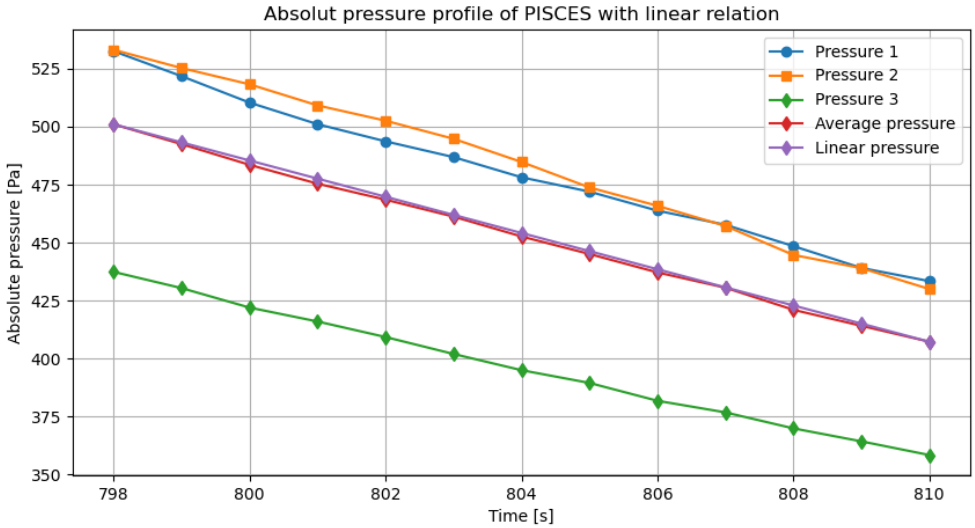


Figure 3.16 Pressure profile of PISCES between about 500 Pa and 400 Pa, the average pressure and linear relation obtained in that pressure range

To obtain the required volumetric flow rate the available 8 bar compressed airline in the aircraft hall of the faculty can be used to feed dry air into the PISCES chamber. However additional instrumentation and valves are required to control the volumetric flow rate entering the chamber. A mass flow controller should allow to control the volumetric flow rate of the dry air. However these controllers were not available and are very expensive. Due to this, this pressure regulation method has not been used even though it would be able to more accurately maintain and regulate the pressure inside PISCES than the method that is used.

Stabilizing pressure with pump valve

Another method to stabilize the pressure inside PISCES is by starting the pumps and once the desired pressure is reached manually adjust the valve in the path from the pump towards the PISCES chamber. This alters the pumping capacity. Eventhough it is hard to get the exact pressure you desire in the chamber and the pressure slightly changes over time, this method was chosen as it could be used immediately without the need to purchase extra components.

Solar simulation

To simulate the Martian solar insolation at the surface of the ice/snow the same lamp will be used as in the EPS setup. This lamp will be placed on top of PISCES and the ice/snow inside PISCES will be illuminated via the window in the top of PISCES. Since we want to be able to take recordings of the ice surface via the side windows the ice surface shall be below

the side windows. Due to this there is a minimum distance imposed between the lamp and the ice surface, which is equal to 540 mm. However based on the calculations preformed in Section 3.4, the lamp should be capable of achieving an insolation of 400 W/m^2 with this minimum distance when using the spotlight function. In reality however the lamp was not capable of achieving this insolation when placed on top of PISCES. However the insolation actually received was approximately 300 W/m^2. Eventhough this is less than was first established in the requirements, this insolation is still sufficient to form penitentes as it is close to the insolation values used by Bergeron in his experiments and higher than the insolation value used by Nyugen in his model simulations. Due to this no additional measures were taken to increase the solar insolation in this setup.

Final setup with PISCES

The final PISCES setup used for one of the experiments can be seen in Figure 3.17. While the exact setup slightly altered overtime with each experiment the main setup remained the same during each experiment. This main setup includes the temperature regulation using cooled aluminium pellets and insulation, the pressure regulation using the pump valve (if the experiment was performed at Martian pressures), the HEDLER lamp hung above the PISCES window and the measurement instrumentations used. These measurement instrumentations include six thermocouples, one relative humidity sensor and three pressure sensors. To make pictures a camera was used, placed outside the chamber in front of one of the side windows. For some experiments the coldfinger inside the chamber was used to prevent excess moisture inside the chamber and lower the relative humidity. While performing experiments at ambient pressure the EPS box was also placed inside the chamber as extra insulation layer, however this could not be used when the vacuum pumps were on as styrofoam does not remain its structure at lower pressures. When the vacuum pumps were used a small plexiglass cover was placed beneath the GN container for insulation between the GN container and PISCES floor.



(a) (b)

Figure 3.17 The outside (a) and inside (b) of the PISCES setup

Some additional add-on's to the setup that were later on used in some experiments were: silica gel grains and packets, cooled aluminium pellets and a small ventilator. The silica gel grains and packets were used to lower the relative humidity inside the chamber. The cooled aluminium pellets were used to keep the temperature cool during the experiments while not adding extra moisture in the air (as the crushed ice did in the EPS setup). These aluminium pellets were cooled in the -25 or -80 °C freezer before experiment conduction. A small ventilator was later on added to some of the experiments to test the effect of a small wind flow over the surface on penitente formation. All of the components used in each individual experiment and more details can be found in Appendix A.

3.6 Penitente growth model equations

The penitente growth model used to calculate the theoretical penitente growth rate and spacing is based on Claudin's penitente dispersion model [18]. This model will be used to verify experimental results obtained with the laboratory experiments. Moreover the model will be used to further investigate the possibility of penitente formation at Martian temperatures and pressures and to further investigate the key factors influencing penitente formation. Additionally this model will be used to investigate the effect of the dust content on the formation duration of penitentes on Mars.

In this section all the equations used in this model to obtain the theoretical growth rate and penitente spacing will be presented. The input conditions used to calculate the theoretical results using this model can be found in Appendix B. The python code of the model used, which contains all these equation and which is used to obtain the model results, can be found in Appendix B aswell. All of the symbols used in this model, together with their units

and descriptions can be found in Table 3.6.

Model equations

The model equations used to calculate the growth of penitentes are based on the principles of sublimation and self-illumination, as was presented in Section 2.4. The growth of these penitentes can be expressed as dimensionless growth rate and growth rate. The dimensionless growth rate only takes into account the sublimation and self-illumination factor, while the growth rate is also based on the amount of solar flux received by the snow/ice surface. The growth rate is thus the final factor which takes into account all of the penitente growth conditions and which determines the rate at which penitentes can form and grow. The dimensionless growth rate is however an important parameter as it determines the peak spacing between the penitentes.

The dimensionless growth rate $\frac{\rho_s L}{\psi_a}\sigma$ and the growth rate σ are calculated using the dispersion relation, Equation 3.12.

$$\frac{\rho_s L}{\psi_a}\sigma = \frac{k\Lambda}{1 + Ptanh(kl) + Rk\Lambda} \times \left[\left(1 - \frac{1}{\sqrt{1 + k^2\Lambda^2}}\right) + \Omega\left(1 - \frac{k\Lambda}{\sqrt{1 + k^2\Lambda^2}}\right) - \left(1 - \frac{1}{cosh(kl)}\right)P\right] \tag{3.12}$$

This dispersion relations uses two dimensionless numbers, P and R, which are calculated using Equation 3.13 and 3.14, respectively. P represents the influence of the mass diffusion and heat conductivity, while R represents the influence of the heat conductivity and kinetics [18]. In order to calculate these two dimensionless numbers, the first derivative of the saturated vapor density must be known. Equation 3.15 is used to calculate this first derivative of the saturated vapor density. The get this first derivative the saturated vapor density must be known. The saturated vapor density can be calculated using the ideal gas law, Equation 3.16, and the saturated vapor pressure which can be calculated using the Goff-Gratch equation, Equation 3.17 [19]. It should be noted that the Goff-Gratch equation is only valid for H_2O and no other ablation materials.

$$P = \frac{\kappa_s}{\rho'_{sat} D_\rho L} \tag{3.13}$$

$$R = \frac{\kappa_s}{\rho'_{sat} \alpha \Lambda L} \tag{3.14}$$

$$\rho'_{sat}(T_0) = \frac{\rho_{sat}(T_0)}{T_0}\left(\frac{M_s L}{R T_0} - 1\right) \tag{3.15}$$

$$\frac{p}{\rho} = \frac{RT}{M_s} \tag{3.16}$$

$$log_{10} P_s = -9.09718(\frac{273.16}{T} - 1) - 3.56654 log_{10}(\frac{273.16}{T}) + 0.876793(1 - \frac{T}{273.16}) \tag{3.17}$$

The mixing length l is calculated using Equation 3.18. The mixing length represents the laminar sublayer thickness in which the vapor content is homogeneous [18] [29]. At ambient pressures an atmospheric density of 1 was used to calculate this mixing length and thus the dimensionless growth rates. The value of 1 was used as this is close to the actual atmospheric density and in order to be consistent with simulations performed by Claudin, which used a value of 1 [18]. At non ambient pressures, the atmospheric density was determined using the ideal gas law.

To calculate the dimensionless growth rate the albedo was not directly taken into account but instead a factor of self-illumination was introduced, which is calculated using Equation 3.19.

$$l = l_v \approx \frac{5\nu}{u_* \rho_{atmos}} \tag{3.18}$$

$$\Omega = \frac{\omega}{\pi} \tag{3.19}$$

Using all the equations presented above the dimensionless growth rate can be calculated and the penitente spacing can be determined. To find the penitente spacing the dimensionless growth rates have been calculated for wavelengths of 0.001 m to 500 m with steps of 0.001 m using a while loop in python. In order to obtain the dimensionless growth rates for all of these wavelengths, the wavelengths were first converted into a wavenumber using Equation 3.20. Once all the dimensionless growth rates for these wavelengths were obtained the maximum dimensionless growth rate was determined using the max function in python. Using this maximum dimensionless growth rate the penitente spacing could be obtained. The penitente spacing is the wavelength belonging to the maximum dimensionless growth rate.

$$k = \frac{2\pi}{\lambda} \tag{3.20}$$

Lastly the growth rate of the penitentes can be determined by multiplying the maximum dimensionless growth rate by $\frac{\psi_a}{\rho_s L}$. The flux of light absorbed by the ablation material required to obtain the growth rate can be calculated using Equation 3.21.

$$\psi_a = \frac{(1-\omega) J_0^{\psi}}{\Lambda} \tag{3.21}$$

Table 3.6 Description of terms used in Claudin's model [18]

Parameter	Unit	Description
ρ_s	kg/m^3	ice density
L	J/kg	Latent heat of sublimation
ψ_a	W/m^3	interfacial value of absorbed light volumetric power
ψ	W/m^3	light volumetric power
J_0^{ψ}	W/m^2	light power flux due to direct sun illumination

ω	-	albedo
Λ	m	light penetration distance
σ	1/s	growth rate of penitentes
k	-	wave number
l	m	mixing length
κ_s	W/m/K	ice thermal conductivity
D_ρ	m^2/s	diffusion coefficient of vapor in the air
ρ_{sat}	kg/m^3	saturated vapor density
ρ'_{sat}	$kg/m^3/K$	first derivative of the saturated vapor density
M_s	kg/mol	molecular weight of water
R	J/kg/mol	perfect gas constant
P_s	Pa	saturated vapor pressure
T	K	temperature
α	m/s	a velocity scale, in this model they estimate its value between 1 and 100 m/s
Ω	-	a factor of self illumination
ν	m^2/s	air kinematic viscosity
u_*	m/s	wind shear velocity
δ	m	surface roughness
ρ_{atmos}	kg/m^3	atmospheric density
λ	m	wavelength

4 Experiment Descriptions and Results

This chapter aims at presenting the experiments that have been performed to research the factors influencing penitente formation and penitente formation in Mars like conditions, aswell as all the experiment results. Experiments performed to research the effect of the kind of ablation material (snow vs ice) on penitente formation are presented in Section 4.1. The effects of temperature on penitente formation as obtained with the experiments are presented in Section 4.2. Section 4.3 presents the experiments investigating the effect of added airflow to the snow surface on penitente formation. The effects of pressure on penitente formation and the experiments performed to investigate this effect are discussed in Section 4.4. These pressure experiments also represent Mars like conditions and give insight on penitente formation on Mars. Lastly Section 4.5 discusses the results obtained from the performed experiments.

A table of all the experiments performed with their key conditions that were varied to study the influence of these factors can be viewed in Table 4.1. The experiment names used are based on the factors which were researched. M stands for ablation Material, T for Temperature, A for Airflow and P for Pressure. A complete overview of all the conditions of each experiment can be viewed in Tables A.1, A.2, A.3, A.4, A.5 and A.6 in Appendix A. All of the measurements taken during all of the experiments and pictures of the start and end of the snow and ice surfaces of all the experiments can be found in Appendix A aswell.

Table 4.1 All the experiments performed and their key conditions that were varied

Experiment name	Ablation material	Freezer temperature [°C]	Pressure [Pa]	Airflow
M1.CloudyIce	cloudy ice	-20	ambient	none
M2.ClearIce	clear ice	-20	ambient	none
M3.Snow	snow	-20	ambient	none
T1.min25	snow	-25	ambient	none
T2.min25	snow	-25	ambient	none
T3.min80	snow	-80	ambient	none
T4.min80Coldfinger	snow	-80 with coldfinger	ambient	none
A1.BlownAir	snow	-80	ambient	blown airflow
A2.SuckedAir	snow	-80	ambient	sucked airflow
A3.BlownAir	snow	-80	ambient	blown airflow
P1.variable	snow	-20	300 to 800	none
P2.200	snow	-80	200	none
P3.ambient	snow	-80	ambient	none
P4.400	snow	-80	400	none
P5.600	snow	-80	600	none
P6.800	snow	-80	800	none
P7.200	snow	-80	200	none

4.1 Ablation material experiments

The first three experiments were conducted to research the effect of the kind of ablation material on penitente formation and to see if penitentes would form using the EPS setup. In each experiment a slightly different ablation material was used. The three different kinds of ablation materials used in these experiments were: cloudy ice made with ice making method 1, clear ice made with ice making method 2 and granular snow made with snow making method 1. The albedo varied between the cloudy ice and clear ice but the density and grain size remained similar. The snow varied compared to the ices due to a different albedo, grain size and density. Experiment M1.CloudyIce used pure ice made with ice making method 1, experiment M2.ClearIce used pure ice made with ice making method 2 and experiment M3.Snow used snow made with snow making method 1 (without sieving), as described in Sections 3.2 and 3.3. Details of all the parameters and conditions present during these experiment can be found in Table A.1 in Appendix A.

The temperature rise within the ablation material was similar for the cloudy ice made with method 1 and for the snow. Eventhough these temperatures are similar, melting of surface occurred during the experiment performed with cloudy ice while only sublimation occurred when the ablation material was snow. This difference in the kind of ablation between the cloudy ice and snow is a direct result of their properties. Ice has a higher thermal conductivity and a lower albedo than snow. The occurrence of sublimation without melt in the snow sample is of great importance for penitente formation and this shows that penitente formation is more likely when snow is the ablation material instead of pure ice.

The begin temperature of the experiment performed with ablation material clear ice made with ice making method 2 already started close to 0 °C and thus does not form a nice comparison to the other two ablation materials. This higher temperature was due to the added insulation layer added to the GN container while in the freezer. Eventhough the sample was in the freezer for 24 hours, about the same amount of time as the other two samples, this sample did not manage to obtain the same temperature as the other two due to the added insulation. Due to this the clear ice in this experiment had a lot of melt. While the temperature was higher in this experiment than the others similar behavior to the cloudy ice made with method 1 was expected. So even at similar temperatures as the other two experiments melt was still expected to occur.

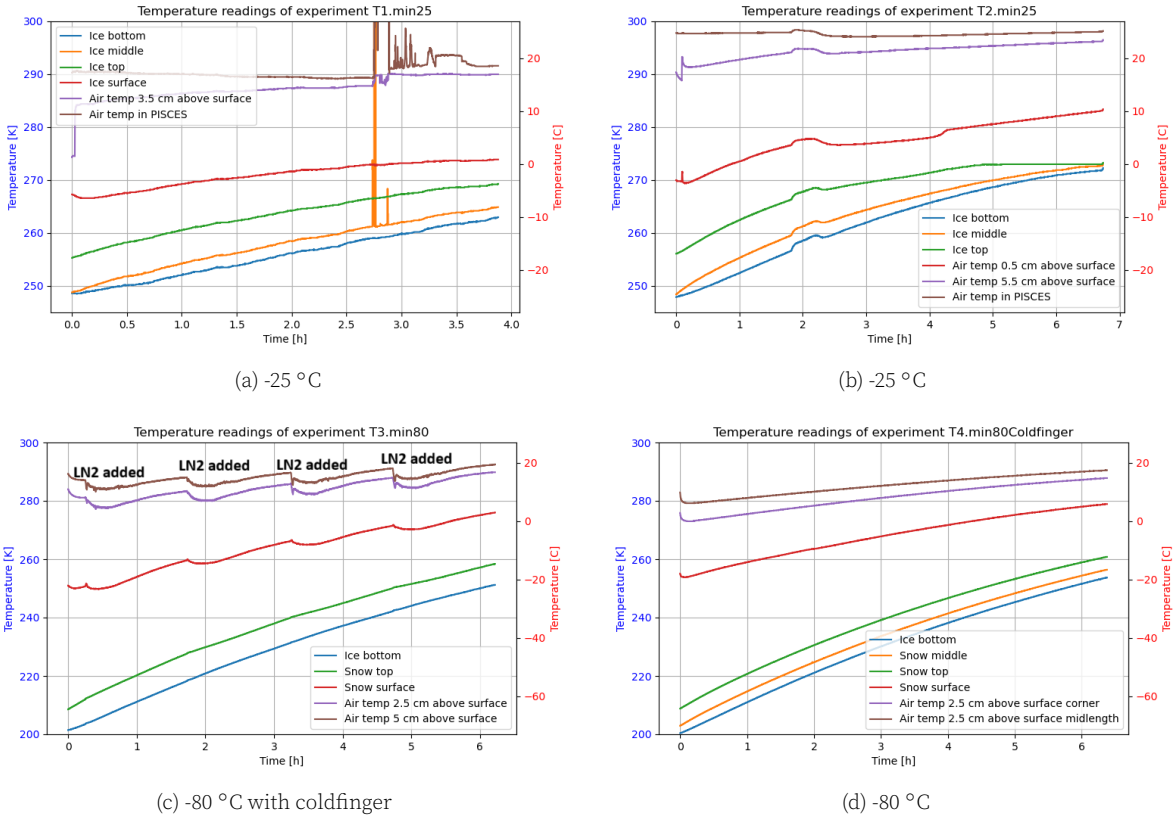
Eventhough no penitentes managed to form in all three experiments the ablation material snow showed the best capability to form penitentes due to the occurrence of sublimation and zero melting. For this reason all the other experiments performed to research other effects on penitente formation will be using snow as ablation material. Penitentes likely did not occur in these experiments due to a too warm temperature.

4.2 Temperature effects experiments

To research the effect of changes in the temperature on penitente formation and to test if penitentes manage to form at lower temperatures in snow three experiments have been performed. The starting temperatures of the snow investigated were -25 °C and -80 °C, additionally one of the -80 °C experiments used the coldfinger to achieve lower temperatures. As the three previous experiments to investigate ablation material effects failed to form penitentes with a start temperature of about -10 °C this temperature was not investigated further in this

temperature research.

For these temperature effect experiments the PISCES setup was used as a lower relative humidity could be achieved with this setup compared to the EPS setup. To ensure consistent low relative humidity, humidity absorbers were also added inside PISCES. The experiments that investigate this temperature effect are: experiment T1.min25, T2.min25, T3.min80 and T4.min80Coldfinger. The temperature progressions during each of these experiments is presented in Figure 4.1, the temperature stated beneath each subfigure is the temperature to which the snow sample was cooled before the experiment conduction. The -25 °C experiment was conducted twice as the first experiment had a malfunction after about 2.5 hours which affected the temperature and relative humidity within the PISCES chamber.



(a) -25 °C

(b) -25 °C

(c) -80 °C with coldfinger

(d) -80 °C

Figure 4.1 Temperature progression of experiments T1.min25, T2.min25, T3.min80 and T4.min80Coldfinger with their snow sample begin temperature

In the experiments starting at -25 °C, sublimation of the surface occurred. In experiment T1.min25 before the malfunctioned occurred this was less prominent than experiment T2.min25 due to the time duration of the experiments. In experiment T2.min25 the snow surface height decreased by 2 cm due to sublimation, indicating that sublimation conditions required for penitentes to form are present. However while these conditions were present penitentes failed to form, most probably since the sublimation rate at these temperatures exceeds the rate at which penitentes can grow.

In the experiments starting at -80 °C, both with and without the coldfinger, the snow surface temperature was in the temperature zone of -20 to -10 °C for more than 2 hours, which is the temperature zone and duration Bergeron managed to form penitentes in. Interestingly penitentes still failed to form. It is unknown why penitentes failed to form in these experiments,

as similar solar insolation and relative humidity conditions to Bergeron's experiments were present aswell as the 2 hours time period of the temperature conditions and similar snow properties. It is thus clear that still a factor is missing that prevents penitente formation.

In these experiments the main effect of the temperature differences was on the sublimation rate of the snow surface. While in the -25 °C experiments sublimation was clearly visible over time this effect was less in the -80 °C experiments. In the -80 °C experiments some sublimation did occur but less than 0.5 cm of the snow surface height sublimated away. The addition of the coldfinger did not have an added effect on this and its cooling capabilities were less pronounced than expected and only had a short influence duration on the temperature.

While penitentes failed to form, the -80 °C start temperature is most likely to form penitentes in future experiments while other factors will be tested. This is due to the fact that the temperature zone of -20 and -10 °C for two hours is reached with this temperature while the -25 °C start temperature failed to achieve this.

4.3 Airflow effects experiments

As penitentes failed to form in the previous experiments the influence of an added airflow over the snow surface has been tested. An airflow was introduced as Bergeron's experiments also had a small airflow present. This effect of an added airflow has been investigated with experiments A1.BlownAir, A2.SuckedAir and A3.BlownAir. In two of the experiments air was directly blown onto the snow surface using a small ventilator, while in the other one an airflow was created by inverting this ventilator so air was being sucked away from the snow surface. All the details of the experiments are presented in Table A.3. Unfortunately in experiment A1.BlownAir the ventilator lost power after 3 hours, however this did give great insight in the effect of a sudden stop in air flow on the snow ablation.

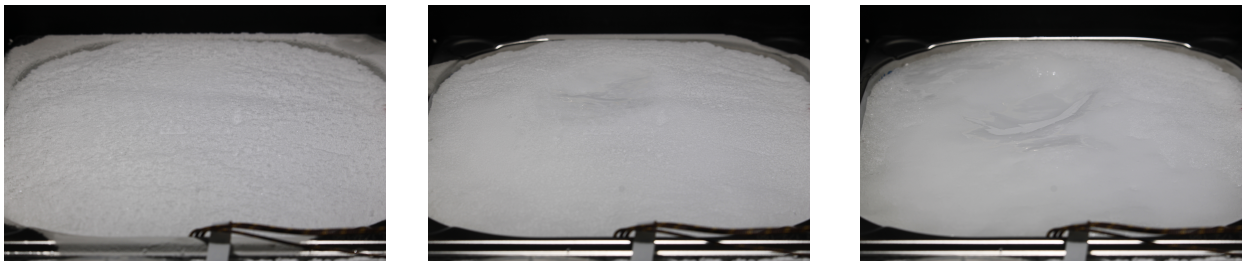
The progression of the snow surface due to an added airflow by blowing wind onto the snow surface can be seen in Figure 4.2. In this figure the influence of the added airflow can clearly be seen. Small structures already in the surface at the start of the experiments dissapeared, while locally some troughs appeared in the snow surface as can be seen in Figure 4.2b. After this photo was taken the small ventilator lost power cutting out the airflow over the surface. The sudden loss of airflow resulted that the created troughs and other features due to the added airflow in the snow slowly disappeared again over time, this can be seen in Figure 4.2c.



(a) Start experiment (b) Middle experiment (c) End experiment

Figure 4.2 Snow surface progression of experiment A1.BlownAir with the addition of blowing wind onto the surface. The pictures were taken at the start of the experiment, at about 3 hours into the experiment just before the ventilator lost power and at the end of the experiment about 1.5 hours after the ventilator lost power

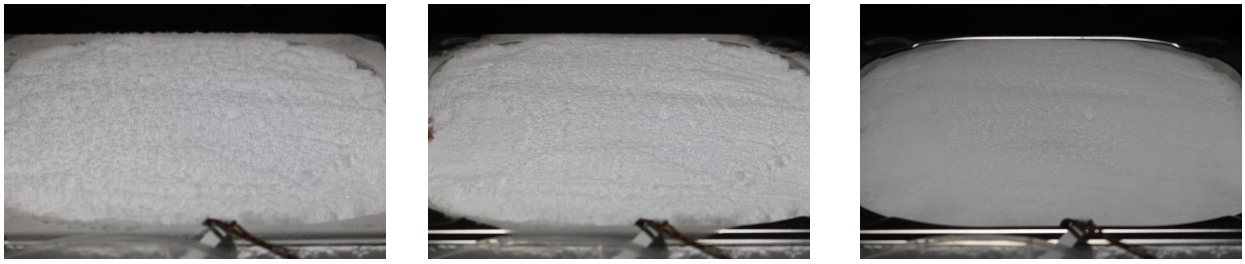
As some surface features started to appear in the snow surface due to the added airflow a second experiment was performed which added an airflow by blowing wind onto the snow surface. However it was now made sure that no power was lost during the experiment. During the first two hours of this experiment similar snow surface progression was present as the last one, the initial structures disappeared and troughs started to form in the surface. However these troughs did not result in penitentes but acted as a local hub were melting was present. At the end of the experiment a large pool of water had collected in these troughs. The progression of the snow surface throughout this experiment can be seen in Figure 4.3. This strong melting in the troughs occurred due to a too large airflow onto the snow surface and/or due to warmer air from PISCES being blown onto the surface instead of cold air.



(a) Start experiment (b) Middle experiment (c) End experiment

Figure 4.3 Snow surface progression of experiment A3.BlownAir. These pictures were taken at the start, middle and end of the experiment

To test the effect of a smaller airflow while no warmer air is blown onto the snow surface an experiment was done that sucked air away from the snow surface. The effect of this is shown in Figure 4.4. This sucking prevents warmer air from inside PISCES, that may cause melt, being directly blown onto the surface. Like the previous two experiments with added ventilator the initial surface features in the snow disappeared over time. However no other features like troughs were created due to this added airflow and thus also no penitentes did appear.

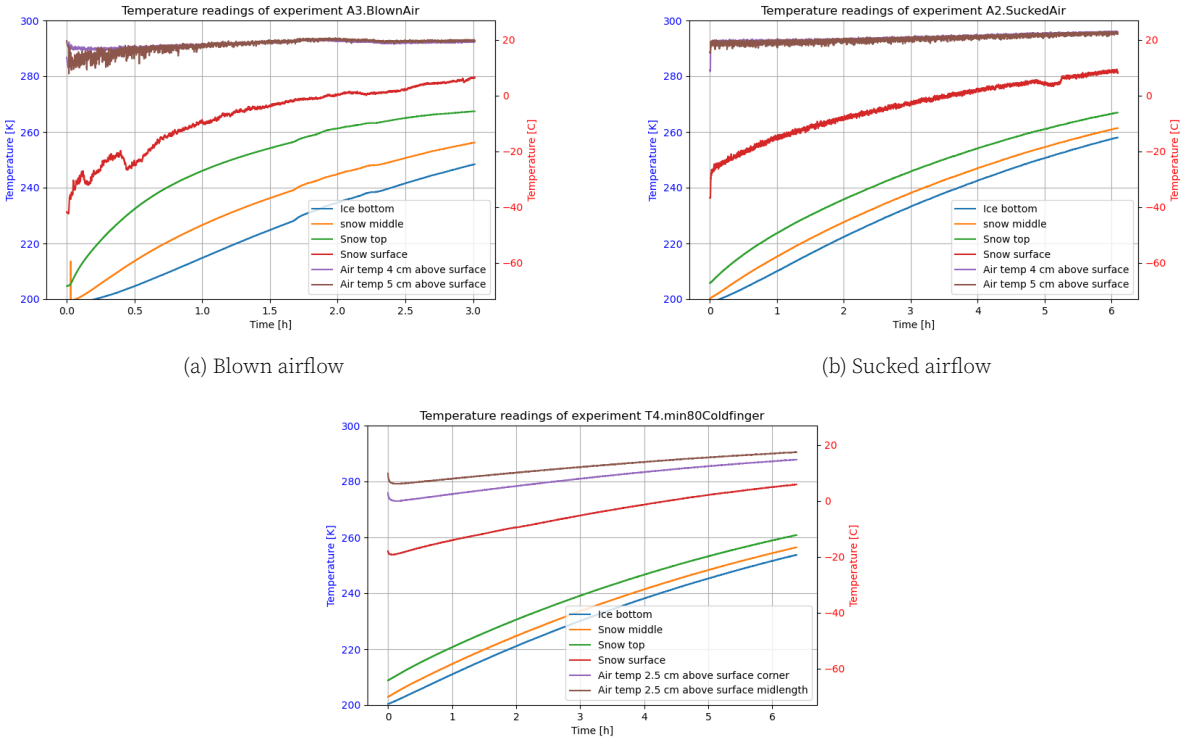


(a) Start experiment (b) Middle experiment (c) End experiment

Figure 4.4 Snow surface at the start, middle and end of experiment A2.SuckedAir

Besides the surface effects, the airflow also had an effect on the temperature of the snow/ice sample. This effect can be seen in Figure 4.5. The temperature in the experiments where air was blown onto the surface has a much steeper increase than the experiment where the air was sucked away from the surface and an experiment where no airflow was present. Due to this steep temperature increase the temperature did not remain between -20 and -10 °C for long enough to form penitentes. This increase in temperature due to the addition of airflow by sucking air from the surface is less pronounced. While this increase in temperature is slightly steeper than the no airflow case small temperature variations in the snow surface and air temperature are clearly present while this is absent when no airflow is present. Even-though the snow surface temperature had a slight steeper temperature incline compared to the no airflow case this temperature did stay between -20 and -10 °C for about 2 hours, how-ever no penitentes formed.

This last factor of a small airflow was added to the test setup as this was still the only factor missing in this setup as compared to Bergeron's setup. However even with this additional factor still no penitentes were formed. It is unknown what the still missing factor is that prevents penitentes to form. As an airflow did not have an effect on the snow surface except increasing the temperature slightly it was chosen to omit this factor in future experiments.



(a) Blown airflow

(b) Sucked airflow

(c) No airflow

Figure 4.5 Temperature readings of experiments A3.BlownAir, A2.SuckedAir and T4.min80Coldfinger (With blown airflow, sucked airflow and no airflow)

It has failed to recreate the penitente experiments by Bergeron while all of the contributing factors were present in these thesis experiments. Penitentes are thus very sensitive to the climatic conditions and very specific conditions are required for them to form. It is however unknown what the missing conditions were during the thesis experiments as all of Bergeron's conditions had been recreated.

4.4 Pressure effects experiments

Lastly the effect of pressure has been tested on penitente formation. As previous experiments had failed to form penitentes from scratch, all of these pressure experiments, except P1.variable, have already preformed penitentes in the snow surface. With these preformed penitentes in part of the snow surface the stability of these penitentes in different pressure regimes could be investigated. The pressure regimes in these experiment represent the Martian atmospheric pressure. The temperature and pressure of each of these experiments compared to the penitente formation zone with respect to the phase change graph of water is presented in Figure 4.6. The penitente formation zone is based on the temperature and pressure regions where Berisford managed to form penitentes. The penitente formation zone was considered to be within 100 Pa of the saturated water vapor curve.

All of the experiments using preformed penitentes started at a temperature of −80°C. At pressures of 200 Pa, 400 Pa, and 600 Pa these preformed penitentes remained stable throughout the whole experiment duration. Stability of these penitentes was expected for temperature and pressure combinations to the left of the saturated vapor curve as this is the region where the state of water is solid and no ablation occurs. However even when the temperatures hit the penitente formation zone no changes in these penitentes occurred. Thus penitentes will

remain stable within the penitente formation zone and to the left of the saturated vapor curve. As Martian pressures and temperatures often lay within this same regions penitentes that have already formed on Mars will remain stable if temperatures and pressures will remain within this region. When temperatures suddenly increase, knocking the temperature and pressure conditions out of this region, it is expected that the sublimation rate will exceed penitente growth rate resulting in the disappearance of already formed penitentes.

In experiment P2.200 the temperature and pressure condition was mostly within the penitente formation zone, but no change in the preformed penitentes or snow surface occurred. The temperature stayed within this zone for about 2 hours, however at lower pressure the growth rate of penitentes is lower than at ambient pressure as will be explained in Chapter 5. Thus 2 hours is not enough for penitentes to form at these lower pressures while it was enough in Bergeron's experiments at ambient pressure.

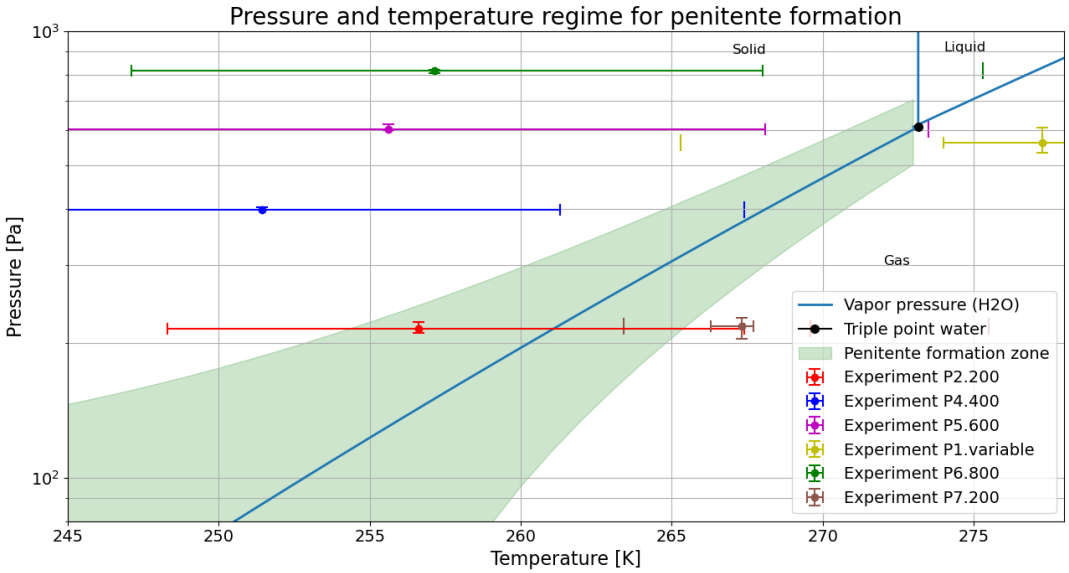
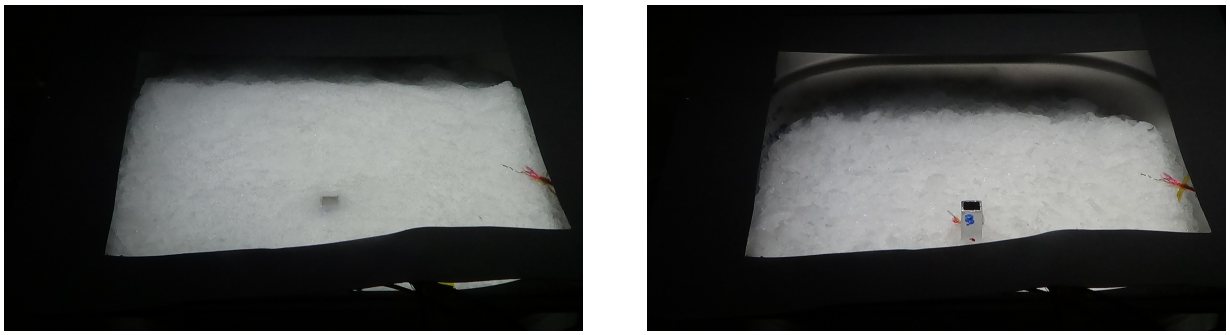


Figure 4.6 Temperature and pressure regime of all experiments performed at Martian like pressures compared to the saturated water vapor curve in the water phase diagram and the likely penitente formation zone, as established using Berisford's results [1]

At the end of experiment P6.800 some light melting occurred at some of the peaks of the preformed penitentes, as can be seen in Figure 4.8b. At the end of this experiment the warmer temperatures caused slight melting at this pressure of 800 Pa as they were within the liquid phase of the water phase change diagram. Thus melting was expected. However the temperature was within this liquid region for about one hour and only slight melting was noticeable.

After about five hours in experiment P6.800 the pressure was lowered from 800 to 200 Pa and was renamed to experiment P7.200. This was done to investigate what would happen with the preformed penitentes if the temperature and pressure is well within the gas region of the water phase change diagram. As can be seen in Figure 4.6 the temperature of experiment P7.200 was only within the penitente formation zone at the very beginning and was within the gas region for the remainder of this experiment. Strong sublimation was expected to occur, as strong sublimation occurred during experiment P1.variable when temperatures reached above the freeze point, as can be seen in Figure 4.7. However no visible sublimation

did occur and the preformed penitentes remained stable throughout this experiment. But the melt that had occurred when the pressure was at 800 Pa fully disappeared, as was expected. Thus penitentes will remain stable at higher temperatures in this short experiment duration than was first expected while in the gas region of the phase change diagram.



(a) Start experiment (b) End experiment

Figure 4.7 Ice surface at start (a) and end (b) of experiment P1.variable

The changes in the surface throughout experiments P6.800 and P7.200 can be seen in Figure 4.8. A change in the penitente shapes is visible between the start and middle of the experiment. Some of the snow did sublime, however this snow which sublimated was the frost that was deposited onto the preformed penitente shapes. No sublimation of the original penitente shapes occurred once the frost was completely sublimated. This occurrence of frost happened in all of these pressure experiments with preformed penitente shapes and most likely occurred due to the vast temperature difference of the snow sample and the air temperature.



(a) Start experiment (800 Pa) (b) middle experiment (800 Pa) (c) End experiment (200 Pa)

Figure 4.8 Snow surface progression of experiment P6.800 into P7.200 , where the picture of surface at the middle experiment was taken just before the pressure was lowered to 200 Pa

4.5 Discussion of experimental results

In this section the obtained results from the experiments will be discussed. In none of the experiments penitentes managed to form. While no penitentes formed in the experiments researching the type of ablation material, snow still showed more favorable properties for penitente formation than ice. This is similar to what was found by Bergeron's experiments. In order to better study the effect of the ablation material in the future it is recommended to perform these experiments at steady and lower temperatures were penitentes are likely to form, as current temperatures were likely too high.

At various lower temperatures at ambient pressures penitentes also failed to form. In Bergeron's experiments penitentes only formed in temperatures between -20 and -10 °C in approximately two hours [12]. The snow surface temperature was not within this range for this time duration in the experiments with start temperature -25 °C and may be the reason why no penitentes did occur in these experiments. However this condition of -20 to -10 ° C for two hours was achieved in the experiments with start temperature -80 °C. As it was not possible to stabilize the temperature within the test setup it is recommended for future laboratory experiments to stabilize the temperature within the test setup so penitente formation at prolonged stable conditions can be studied. It is namely believed that great fluctuations in temperature during the experiments may have halted penitente formation.

As a factor of wind was the only missing variable that separated the experimental conditions starting at temperature -80°C compared to Bergeron's conditions the influence of airflow effects at this temperature was also tested. However even when wind was introduced no penitentes managed to form. As almost the exact conditions as Bergeron's experiment were present during these experiments it is unknown why penitentes failed to form. There is a possibility that an undocumented factor which Bergeron used was still missing preventing formation of penitentes. Another reason why penitentes still failed to form is that some of the conditions very slightly differed from Bergeron's preventing penitente formation. While the exact reason is unknown these results show that penitentes are very sensitive to climatic conditions and that very specific conditions are required for them to form.

While an addition of wind did not influence penitente formation or halted penitente formation in the experiments at ambient pressures, the effect of wind was not tested at Martian pressures. As Mars has some varying near-surface winds throughout a sol and Martian year it is recommended for future research to experiment with and test the effects of these wind velocities on penitente formation and stability at Martian pressures.

It was shown that melt of preformed peaks does occurs when the temperature and pressure are within the liquid region of the phase change diagram. This did not happen when the conditions stayed within the solid region, were preformed penitentes remained stable. Thus penitentes will not remain stable when pushed inside the liquid region of the water phase diagram. It is however recommended to perform additional experiments where the temperature is kept within this region for a longer time to investigate the long lasting effects and the time it takes for penitentes to fully ablate.

In experiment P1.variable strong sublimation occurred as the temperature and pressure conditions were well within the gas region of the water phase diagram. Unfortunally no preformed penitentes were present in this experiment and their stability could not be researched. However it is expected that they do not remain stable as the sublimation rate exceeds the penitente growth rate in this region. Berisford found similar results when conditions were well within this gas region. In his experiments the snow quickly sublimated away in these conditions while no penitentes formed [1]. Thus these condition well within the gas region do not support penitente formation and most likely ablate pre-existed penitentes completely. For future research it is recommended to perform more experiments with preformed penitentes in these gas regions at more extended durations to determine the longitudinality of penitente stability in this region.

At Martian like pressures penitentes did not manage to form on its own during the experi-

ments but all the preformed penitentes were stable. While Berisford managed to form penitentes at temperatures and pressures close to the water vapor curve no clear indication of the time in which these penitentes formed was present in his paper. However in Berisford's experiments experimenting with preformed penitentes, a change in penitente height occurred over the duration of one months [23]. Thus while the temperature and pressure conditions were sufficient for a period of time in some of the experiments performed the experiment durations were too little to see changes in the preformed penitentes or to form penitentes at Martian pressures. However the experiments which use preformed penitentes showed that penitentes remain stable and thus can exist at Mars pressures when the temperature and pressure stay close to the water vapor curve or within the solid region of the phase change diagram.

5 Penitente Growth Model Results and Discussion

While the experiments performed gave an insight in the factors influencing penitente formation and penitente stability at Martian conditions a penitente growth model will be used to more thoroughly study the exact effects of these influence factors and if penitente growth is possible at certain Martian temperatures and pressures. Moreover this model is used to investigate the effect of dust content in snow and ice on penitente formation on Mars, as this factor had not been investigated yet with the performed experiment. This chapter aims at documenting the results obtained using Claudin's penitente model. Using this model in combination with the experiment results all the research questions presented in Chapter 2 can be answered. The dispersion relations and equations used for these simulations were presented in Chapter 3. In Section 5.1 the theoretical penitente growth and spacing that could be obtained in the experimental conditions that were conducted are investigated and are compared to the experimental results obtained to further investigate the exact effects of the influence of the key factors varied during the experiments and to validate some of the experimental results. In Section 5.2 the model is used to simulate penitente formation at certain Mars conditions. Additionally the model is used, combined with results obtained from the experiments, to investigate if penitente formation is possible at certain locations on Mars and the stability of possibly formed penitentes in these locations. A short study of the influence of added dust to snow and ice on penitente formation and a discussion of the influence of these results on penitente formation on Mars has been performed in Section 5.3. Lastly a discussion of the results is presented in Section 5.4.

5.1 Model results for experimental conditions

The dispersion relation has been used to calculate the dimensionless growth rate, growth rate and penitente spacing for each of the experimental conditions that have been performed using the EPS and PISCES setup. Using this dispersion relation the influence of the factors investigated during the experiments on the growth rate and spacing are desired to be investigated and compared to the experiment results. These model results are presented in Table 5.1. As can be seen in these results the dimensionless growth rate, growth rate and penitente spacing differ for each of these experiments due to their different experimental conditions. The inputs to this model, which represent the experimental conditions, can be found in Table B.1 in Appendix B. In this section the causes of these different model results between each experimental conditions will be presented and related to the actual experiment results to find the key factors that influence penitente formation.

Firstly a noticeable difference in the growth rates and penitente spacing can be seen in the experiments which used pure ice as ablation material (experiments M1.CloudyIce and M2.ClearIce) as compared to the rest of the experiments which used snow. While the growth rate in pure ice is lower, about 1/3rd of the growth rate in snow, the penitente spacing is about twice that of snow. This difference in penitente spacing and dimensionless growth rate is due to the higher thermal conductivity of pure ice as compared to snow. While the density of pure ice is also much higher than snow, an increase in only the density did not result in higher theoretical penitente spacing and dimensionless growth rate, however it resulted in

a decrease in the growth rate of penitentes. As the dimensionless growth rate directly impacts the growth rate of penitentes both the thermal conductivity and the density greatly influence the growth rate on penitentes. An increase in either of these immediately results in a lower growth rate. Thus the properties of the ablation material are of great influence on the penitente formation.

Eventhough penitentes did not form during the experiments this effect of the kind of ablation material was also seen in the conducted experiments, as explained in Section 4.1. In these experiments penitentes are less likely to form in pure ice as compared to snow. Moreover Bergeron achieved similar results in his experiments, were penitentes took about twice as long to form in pure ice as compared to snow.

Moreover the effect of the albedo was investigated using the model. In the experiments this effect was not investigated as the same ice/snow samples were used throughout all of the experiments. By increasing the albedo in the model inputs from 0.7 to 0.9 ,while all other inputs remain constant, the penitente spacing is not adjusted. However this increase in albedo interestingly slightly increases the dimensionless growth rate with about 0.006% while decreasing the growth rate with about 66%. As these dimensionless growth rate and growth rate have a direct impact on each other this seems contradictory.

Secondly the temperature during the experiments has a great influence on the dimensionless growth rate, growth rate and penitente spacing calculated by the model. In this model the temperature unit of Kelvin will be used instead of °C, as the temperature input of the penitente model is in Kelvin. The influence of the temperature on penitente growth and spacing can most clearly be seen when comparing the model results of experiments A2.SuckedAir, A3.BlownAir and P3.ambient. The conditions of these three experiments are very similar to one another except for the temperatures which are 262 K, 272 K and 243 K respectively. It should be noted that the factor of wind speed is not considered in the model equations making the conditions of these three experiments similar to one another in the model. A lower temperature results in a smaller dimensionless growth rate, resulting in smaller growth rate. Moreover a lower temperature results in a much larger penitente spacing. This difference in temperature on the growth rate and spacing is also visible at lower pressure when comparing experiment P2.200 and P7.200. The drastic decrease in dimensionless growth rate by a drop of 20 K, when comparing experiment A2.SuckedAir and P3.ambient, could explain the lower limit of the temperature zone where penitentes formed in Bergeron's experiments. However for visible penitentes to form the spacing must not be too small resulting that the temperature should also not be too high.

This effect of temperature was also clearly seen in experiment P1.variable. Once temperatures reached the freezing point the snow surface decreased by 2 cm in about 2 hours due to sublimation. However no penitentes were carved out during this sublimation as the sublimation rate was too great due to the high temperature. It is believed this is the main reason why no penitente solution was found as the penitente growth rate was most probably too small in comparison to the sublimation rate.

Thirdly the pressure greatly affects the penitente dimensionless growth rate, growth rate and penitente spacing. This can clearly be seen when comparing all the experiments performed at ambient pressure as compared to the experiments performed at the Martian pressure regime. The pressure greatly affects the air density which has a great impact on the mixing

length l, as can be noticed when investigating Equation 3.18 in combination with the ideal gas law presented in Chapter 3. Moreover the diffusion coefficient of vapor in the air is dependent on the pressure. The experiments performed at Martian pressure regimes have a lower air density (about 500 times lower) and have a higher diffusion coefficient (about 10 times as high) as these are dependent on the pressure. While this diffusion coefficient was not measured, the value of 0.0004 at Martian pressures was copied from Nguyen as this coefficient is dependent on pressure and this experiment was performed in the Martian pressure regime [19]. A value of 0.00003 was used for ambient pressures, as this is a typical value for ambient conditions [18]. The air density was calculated using the ideal gas law for the Martian pressures used while a value of 1 was used for ambient pressure to be consistent with Claudin's model.

A lower pressure immediately resulted in much smaller growth rates while the penitente spacing greatly increased. For experiment P1.variable the model found no solution due to a too high temperature, by lowering the input temperature by only 6 K in the model for this experiment a solution is found. This shows that at Martian pressures a low temperature is a requirement for penitentes to form and again stresses the importance of the factor of temperature on penitente formation.

Fourthly the insolation at the snow surface has some impacts on the growth rate of the penitentes. It should be noticed that the dimensionless growth rate and penitente spacing are not impacted. This is as the model equations only take the insolation into account when calculating the growth rate, and not the dimensionless growth rate. When increasing the insolation by a certain factor the growth rate is immediately increased by the same factor. This shows that a strong solar insolation indeed speeds up the progress of penitente formation, as it is already widely known in current literature. This effect could not clearly be seen in the performed experiments, firstly as no penitentes were formed and secondly as the insolation between each experiments were quite similar to one another.

Table 5.1 Theoretical dimensionless growth rate, growth rate and penitente spacing of the experimental conditions calculated with Claudin's model [18]

Experimental conditions	Dimensionless growth rate	Growth rate [1/s]	Penitente spacing [mm]
M1.CloudyIce	1.20	6.55E-06	12
M2.ClearIce	1.38	7.54E-06	11
M3.Snow	5.32	2.97E-05	5
T1.min25	6.84	2.45E-05	4
T2.min25	4.98	1.63E-05	5
T3.min80	2.86	1.11E-05	7
T4.min80Coldfinger	3.54	1.35E-05	6
A1.BlownAir	7.28	2.62E-05	4
A2.SuckedAir	3.54	1.18E-05	6
A3.BlownAir	6.84	2.69E-05	4
P1.variable	-	-	- (no penitente solution found)
P2.200	0.009	3.06E-8	1205
P3.ambient	0.76	2.90E-6	15
P4.400	0.01	3.39E-8	904

P5.600	0.02	6.66E-8	426
P6.800	0.03	8.09E-8	366
P7.200	0.01	3.95E-8	911

5.2 Model results for Martian conditions

To investigate the theoretical growth and spacing of penitentes on Mars, Claudin's model has also been used. Firstly some initial inputs were given to the model that represent Martian conditions, aswell as one condition that represents the conditions here on Earth were it is known that penitentes are formed (The Santiago Andes). Input conditions used for Mars penitente modelling by Nguyen where used. With these conditions the model was validated, as the same results were found as Nyugen when using his input conditions. The main difference between the input for the Mars conditions compared to Earth is the air molar mass. For Mars the molar mass of CO_2 has been used, as the Martian atmosphere mainly consists out of CO_2. The input conditions used for these Mars model simulations can be found in Table B.2 in Appendix B.

To get an first insight in possible penitente formation on Mars, at first five input conditions were put into the model. These five inputs have been chosen as Mars has a vast range in temperatures and pressures. The average climatic conditions, as presented in Chapter 2, were used as input to investigate if penitentes could form in these. The conditions at the Phoenix landing site and the Mars North pole were used as these are locations where it is known that water ice is present. The temperature, pressure and snow properties used as input for the Phoenix condition is based on measurements taken by the Phoenix rover at $L_s = 90°$ [10] [8] [3] [2]. The temperature, pressure and insolation used as input for the Mars North Pole is based on the Mars Climate database model at $L_s = 90°$ at t= 12 h [35] [36]. More over the properties of pure ice were used to simulate the ice cap at the Martian North Pole [3] [2] [51]. Additionally Nguyen's conditions were used to validate the model results and an update to Nguyen case had been made to the thermal conductivity in the ice used to better represent the ice conditions on Mars, as was presented in Chapter 2. Moreover an input condition for the Santiago Andes was added for comparison material for Mars vs Earth penitentes.

The model results of these five input conditions are presented in Table 5.2. Noticeable is the large impact due to a change of the thermal conductivity in the results by Nguyen. Especially the penitente spacing increases greatly, thus results originally found by Nguyen are not entirely correct. Moreover the growth rates of the Martian conditions are so small that penitentes require a vast of amount of time to form. In the Santiago Andes penitentes of about 30 cm managed to form within one week. The growth rates on Mars are in the order of 1000 times smaller. Thus penitentes would take several years to form in these regions, as also was concluded by Nguyen in his research [19]. However it should be noted that the temperature and pressure in these chosen regions do not fall within the established penitente formation zone which could result in these very small growth rates and large spacings. Thus locations may be present were these two conditions fall within this zone were penitentes are more likely to form.

Table 5.2 Theoretical dimensionless growth rate, growth rate and penitente spacing of various Martian conditions calculated with Claudin's model [18]

Input conditions	Dimensionless growth rate	Growth rate [1/s]	Penitente spacing [cm]
Nguyen	6.68E-5	1.06E-10	2500
Updated Nguyen	4.55E-5	7.22E-11	3258
Mars average	8.56E-4	4.31E-9	519
Phoenix	1.07E-3	2.00E-9	397
Mars North pole	4.73E-3	1.08E-8	118
Santiago Andes	9.44E-1	1.05E-5	1.5

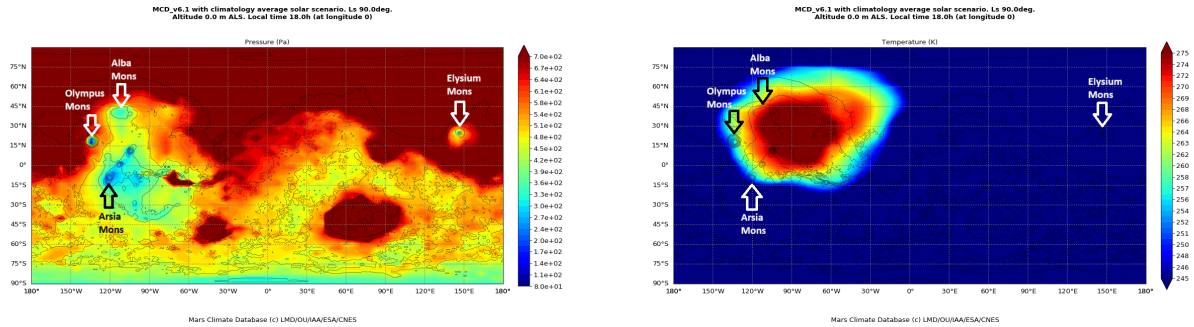
More plausible regions for penitente formation have been found using the key factors influencing penitente formation and the established penitente formation zone based on the saturated water vapor curve as presented by Berisford. These specific regions where penitente formation could occur can be pinpointed using the Mars Climate Database (MCD) [35] [36]. The regions where penitente formation might be possible is highly dependent on the season as the temperature and pressure throughout a Martian year have a high seasonal dependence. Due to this the MCD was used to simulate the Martian temperature, pressure and insolation at its spring equinox ($L_s = 0°$), summer solstice ($L_s = 90°$), autumn equinox ($L_s = 180°$), and the winter solstice ($L_s = 270°$) [35] [36]. To take into account the diurnal variations in these three factors MCD simulations were done for times 0h, 6h, 12h and 18h for each of the four mentioned solar longitudes. All of the temperature, pressure and solar insolation plots obtained at these solar longitudes and diurnal times using the MCD can be seen in Appendix B.

An example of these MCD simulations can be seen in Figure 5.1. It should be noted that the pressure in these simulations was only plotted in between the range of 80 to 700 Pa. Any pressures that are at exactly 80 or 700 Pa and thus outside of the range in these plotted graphs may in reality be lower or higher. It was specifically chosen to do this as penitente formation outside this range is unlikely at Martian temperatures and to increase the accuracy and visibility of pressure differences within this range in the plot. For these same reasons the temperature was also given a range, namely 245 to 275 K. With these plots obtained from the MCD the pressure and temperatures at the various locations on Mars were compared to the penitente formation zone and locations on Mars within the penitente formation zone could be pinpointed.

Using the MCD simulations and the penitente formation zone depicted in Figure 4.6, four interesting locations were found at which penitente formation would be possible, these are: Olympus Mons, Elysium Mons, Arsia Mons, Alba Mons. At each of these locations penitente formation is possible at certain hours throughout the sol for multiple seasons. These four locations and their pressure and temperature during $L_s = 90°, t = 18h$ can be seen in Figure 5.1. At this time the temperature and pressure at Olympus Mons ($T = 255K$, $P = 190Pa$), Alba Mons ($T = 267K$, $P = 350Pa$) and Arsia Mons ($T = 247.5K$, $P = 140Pa$), as obtained using Figure 5.1, are within the penitente formation zone. The temperature and pressure at Elysium Mons ($T < 245K$, $P = 450Pa$) fall outside the formation zone at this time. Thus at $L_s = 90°, t = 18h$ penitente formation is possible at Olympus Mons, Alba Mons and Arsia Mons.

Using this same method the multiple seasons and times have been found where penitente

formation is possible at these locations. The seasons and times when penitente formation is possible at these pinpointed locations can be seen in Figure 5.2, where their temperatures and pressures are plotted over the penitente formation zone. At Olympus Mons penitente formation is even possible throughout the Martian year, as can be seen this Figure. Penitente formation is possible in these regions as these regions on Mars as they have a higher elevation than the rest of the terrain resulting in a generally lower pressure in these regions. Combined with the low temperatures on Mars the pressure temperature regime in these region fall within the penitente formation zone at certain times of the day. On the rest of Mars, except the South polar region which will be addressed later in this section, the pressure and temperatures fall out of the penitente formation zone throughout the Martian year and thus no penitente formation will be possible outside of the pinpointed regions.

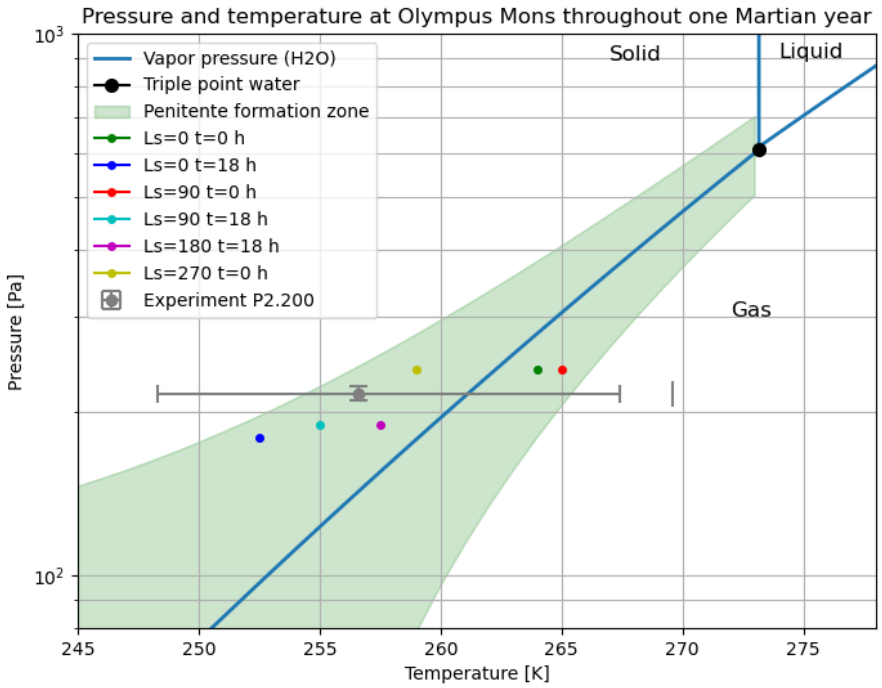


(a) Pressure

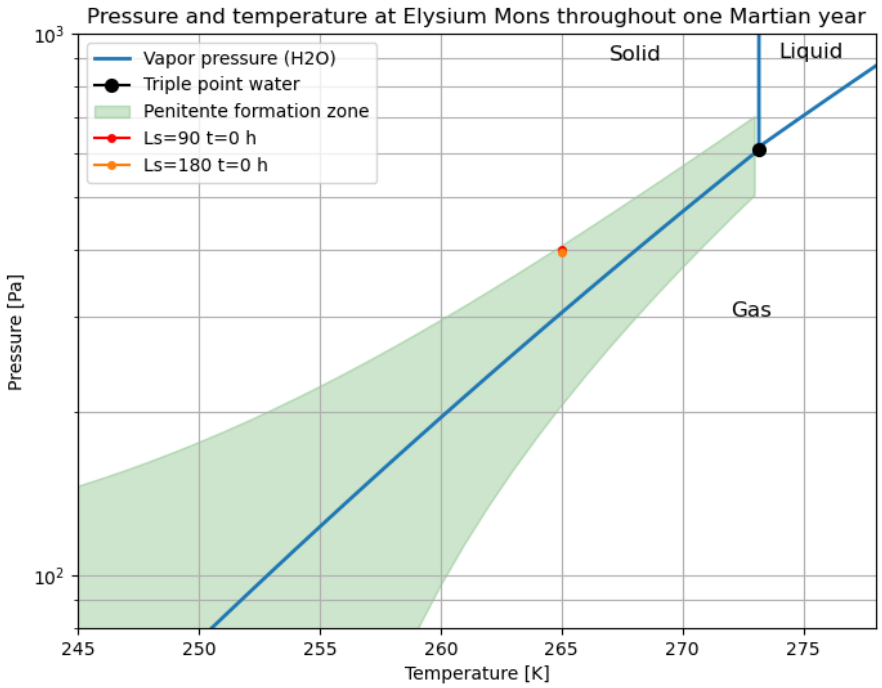
(b) Temperature

Figure 5.1 Pressure (from 80 to 700 Pa) and temperature (from 245 to 275 K) at Mars at $Ls = 90°$ and $t = 18h$. Actual pressure and temperatures outside of the given range could be higher or lower but were left out for analytical reasons

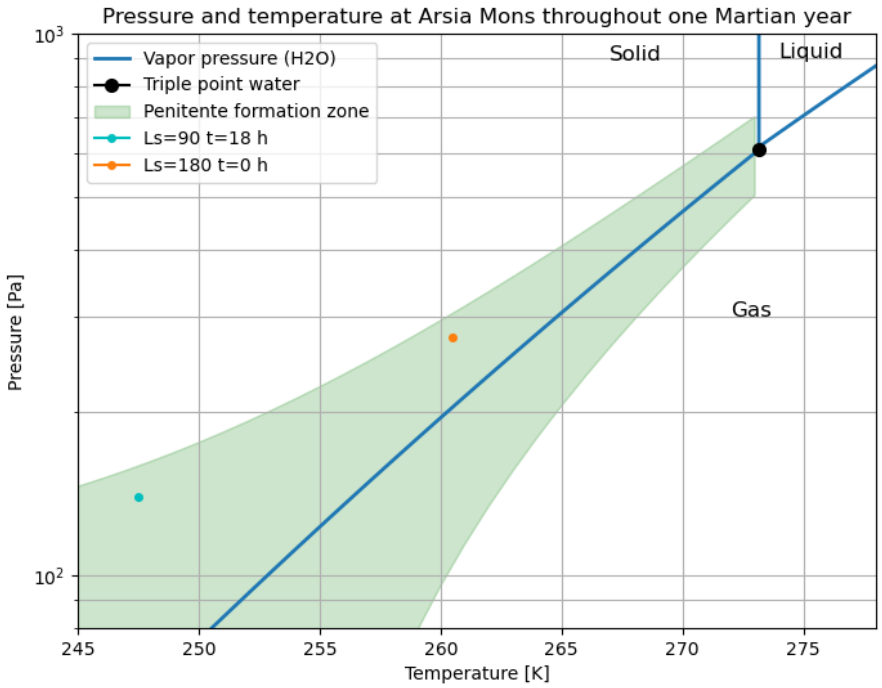
The temperature and pressure conditions of experiment P2.200 are very close to the temperatures and pressures at Olympus Mons, as can be seen in Figure 5.2. This allows for a direct comparison between the two. While penitentes failed to form on its own during experiment P2.200, preformed penitentes remained stable throughout the experiment. Thus if penitentes could form on Olympus Mars, they will remain stable in these temperature and pressure regimes. However these exact temperature and pressure regimes on Olympus Mons only exists for a few hours during a sol. If the temperature were to drastically increase while the pressure remains stable, which happens when the Sun is overhead, the temperature and pressure condition will be pushed outside of the penitente formation zone and well within the gas region of the graph. In this gas region sublimation will quickly take place and preformed penitentes will likely sublime away. On the otherhand if penitentes were to form within the temperature and pressure regimes depicted in the figure and the temperature suddenly drops, as does during local night fall, the already formed penitentes will remain stable as no sublimation will take place to the left of the saturated water vapor curve, as was found with the conducted experiments.



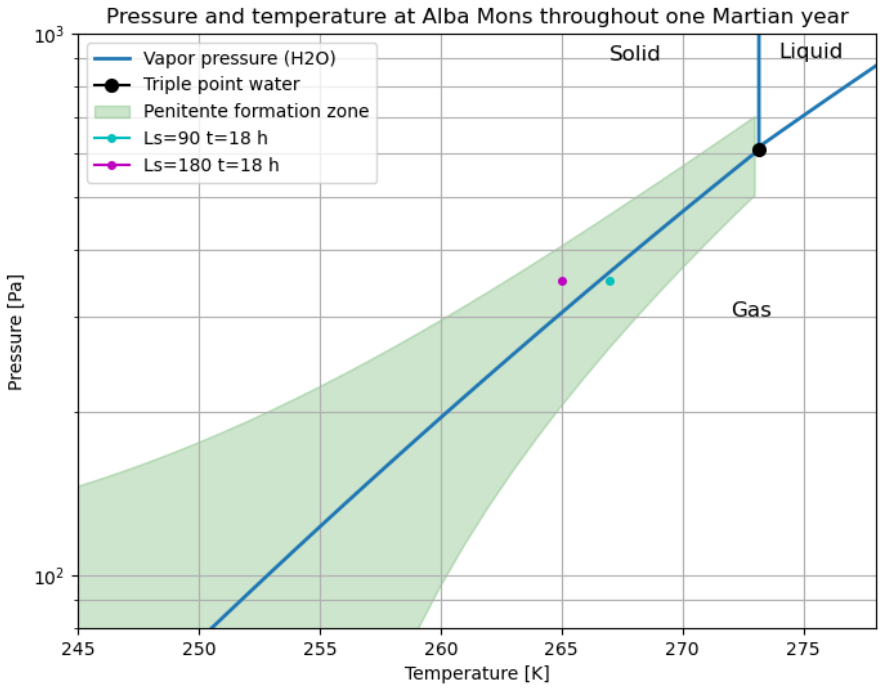
(a) Olympus Mons



(b) Elysium Mons



(c) Arsia Mons



(d) Alba Mons

Figure 5.2 Temperature and pressure conditions on Olympus, Elysium, Arsia and Alba Mons throughout one Martian year compared to the likely penitente formation zone

To investigate if theoretically penitentes could form in these locations at the times where temperatures and pressures fall within in penitente formation zone the conditions were put into the penitente model. These results are presented in Table 5.3. The input conditions used to get these results can be found in Table B.3 in Appendix B. The great effect of the pressures on the growth rate and penitente spacing, as was discussed in the previous sec-

tion, can again clearly been seen in these results. Due to the low pressure on Olympus Mons, the growth rate is very low. On Earth in the region of the Santiago Andes the growth rate of penitentes is about 1.05E-5 with a penitente spacing of 1.5 cm. Within this region penitentes grew about 30 cm in one week [20]. The theoretical growth rate on Earth is thus about 300 times higher than the growth rates in these Martian locations. It is thus very unlikely that penitentes would have enough time to establish in Modern Martian conditions in these locations, as the growth rate is too little and the time in which the temperature and pressure conditions are within the penitente formation zone is too little. A region should be found where the temperature and pressure regime is within the penitente formation zone and the temperature should never increase, or pressure decrease, so much that the regime is pushed outside the penitente formation zone into the gas region of the phase change graph as rapid sublimation will take place and destroy the formed penitentes.

Table 5.3 Theoretical dimensionless growth rate, growth rate and penitente spacing of Martian conditions at potential locations where penitentes could form calculated with Claudin's model [18]

Solar longitude [°]	Local time [h]	Dimensionless growth rate	Growth rate [1/s]	Penitente spacing [cm]
Olympus Mons				
0	0	1.61E-2	5.71E-10	74
0	18	7.02E-3	2.78E-8	157
90	0	1.69E-2	5.97E-8	71
90	18	8.44E-3	3.34E-8	134
180	18	9.56E-3	4.19E-8	120
270	0	1.28E-2	3.99E-8	91
Elysium Mons				
90	0	2.72E-2	1.12E-7	41
180	0	2.68E-2	1.23E-7	42
Arsia Mons				
90	18	4.17E-3	1.52E-8	249
180	0	1.55E-2	4.85E-8	75
Alba Mons				
90	18	2.61E-2	1.09E-7	44
180	18	2.39E-2	1.12E-7	48
South polar region				
270	0	3.43E-2	1.43E-7	31

At $L_s = 270°$ at local noon the temperature and pressure regime in the South polar region is within the penitente formation zone, as presented in Figure 5.3. Penitentes could thus form at these times. Moreover these conditions are the maximum temperature and pressure conditions that occur within this region, resulting that formed penitentes in this region would not sublimate away due to a sudden increase in temperature pushing the temperature and pressure conditions well within the gas zone of the water phase diagram.

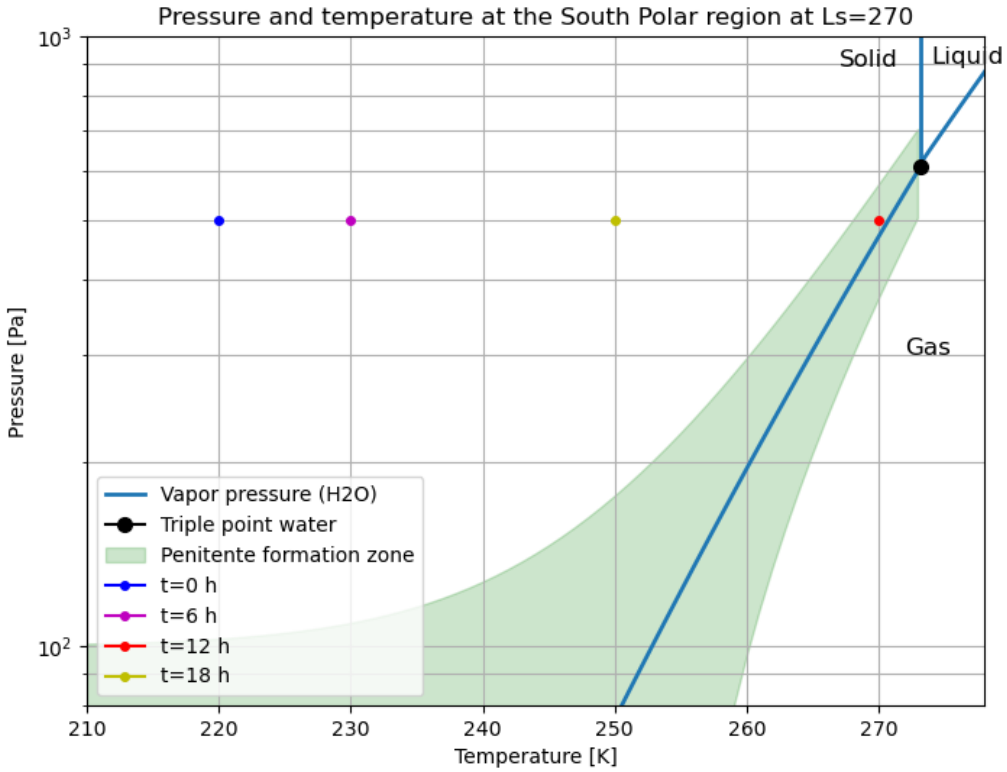


Figure 5.3 Temperature and pressure conditions in the South polar regions during $L_s = 270°$

5.3 Dust influence on theoretical penitente growth and spacing

As ice and snow on Mars is known to contain a small percentage of dust a small investigation has been performed in the influence of this dust on the theoretical penitente growth and spacing. As presented in Chapter 2, dust added to snow or ice influences its albedo. Moreover added dust to snow or ice increases the bulk density of the medium as Martian dust has a higher density ($1300 kg/m^3$) than both snow and ice [3].

The influence on added dust to pure ice has been investigated with Nguyen conditions with ablation material pure ice. The effect of added dust can be seen in Table 5.4. An addition of dust to the ice decreases the dimensionless growth rate and growth rate while increasing the penitente spacing. Thus dust added to pure ice may hinder penitente formation.

On the otherhand an addition of dust to snow decreases the dimensionless growth rate while increasing the growth rate and spacing, as can be seen in Table 5.5. However at lower dust rates this is not the case as the dust rate is too low to alter the albedo and only very slightly alters the density. However at higher dust content the albedo is influenced, as can be seen in Figure 2.3 in Chapter 2. Thus added dust may promote penitente formation in snow.

On Mars typically dusty snow is present with a dust content in the order of 0.01%, as presented in Section 2.6. This dust content is high enough for the dust to have an enhanced effect on the penitente growth, as can be seen in Table 5.5. However the growth rate increases only by about 15% as compared to the clear snow. As the growth rates on Mars are

already really low the added dust will not significantly influence their growth. Still several years are required for penitentes to form in dusty snow on Mars.

Table 5.4 Influence of added dust to pure ice on the theoretical dimensionless growth rate, growth rate and penitente spacing

Input conditions	Dimensionless growth rate	Growth rate [1/s]	Penitente spacing [cm]	Albedo
Updated Nguyen	4.55E-5	7.22E-11	3258	0.5
Updated Nguyen 0.1% dusty ice	2.66E-5	5.90E-11	3884	0.3
Updated Nguyen 0.01% dusty ice	3.13E-5	6.45E-11	3683	0.35
Updated Nguyen 0.001% dusty ice	4.36E-5	7.19E-11	3304	0.48
Updated Nguyen 0.0001% dusty ice	4.55E-5	7.22E-11	3258	0.5

Table 5.5 Influence of added dust to snow on the theoretical dimensionless growth rate, growth rate and penitente spacing

Input conditions	Dimensionless growth rate	Growth rate [1/s]	Penitente spacing [cm]	Albedo
Updated Nguyen snow	3.67E-4	5.35E-10	938	0.8
Updated Nguyen 0.1% dusty snow	2.46E-4	8.04E-10	1066	0.55
Updated Nguyen 0.01% dusty snow	3.42E-4	6.23E-10	958	0.75
Updated Nguyen 0.001% dusty snow	3.67E-4	5.35E-10	938	0.8
Updated Nguyen 0.0001% dusty snow	3.67E-4	5.35E-10	938	0.8

5.4 Discussion of results

The model results show four main key factors that influence penitente growth and spacing: the kind of ablation material, the temperature, the pressure and the insolation. The ablation material effects the growth rate of penitentes greatly, in pure ice the growth rate is much smaller than in snow. This result found is in accordance with results obtained by Bergeron and with results obtained with the experiments. It should however be noted that current literature states that the albedo of the ablation material is the main factor which influences penitente growth and that a higher albedo should lead to a greater growth rate. However the model results oppose this as it was found that an increase in only the albedo actually greatly reduces the growth rate. In reality the albedo is dependent on the grain size and density of the ablation material which was kept constant to obtain these results. A smaller grain size and density of snow/ice results in a greater albedo but also in a lower thermal conductivity. As the growth rate in snow is greater than in ice the density and thermal conductivity have a far greater impact than is currently believed in literature. Thus the kind of ablation material is of great influence on penitente growth and formation but the albedo is not the leading factor in this difference as current literature suggests. The current theory that albedo is the main influence factor should be reconsidered and further investigated, as

density may have a far greater impact than thought. However to ensure this future studies should be performed on this.

The great impact of temperature on the growth rate obtained using the model is in accordance to current literature. The lower the temperature the smaller the growth rate which could explain the lower temperature limit observed by Lliboutry and by Bergeron in his experiments. However a too great temperature could mean that the snow sublimates or melt faster than penitentes could grow as was observed in model results of experiment P1.variable, in the performed experiments and the experiments by Bergeron.

The result that a lower pressure decreases the penitente growth rate is also in accordance with current literature. At ambient pressure Bergeron managed to form penitentes in a matter of hours while at lower pressure Berisford only noticed changes in preformed penitentes over the course of a month. The low penitente growth rates at Martian pressures can also be the reason why no penitentes were formed during the experiments at Martian pressures. In the experiments at Martian pressures no penitentes were able to form while conditions were within the penitente formation zone for some hours at some of these experiments. No penitente formation likely occurred due to small growth rates of penitentes at these lower pressures. Thus the experiment duration was too little to form penitentes at these pressures. It is thus recommended to prolong experiment duration for future research and to ensure stable temperatures and pressures during the experiment duration.

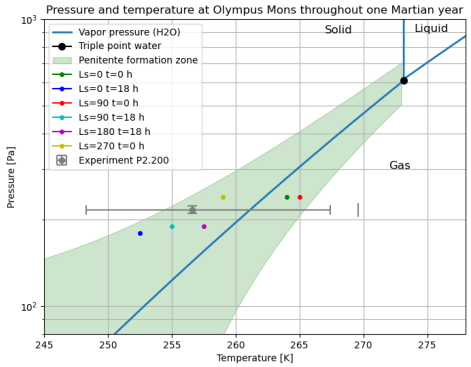
As obtained from the experiment results and model results the possibility of penitente formation on Mars is greatly dependent on the temperature and pressure. Nguyen stated that penitente formation is possible at all locations on Mars within $\pm$ 60° latitude [19]. However the obtained experiment and model results oppose this as penitente formation is only possible close to the water vapor curve as stated by Berisford. Not all regions within this latitude specified by Nguyen have the temperature and pressure conditions required for penitente formation. These conditions are only met at the certain specific locations mentioned (Olympus, Elysium, Alba and Arsia Mons) for only a limited amount of time, as can be seen in Figure 5.4. In these locations the pressure is generally lower as compared to the overall Martian pressure. While penitentes are possible to form in these locations several years are required for them to grow, due to their small growth rate caused by the low pressure on Mars. This is also in accordance with the growth rates on Mars found in Nyugen's research. However the temperature and pressure conditions at Olympus, Elysium, Alba and Arsia Mons only stay within the penitente formation zone for a limited amount of time and are pushed well within the gas phase region of the water phase change diagram at local noon. In this region preformed penitentes likely sublimate completely away as was estimated with the experimental results and was seen in Berisford's experiments. Thus while penitente formation is possible at these four locations the pressure and temperature will not remain stable for enough time for penitentes to actually form.

In the South polar region the temperature and pressure conditions are within the penitente formation zone for limited time, as can be seen in Figure 5.4. At the other time periods the temperature and pressure are within the solid region where preformed penitentes will remain stable as was seen in the experiment results. Thus this region allows for time for penitentes to form, where they could grow during the day during local summer while remaining stable at night and during the other seasons. However CO_2 snow covers the landscape in the South polar region during local winter, it is unknown if the CO_2 cover could interrupt and

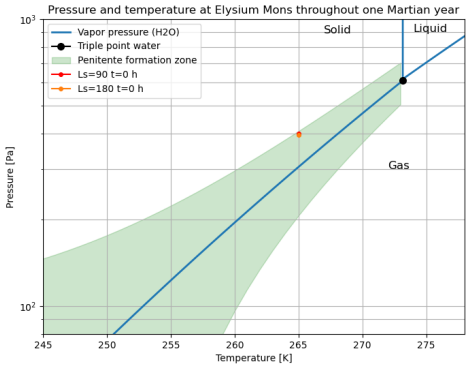
destroy formed micropenitentes which may have formed during the local summer. It is recommended to investigate the effect of CO_2 snow covering preformed penitentes in future research in order to conclude if preformed penitentes could remain stable when covered with CO_2 snow. If preformed penitentes could remain stable in these conditions penitente formation is possible in the South polar region and penitentes are expected to be found in this region on Mars.

As Martian dust typically contains dust in the order of 0.01% it is unlikely that large penitentes can form as melt will not take place at these temperature and pressure conditions. If snow or ice present in this South polar region would however have a dust content of 0.1% or more, melt might occur which could mean larger penitentes would be possible. While in theory dust content does not have a great enough effect on the growth rate of penitentes at Martian pressures it is still recommended to perform future laboratory experiments that take the dust content into account in future experiments of penitentes on Mars as to research if a larger dust content could indeed induce melt and possibly create larger penitentes.

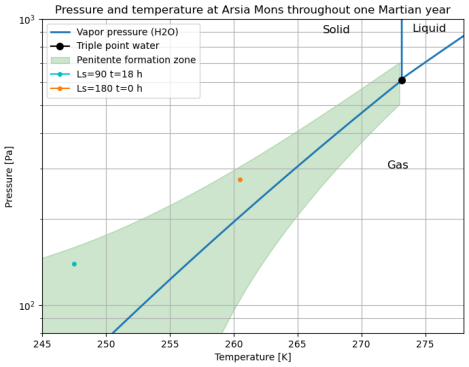
In order to best replicate Martian conditions it is also recommended to simulate the Martian atmospheric composition in future experiments, as this was taken into account in the model results but was left out of the laboratory experiments. Moreover it is recommended to investigate if penitentes could also form in CO_2 snow and ice as this is present in certain regions on Mars during local winter.



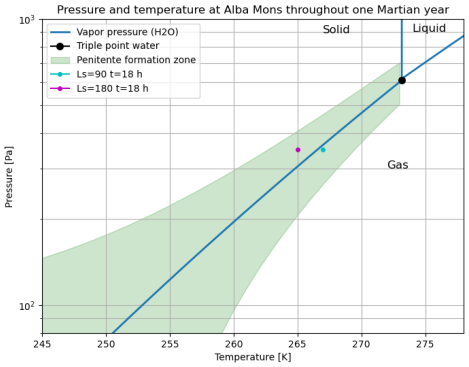
(a) Olympus Mons



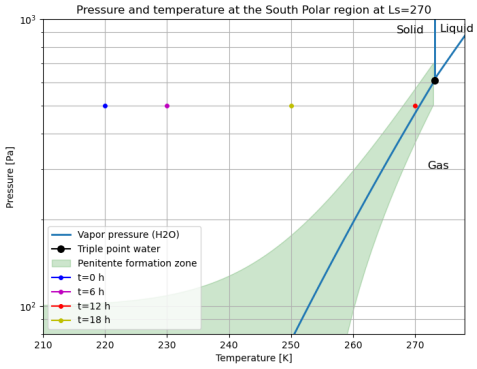
(b) Elysium Mons



(c) Arsia Mons



(d) Alba Mons



(e) South polar region

Figure 5.4 Temperature and pressure conditions on Olympus, Elysium, Arsia, Alba Mons and the South polar region throughout one Martian year compared to the likely penitente formation zone

6 Conclusion

The aim of this report was to study in which temperature and pressure regimes penitentes can form on Mars. In order to answer this research question four sub questions were established:

- **Which factors have a key influence on penitente formation on Mars?**
- **Are penitentes able to form in known temperature and atmospheric pressure conditions on Mars?**
- **At which temperatures can penitentes form on Mars at various Martian pressures?**
- **What is the effect of the dust content on the formation duration of penitentes on Mars?**

These questions have been answered by performing laboratory experiments which were used to study the effect of the kind of ablation material, temperature, airflow and pressure on penitente formation. Moreover the experiments were used to study if penitentes could form under Martian condition and if penitentes will remain stable in these conditions. Additionally a penitente model was used to further study the exact effects of the influence factors studied with the experiments and to study the growth rates and peak spacing of penitentes at temperatures and pressures on Mars in which it is believed penitentes can form. Moreover the model was used to research the effect of dust content added to snow and ice on the growth rate and peak spacing at Martian conditions.

The factors that influence the penitente formation on Mars are the properties of the snow and/or ice, the surface temperature, the pressure of the atmosphere, the presence or absence of an airflow over the surface, the solar insolation at the surface and the percentage of dust content within the snow or ice. Snow is more likely to form penitentes as it has a lower density and thermal conductivity than ice resulting in faster formation of penitentes as compared to ice. A too low temperature limits penitente formation as it decreases the growth rate, on the other side a too high temperature limits penitente formation as well as the snow/ice sublimates or melts faster than penitentes could grow. The exact temperature region where penitentes could form is dependent on the atmospheric pressure. A lower pressure results in a decrease in penitente growth rate and penitentes will thus need a longer time period to form at lower pressures. The presence of an airflow can obstruct penitente formation if warmer air is blown onto the snow/ice surface, however when cold air is blown onto the snow/ice surface a small airflow did not influence penitente formation. Lastly the amount of solar insolation received by the snow/ice surface influences penitente formation. The higher the insolation the higher the penitente growth rate and the quicker penitentes will appear within the snow/ice.

Penitentes are able to form in temperatures and pressures currently present on Mars. However the temperatures and pressures required for penitentes to form are only present at a few very specific locations on Mars. Penitentes can only form in temperature and pressure conditions which are close to the saturated water vapor curve, called the penitente formation zone. These conditions only occur in five locations: Olympus Mons, Elysium Mons, Alba Mons, Arsia Mons and the South polar region. It should be noted that the temperature and pressure condition are only within the penitente formation zone at specific times and seasons in these regions.

At Olympus, Elysium, Alba and Arsia Mons the temperature rises during local noon pushing the temperature and pressure conditions out of the penitente formation zone and well within the gas region of the water phase change diagram. In this region quick sublimation of the snow/ice takes places and preformed penitentes likely disappear completely. On Mars penitentes take several years to form due to the low pressure causing a very low penitente growth rate. Due to this not enough time is available at Olympus, Elysium, Alba and Arsia Mons for penitentes to form before their formation is disrupted due to a temperature increase. Thus while penitentes formation is possible at these locations during some time period not enough time is available for penitentes to actually form.

In the South polar region the temperature and pressure conditions are within the penitente formation zone for a small amount of time. However these conditions occur at maximum temperature at the South polar region. On the South polar region conditions are never within the gas region of the phase change diagram resulting that preformed penitentes will not disappear due to strong sublimation. At the times when penitente formation is not possible temperature and pressure conditions remain within the solid region of the phase change diagram. In this region preformed penitentes remain stable. Due to this enough time is present at the South polar region for penitentes to form, but it will take several years for them to form and they will remain small if the dust content of the snow/ice present is below 0.1%. However in the local winter the South polar region gets covered with CO_2 snow and it is unknown if this CO_2 snow on top of preformed penitentes will make them disappear. It is thus recommended to investigate the effect of CO_2 snow covering preformed penitentes in future research in order to conclude if preformed penitentes could remain stable when covered with CO_2 snow. If these preformed penitentes remain stable under these conditions micro-penitentes are expected to exist at the South polar region on Mars.

While dust added to snow or ice influences the penitente growth rate dependent on the percentage of dust in the snow or ice its effect is so small at Martian conditions that it does not significantly influence the duration of penitente formation. Thus regardless of dust present in snow or ice penitentes only form in snow or ice after several years on Mars.

In conclusion penitente formation in the water snow/ice on Mars is possible when the temperature and pressure are within the penitente formation zone and penitentes stay stable only when the temperature and pressure will not be pushed out of this zone well into the gas region of the water phase change diagram. This only occurs in the South polar region on Mars, but several years are required for penitentes to form in this region if the process is not halted by CO_2 snow covering the region in local winter.

For future studies on this topic some recommendations are proposed. Firstly it is proposed to stabilize the temperature within the test setup so penitente formation at prolonged stable conditions can be studied. It is believed that this is the reason why no penitentes were formed during some of the experiments. Secondly it is recommended to further study the effect of prolonged temperature and pressure conditions in the gas region of the water phase diagram for Martian pressures. In this study only a short experiment was performed in this region and this time was too little to see clear effects and draw substantial conclusions. Thirdly it is recommended to take dust content within the snow into account in future experiments of penitentes on Mars. Fourthly it is recommended to simulate the Martian atmosphere composition while performing experiments. Lastly it is recommended to investigate if penitentes could also form in CO_2 snow and ice as this is also present on Mars.

Bibliography

[1] D. Berisford, J. Foster, J. Kosberg, B. Furst, M. Poston, T. Daimaru, M. Lang, and L. Backman, "Laboratory formation of micro-penitentes at temperatures and pressures relevant to earth and other worlds," *Journal of Glaciology*, pp. 1–9, 2024. [Online]. Available: https://www-cambridge-org.tudelft.idm.oclc.org/core/journals/journal-of-glaciology/article/laboratory-formation-of-micropenitentes-at-temperatures-and-pressures-relevant-to-earth-and-other-worlds/6009A24E88E9FBCC5C8D3F5E2BFE7DB4

[2] A. Khuller, P. Christensen, and S. Warren, "Spectral albedo of dusty martian h2o snow and ice," *Journal of Geophysical Research: Planets*, vol. 126, Aug 2021. [Online]. Available: https://doi.org/10.1029/2021je006910

[3] A. Khuller and P. Christensen, "Evidence of exposed dusty water ice within martian gullies," *Journal of Geophysical Research: Planets*, vol. 126, Jan 2021. [Online]. Available: https://doi-org.tudelft.idm.oclc.org/10.1029/2020JE006539

[4] E. Pierazzo, N. Artemieva, and B. Ivanov, "Starting conditions for hydrothermal systems underneath martian craters: Hydrocode modeling," *Special Paper of the Geological Society of America*, vol. 384, 02 2004. [Online]. Available: https://www.researchgate.net/publication/23852341_Starting_Conditions_for_Hydrothermal_Systems_Underneath_Martian_Craters_Hydrocode_Modeling

[5] A. Witkowski, M. Majkut, and S. Rulik, "Analysis of pipeline transportation systems for carbon dioxide sequestration," *Archives of Thermodynamics*, vol. 35, pp. s. 117–140, 03 2014.

[6] L. Duc, V. Horak, T. Lukac, and Q. Mai, "Study of phase behavior of carbon dioxide as the power gas for gas guns," 07 2015.

[7] J. S. Levine, D. R. Kraemer, and W. R. Kuhn, "Solar radiation incident on mars and the outer planets: Latitudinal, seasonal, and atmospheric effects," *Icarus*, vol. 31, no. 1, pp. 136–145, 1977. [Online]. Available: https://www.sciencedirect.com/science/article/pii/0019103577900768

[8] G. Martínez, C. Newman, A. D. Vicente-Retortillo, E. Fischer, and N. Renno, "The modern near-surface martian climate: A review of in-situ meteorological data from viking to curiosity," *Space Science Reviews*, vol. 212, pp. 295–338, Oct 2017. [Online]. Available: https://doi.org/10.1007/s11214-017-0360-x

[9] B. Pál, Ákos Kereszturi, F. Forget, and M. D. Smith, "Global seasonal variations of the near-surface relative humidity levels on present-day mars," *Icarus*, vol. 333, pp. 481–495, 2019. [Online]. Available: https://www.sciencedirect.com/science/article/pii/S0019103518305529

[10] M. A. Mischna, "Chapter 1 - orbital (climatic) forcing and its imprint on the global landscape," in *Dynamic Mars*, R. J. Soare, S. J. Conway, and S. M. Clifford, Eds. Elsevier, 2018, pp. 3–48. [Online]. Available: https://www.sciencedirect.com/science/article/pii/B9780128130186000017

[11] HEDLER Systemlicht. Hedler profilux led 1000 (focusable, dimmable). [Online]. Available: "https://www.hedlershop.de/en/led-lights/hedler-profilux-led-1000-focusable-dimmable"

[12] V. Bergeron, C. Berger, and M. D. Betterton, "Controlled irradiative formation of penitentes," *Phys. Rev. Lett.*, vol. 96, p. 098502, Mar 2006. [Online]. Available: https://link.aps.org/doi/10.1103/PhysRevLett.96.098502

[13] D. Singh and M. Flanner, "An improved carbon dioxide snow spectral albedo model: Application to martian conditions: Carbon dioxide snow albedo model," *Journal of Geophysical Research: Planets*, vol. 121, 09 2016.

[14] Industrial Water Solutions. Sodium chloride brine tables for 60 f. [Online]. Available: "https://industrialh2osolutions.com/wp-content/uploads/2019/04/Sodium-Chloride-Brine-Table.pdf?x51065"

[15] North American Salt Company and Sifto Canada Corp. (2013) Mgcl2 magnesium chloride technical manual. [Online]. Available: "https://freezgard.com/sites/default/files/mgcl2_technical_manual.pdf"

[16] A. Eccles. (2023) Chemical tanks | calcium chloride 101. [Online]. Available: "https://www.ntotank.com/blog/calcium-chloride-101"

[17] C. Lamas, C. Vega, and E. Noya, "Freezing point depression of salt aqueous solutions using the madrid-2019 model," *The Journal of Chemical Physics*, vol. 156, p. 134503, 04 2022.

[18] P. Claudin, H. Jarry, G. Vignoles, M. Plapp, and B. Andreotti, "Physical processes causing the formation of penitentes," *Phys. Rev. E*, vol. 92, p. 033015, Sep 2015. [Online]. Available: https://link.aps.org/doi/10.1103/PhysRevE.92.033015

[19] T. G. Nguyen, C. L. Smith, A. C. Innanen, and J. E. Moores, "Simulating the formation of martian penitentes," *Planetary and Space Science*, vol. 174, pp. 21–31, 2019. [Online]. Available: https://www.sciencedirect.com/science/article/pii/S0032063318304483

[20] L. Lliboutry, "The origin of penitents," *Journal of Glaciology*, vol. 2, no. 15, p. 331–338, 1954. [Online]. Available: https://www-cambridge-org.tudelft.idm.oclc.org/core/journals/journal-of-glaciology/article/origin-of-penitents/FACAAF8EF9A38B0F14AE85DC6805B8C7

[21] A. Solon, L. Vimercati, J. Darcy, P. Sekul, D. Porazinska, C. Dorador, and M. Farías, "Microbial communities of high-elevation fumaroles, penitentes, and dry tephra "soils" of the puna de atacama volcanic zone," *Microbial Ecology*, vol. 76, 08 2018.

[22] K. Hand, D. Berisford, and T. Daimaru, "Penitente formation is unlikely on europa," *Nature Geoscience*, vol. 13, pp. 17–19, 2020. [Online]. Available: https://doi.org/10.1038/s41561-019-0496-2

[23] D. Berisford, J. Foster, J. Kosberg, B. Furst, M. Poston, T. Daimaru, M. Lang, L. Backman, A. Macias, and K. Hand, "Erosion of penitentes under experimental conditions relevant to ice-covered airless worlds," *Journal of Geophysical Research: Planets*, vol. 126, no. 10, 2021. [Online]. Available: https://www.scopus.com/inward/record.uri?eid=2-s2.0-85117902551&doi=10.1029%2f2021JE006955&partnerID=40&md5=db864e8fe5d0ec5c2a9176ab4928a053

[24] S. G. Warren, "Snow spikes (penitentes) in the dry andes, but not on europa: a defense of lliboutry's classic paper," *Annals of Glaciology*, vol. 63, no. 87–89, p. 62–66, 2022.

[25] D. Berisford, B. Furst, D. Sahu, M. Poston, J. Foster, A. Hofmann, D. Schoelen, T. Daimaru, and K. Hand, "Laboratory simulation of sublimating planetary surface ices: Experiment design and thermal considerations," 07 2018.

[26] J. Molaro, M. Choukroun, C. Phillips, E. Phelps, R. Hodyss, K. Mitchell, J. Lora, and G. Meirion-Griffith, "The microstructural evolution of water ice in the solar system through sintering," 01 2019.

[27] L. Cathles, D. Abbot, and D. MacAyeal, "Intra-surface radiative transfer limits the geographic extent of snow penitents on horizontal snowfields," *Journal of Glaciology*, vol. 60, 11 2013. [Online]. Available: https://www.researchgate.net/publication/262992033_Intra-surface_radiative_transfer_limits_the_geographic_extent_of_snow_penitents_on_horizontal_snowfields

[28] G. C. Amstutz, "On the formation of snow penitentes," *Journal of Glaciology*, vol. 3, no. 24, p. 304–311, 1958. [Online]. Available: https://www-cambridge-org.tudelft.idm.oclc.org/core/journals/journal-of-glaciology/article/on-the-formation-of-snow-penitentes/B295C525E57B57785BE389557272DF9D

[29] J. Moores, C. Smith, A. Toigo, and S. D. Guzewich, "Penitentes as the origin of the bladed terrain of tartarus dorsa on pluto," *Nature*, vol. 541, pp. 188–190, 2017. [Online]. Available: https://doi-org.tudelft.idm.oclc.org/10.1038/nature20779

[30] M. D. Betterton, "Theory of structure formation in snowfields motivated by penitentes, suncups, and dirt cones," *Phys. Rev. E*, vol. 63, p. 056129, Apr 2001. [Online]. Available: https://link.aps.org/doi/10.1103/PhysRevE.63.056129

[31] S. Byrne, "The polar deposits of mars," *Annual Review of Earth and Planetary Sciences*, vol. 37, pp. 535–560, 2009. [Online]. Available: https://www-annualreviews-org.tudelft.idm.oclc.org/content/journals/10.1146/annurev.earth.031208.100101

[32] G. A. Slack, "Thermal conductivity of ice," *Phys. Rev. B*, vol. 22, pp. 3065–3071, Sep 1980. [Online]. Available: https://link.aps.org/doi/10.1103/PhysRevB.22.3065

[33] European Space Agency. (2018) Comparing the atmospheres of mars and earth. [Online]. Available: "https://www.esa.int/ESA_Multimedia/Images/2018/04/Comparing_the_atmospheres_of_Mars_and_Earth"

[34] D. Williams. (2024) Mars fact sheet. [Online]. Available: "https://nssdc.gsfc.nasa.gov/planetary/factsheet/marsfact.html"

[35] F. Forget, F. Hourdin, R. Fournier, C. Hourdin, O. Talagrand, M. Collins, S. Lewis, P. Read, and J. Huot, "Improved general circulation models of the martian atmosphere from the surface to above

80 km," *Journal of Geophysical Research*, vol. 104, pp. 24 155–24 176, Oct 1999. [Online]. Available: https://doi.org/10.1029/1999JE001025

[36] E. Millour, F. Forget, M. Vals, V. Zakharov, L. Montabone, F. Lefèvre, F. Montmessin, J. Chaufray, A. López-Valverde, F. González-Galindo, S. Lewis, P. Read, M. Desjean, and F. Cipriani. (2018) The mars climate database (version 5.3). [Online]. Available: "https://www.cosmos.esa.int/documents/1499429/1583871/Millour_E.pdf"

[37] M. Allison and R. Schmunk. (2023) Mars24 sunclock - time on mars. [Online]. Available: "https://www.giss.nasa.gov/tools/mars24/help/notes.html"

[38] S. Piqueux, D. M. Kass, A. Kleinböhl, M. Slipski, P. O. Hayne, D. J. McCleese, J. T. Schofield, and N. Heavens, "Mars thermal inertia and surface temperatures by the mars climate sounder," *Icarus*, vol. 419, p. 115851, 2024. [Online]. Available: https://www.sciencedirect.com/science/article/pii/S001910352300430X

[39] D. Atri, N. Abdelmoneim, D. B. Dhuri, and M. Simoni, "Diurnal variation of the surface temperature of mars with the emirates mars mission: a comparison with curiosity and perseverance rover measurements," *Monthly Notices of the Royal Astronomical Society: Letters*, vol. 518, no. 1, pp. L1–L6, 10 2022. [Online]. Available: https://doi.org/10.1093/mnrasl/slac094

[40] E. Fischer, G. M. Martínez, N. O. Rennó, L. K. Tamppari, and A. P. Zent, "Relative humidity on mars: New results from the phoenix tecp sensor," *Journal of Geophysical Research: Planets*, vol. 124, no. 11, pp. 2780–2792, 2019. [Online]. Available: https://agupubs.onlinelibrary.wiley.com/doi/abs/10.1029/2019JE006080

[41] A.-M. Harri, M. Genzer, O. Kemppinen, J. Gomez-Elvira, R. Haberle, J. Polkko, H. Savijärvi, N. Rennó, J. A. Rodriguez-Manfredi, W. Schmidt, M. Richardson, T. Siili, M. Paton, M. D. Torre-Juarez, T. Mäkinen, C. Newman, S. Rafkin, M. Mischna, S. Merikallio, H. Haukka, J. Martin-Torres, M. Komu, M.-P. Zorzano, V. Peinado, L. Vazquez, and R. Urqui, "Mars science laboratory relative humidity observations: Initial results," *Journal of Geophysical Research: Planets*, vol. 119, no. 9, pp. 2132–2147, 2014. [Online]. Available: https://agupubs.onlinelibrary.wiley.com/doi/abs/10.1002/2013JE004514

[42] F. Hourdin, P. Le Van, F. Forget, and O. Talagrand, "Meteorological variability and the annual surface pressure cycle on mars," *Journal of the Atmospheric Sciences*, vol. 50, no. 21, p. 3625 – 3640, 1993, cited by: 133; All Open Access, Bronze Open Access. [Online]. Available: https://doi-org.tudelft.idm.oclc.org/10.1175/1520-0469(1993)050<3625:MVATAS>2.0.CO;2

[43] AZONetwork. Grade 304 stainless steel: Properties, fabrication and applications. [Online]. Available: "https://www.azom.com/article.aspx?ArticleID=2867"

[44] Concept Vacuum Limited. Vacuum compatible materials. [Online]. Available: "https://conceptvacuum.com/materials"

[45] P. R. Michael, D. E. Johnston, and W. Moreno, "A conversion guide: solar irradiance and lux illuminance," *Journal of Measurements in Engineering*, vol. 8, no. 4, pp. 153–166, dec 2020. [Online]. Available: https://doi.org/10.21595/jme.2020.21667

[46] PerlaPlast Kunststofshop. Polycarbonaat plaat helder uv-werend dikte 8mm (lexaan). [Online]. Available: "https://perlaplast-kunststofshop.nl/polycarbonaat-lexan-plaat-helder-uv-werend-dikte-8mm"

[47] A. Helmenstine. (2020) Why salt makes ice colder - how cold ice gets. [Online]. Available: "https://sciencenotes.org/why-salt-makes-ice-colder-how-cold-ice-gets/"

[48] B. Loeffler. (2021) Chloride spotlight: What is potassium chloride? [Online]. Available: "https://blog.iceslicer.com/chloride-spotlight-potassium-chloride"

[49] J. Peeters and R. Delfos, "Me45001 advanced heat transfer (2024/2025)," TU Delft lecture slides, accessed on Feb 10, 2025.

[50] B. Zandbergen, "Thermal Rocket Propulsion (version 2.09)," TU Delft, Faculty of Aerospace Engineering, Tech. Rep., 2022.

[51] H. H. Kieffer, "H2o grain size and the amount of dust in mars' residual north polar cap," *Journal of Geophysical Research: Solid Earth*, vol. 95, no. B2, pp. 1481–1493, 1990. [Online]. Available: https://agupubs.onlinelibrary.wiley.com/doi/abs/10.1029/JB095iB02p01481

[52] L. González-Rodrígeuz, A. de Oliveira, L. Rodrígeuz-López, J. Rosas, D. Contreras, and A. Baeza, "A study of uver in santiago, chile based on long-term in situ measurements (five years) and empirical modelling," *Energies*, vol. 14, p. 368, 01 2021.

[53] L. Lliboutry. (1999) Glaciers of the dry andes. [Online]. Available: "https://pubs.usgs.gov/pp/p1386i/chile-arg/dry/#3"

A Experiment details and graphs

In this appendix all the details of all experiments conducted are presented aswell as measurements taken during these experiments. Additionally pictures of the ice or snow surface at the start and end of each experiment are presented.

Experiment sensor measurements

In this section all of the sensor measurements taken during each experiment are presented including a small text explaining some of the measurements.

Experiment M1.CloudyIce measurements

Figure A.1 shows the temperatures in the ice and test setup during experiment M1.CloudyIce. As can be seen in this figure, the thermocouples which measured the ice bottom and the ice middle had incorrect readings. This was due to faulty wiring of the extension cables of these thermocouples. Some sudden troughs can also be seen in the readings of these thermocouples, it is however unknown why they occurred but most probably also due to the faulty wiring. Noticeable in the temperature measurements is that the temperature of the ice was only below -10 °C at the very start of the experiment.

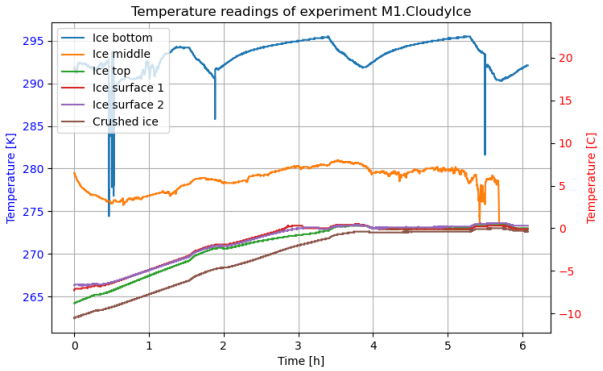


Figure A.1 Temperature readings of experiment M1.CloudyIce

Experiment M2.ClearIce measurements

Figure A.2 shows the temperature in the ice and test setup during experiment M2.ClearIce. The thermocouple wiring that did not work during the previous experiment had been fixed. However a large sudden drop in temperature of the ice surface 2 can be seen after a few minutes in this figure. The thermocouple of ice surface 2 was not properly connected at the start and this sudden drop occurred when the connection got fixed. Noticeable is that the temperature of the ice sample is already close to 0 °C degrees at the start of the experiment. This is probably due to the different ice making method used. To make the ice a foam insulation box was put around the GN container. Ice had been made into this container by freezing water in it for 24 hours in a -20 °C freezer. While this time span was sufficient to make ice for the previous experiment using ice making method 1, it was probably insufficient for ice making method 2 due to the added insulation box. Due to this the ice did not obtain the temperature of the freezer and already had a temperature close to 0 °C at the start

of the experiment.

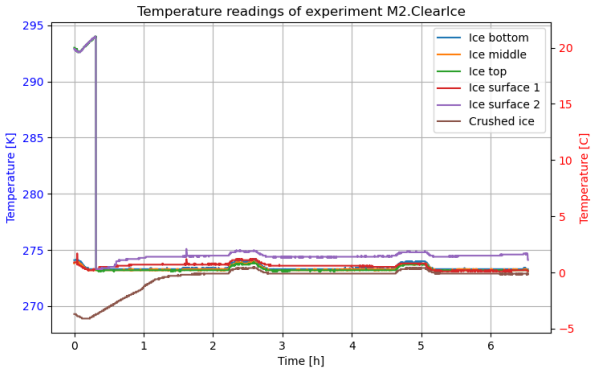


Figure A.2 Temperature readings of experiment M2.ClearIce

Experiment M3.Snow measurements

Figure A.3 shows the temperature in the ice/snow sample and test setup during experiment M3.Snow. Two sudden drops can be seen in the air temperature at annotations A and B. These drops are due to the addition of some liquid nitrogen to the test setup to try and lower the temperature and relative humidity. This temperature decrease did however only last for a few minutes and only affected the air temperature and not the ice/snow sample temperatures. The added liquid nitrogen also failed to decrease the relative humidity, this was most likely since the plexiglass cover had to be lifted to add the liquid nitrogen allowing more humid air from the room to enter the setup.

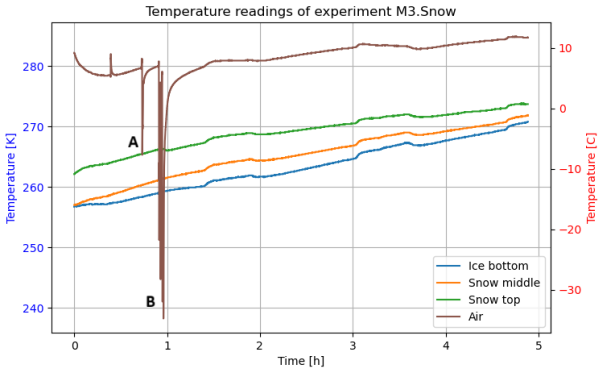
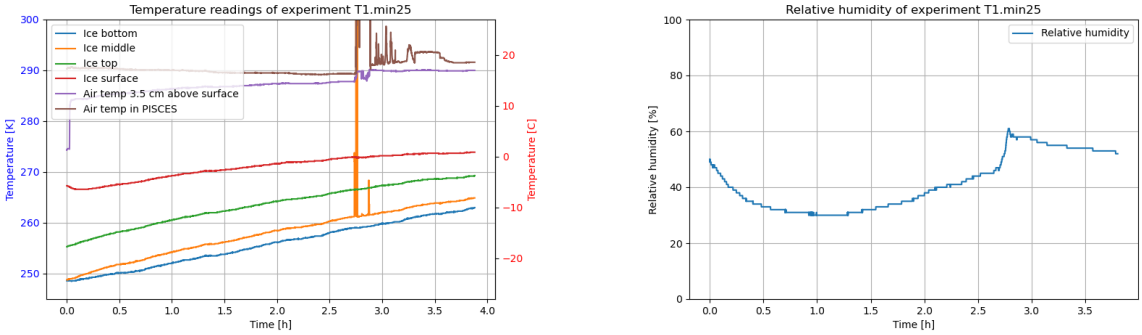


Figure A.3 Temperature readings of experiment M3.Snow

Experiment T1.min25 measurements

Figure A.4 shows the temperature and relative humidity in the test setup during experiment T1.min25. Noticeable in this figure is that the temperature of the ice/snow starts lower than in previous experiments, this is since the ice/snow sample used for this experiment was put in a freezer with lower temperatures compared to the other experiments. The ice/snow sample also remains below 0 °C for a longer time, this is most likely due to addition of the foam insulation box around the GN box. At around 2.7 hours a malfunction occurred which resulted in two thermocouples temporarily reading a value of 3000 Kelvin. Due this malfunction the chamber door had to be opened which resulted in a rise in the air temperature in

PISCES and a rise in the relative humidity.



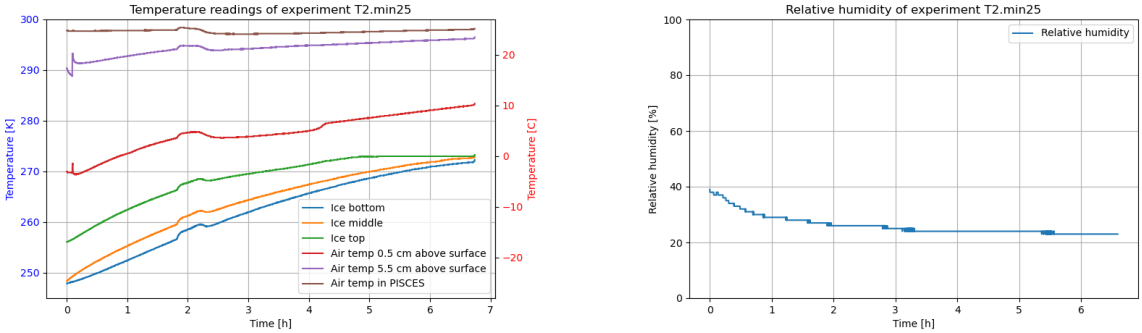
(a) Temperature

(b) Relative humidity

Figure A.4 Temperature and relative humidity readings of experiment T1.min25

Experiment T2.min25 measurements

Figure A.5 shows the temperature and relative humidity in the test setup during experiment T2.min25. A little rise in temperature can be seen around the 2 hour mark, it is however not known why this occurred. For the rest the temperatures during this experiment were quite similar to experiment T1.min25 untill the malfunction. The relative humidity at the start is also quite similar to that of experiment T1.min25, however during this test the relative humidity kept decreasing during the whole experiment. As the surface height lowered about 2 cm during the whole experiment duration and no melt water had accumulated at the end sublimation of the snow had likely occurred.



(a) Temperature

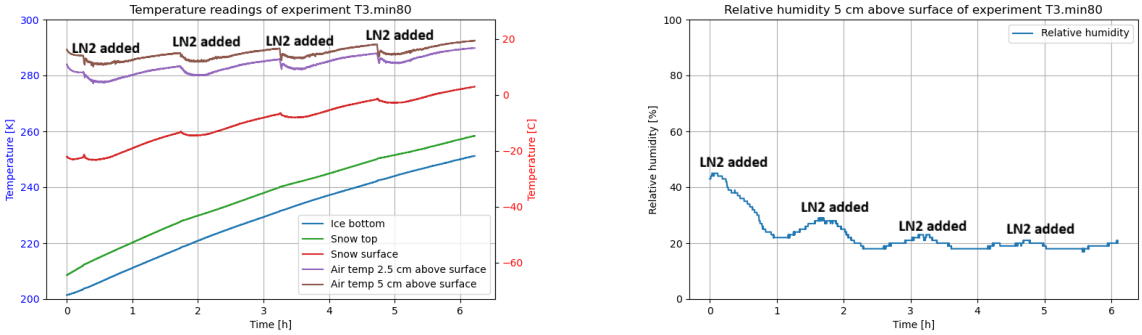
(b) Relative humidity

Figure A.5 Temperature and relative humidity readings of experiment T2.min25

Experiment T3.min25 measurements

Figure A.6 shows the temperature and relative humidity in the test setup during experiment T3.min80. The addition of the liquid nitrogen every 1.5 hours can clearly been seen as a drop in the temperature and the relative humidity. Eventhough the coldfinger decreased the relative humidity in the chamber it did not result in a substantially lower relative humidity compared to the other experiments performed in the PISCES setup. Moreover it can be seen that the measurements of thermocouple 2, which measures the temperature in the very middle of the ice/snow sample, are left out in the graph. This has been done as this thermocouple had not been plugged in correctly and gave incorrect measurements 10 minutes after

the experiment had started.



(a) Temperature

(b) Relative humidity

Figure A.6 Temperature and relative humidity readings of experiment T3.min80

Experiment T4.min80Coldfinger measurements

The temperature during experiment T4.min80Coldfinger can be seen in Figure A.7. The temperature profile within the snow is similar to last experiment, however since no LN2 was added during this experiment no decrease in temperature was present due to LN2. Noticeable is that the temperatures increase somewhat linearly over time when no external factors are added that may increase or decrease the temperature.

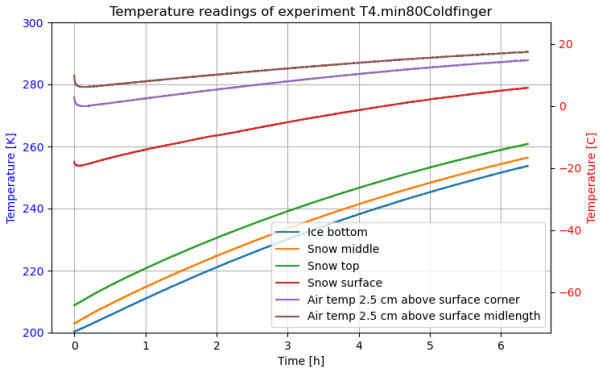
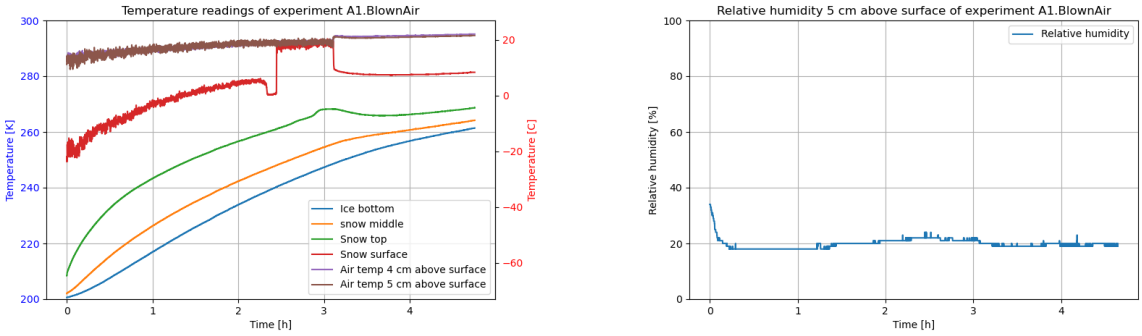


Figure A.7 Temperature readings of experiment T4.min80Coldfinger

Experiment A1.BlownAir measurements

Figure A.8 shows the temperature and relative humidity during experiment A1.BlownAir. From t = 0 h to t = 3 h noise is visible in the temperature measurements of the snow surface and air temperatures. This noise is due to the added airflow introduced by the small ventilator present during this test. At around t = 3 h the ventilator lost power and this could immediately be seen in the temperature measurements as no noise is present anymore from this time onwards in the surface and air temperature measurements. At t = 2.5 h an sudden increase in temperature is visible in the snow surface this is as the thermocouple got loose from the surface and instead of measuring the surface temperature it measured the air temperature.



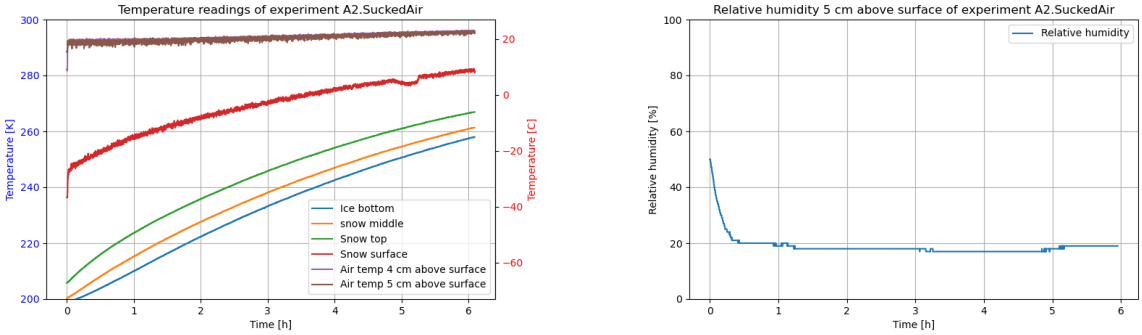
(a) Temperature

(b) Relative humidity

Figure A.8 Temperature and relative humidity readings of experiment A1.BlownAir

Experiment A2.SuckedAir measurements

Figure A.9 shows the temperature and relative humidity in the test setup during experiment A2.SuckedAir. The addition of a small airflow can clearly be seen in the temperature measurements of the air temperatures and the snow surface as small temperature fluctuations, noise, can be seen in these measurements. The measurements in the ice/snow sample do not have these as the airflow did not reach these parts. Like the previous two experiments the snow surface temperature remained below -10 °C for about 2 hours.



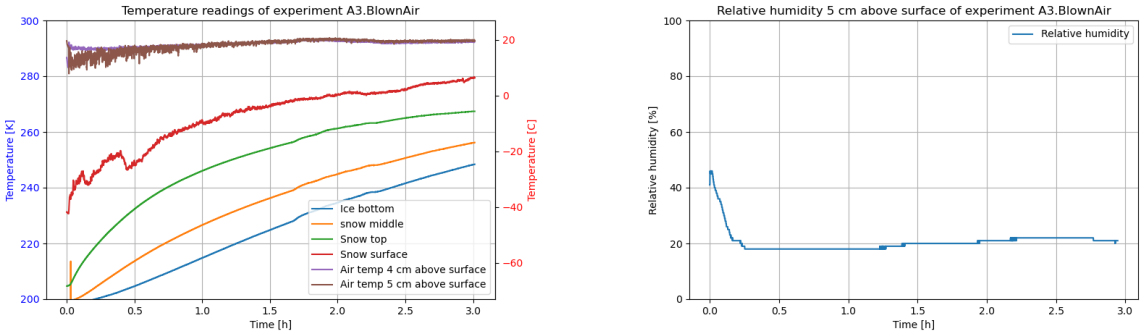
(a) Temperature

(b) Relative humidity

Figure A.9 Temperature and relative humidity readings of experiment A2.SuckedAir

Experiment A3.BlownAir measurements

Figure A.10 shows the temperature and relative humidity in the test setup during experiment A3.BlownAir. Due to the addition of the airflow the temperature of the snow surface drastically increased in a short time. The temperature of the snow surface remained below -10 °C for only about an hour, about half the time of the previous experiments. The relative humidity stayed about the same compared to the previous experiments, thus the airflow mainly influenced the temperature.



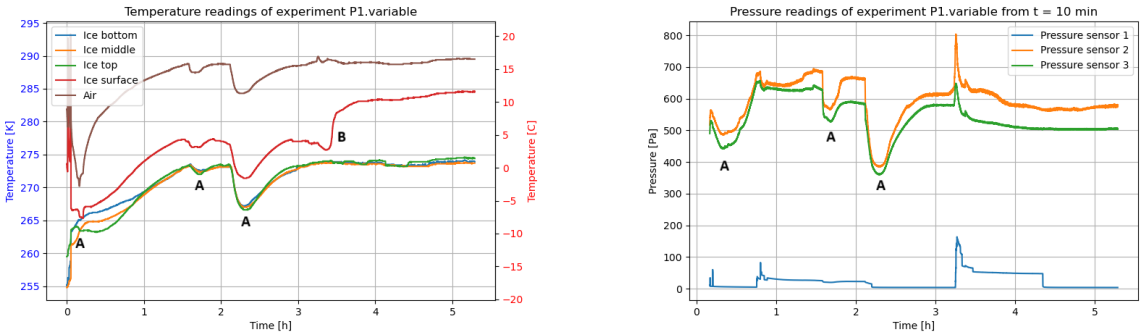
(a) Temperature

(b) Relative humidity

Figure A.10 Temperature and relative humidity readings of experiment A3.BlownAir

Experiment P1.variable measurements

Figure A.11 shows the temperature and pressure in the test setup during experiment P1.variable. It should be noted that the thermocouple that recorded the ice surface did not properly stick to the ice surface so it actually recorded the temperature just above the surface. In the temperature three drops can be noticed at the troughs with annotation A, these drops correspond to the addition of liquid nitrogen to the coldfinger, just as the drops in pressure. A sudden increase in the ice surface temperature can also be seen at annotation B. The reason for this sudden increase is unknown as it could not be seen in the other temperature measurements. The pressure throughout the experiment increased slightly, this was due to the sublimation of the snow adding extra water vapor in the air. Moreover it should be noted that pressure sensor 1 recorded a much lower pressure than the other two sensor, this is as pressure sensor 1 did not measure the pressure in the chamber but in the pump lines between the chamber and the pumps, which were slightly closed off to the chamber by a valve to stabilize the pressure inside the chamber.



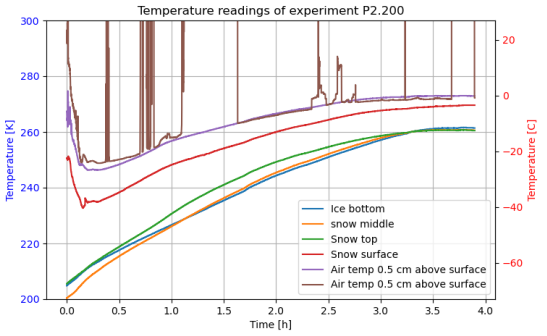
(a) Temperature

(b) Pressure

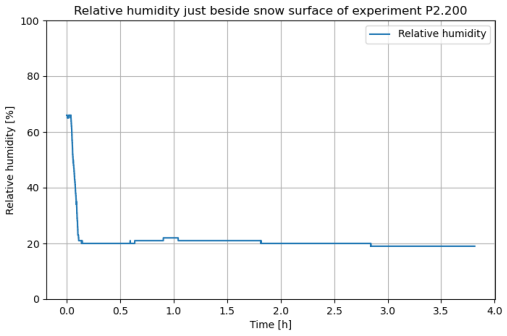
Figure A.11 Temperature and pressure readings of experiment P1.variable

Experiment P2.200 measurements

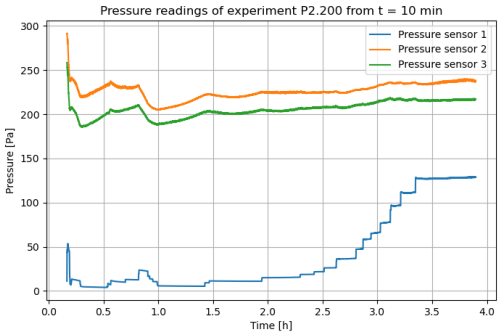
The temperature and relative humidity inside the test setup during experiment P2.200 can be seen in Figure A.12. Noticeable is that the temperature recorded by TC6 at 0.5 cm above the snow surface has some very high peaks in its measurements. These are incorrect measurements caused by a faulty connection. During this experiment somewhere at the the beginning TC2, the thermocouple measuring the snow surface temperature, fell out of the snow surface and got stuck some where at the top rim at the outside of the GN container.



(a) Temperature



(b) Relative humidity

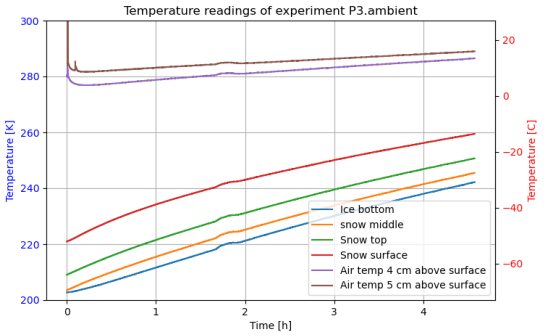


(c) Pressure

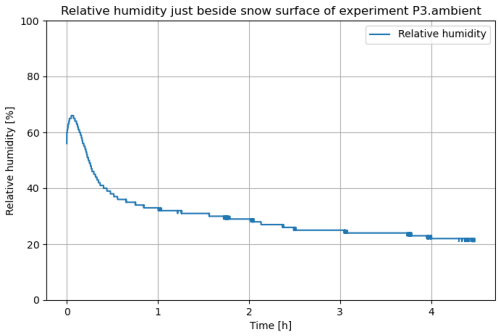
Figure A.12 Temperature, relative humidity and pressure readings of experiment P2.200

Experiment P3.ambient measurements

Figure A.13 shows the temperature and relative humidity during experiment P3.ambient. Noticeable in these measurements is that the relative humidity decreased more slowly as compared to the other experiments. It is unknown why this happened as no changes were made to the setup or experiment conduction. Besides this the temperature profile did not differ from the other experiments with similar test setup (experiment T4.min80Coldfinger).



(a) Temperature



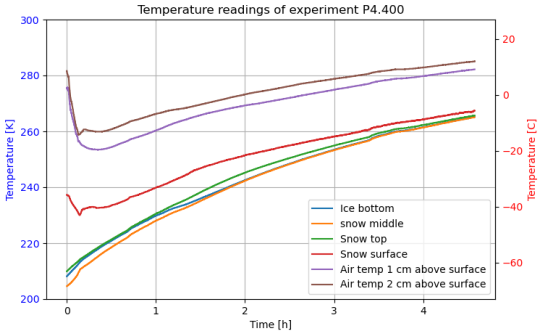
(b) Relative humidity

Figure A.13 Temperature and relative humidity of experiment P3.ambient

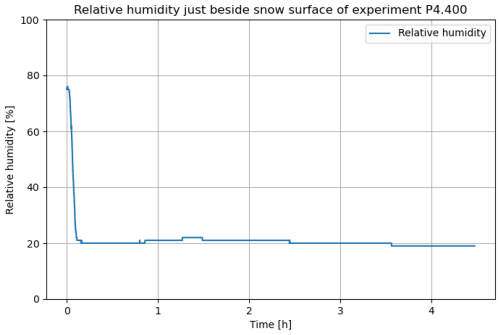
Experiment P4.400 measurements

Figure A.14 shows the temperature, relative humidity and pressure during experiment P4.400. A sudden drop in temperature of the snow surface and air temperature can be noticed at the beginning of the experiment. This drop occurred when the vacuum pumps were turned on. A similar drop can be seen in the relative humidity, this was also caused by the vacuum

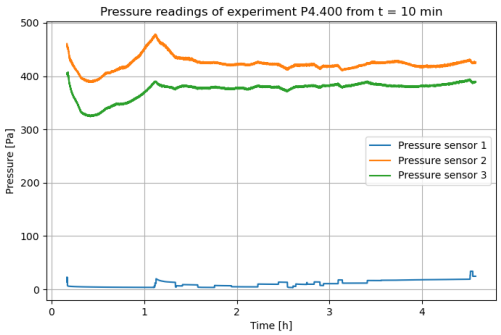
pumps being turned on.



(a) Temperature



(b) Relative humidity

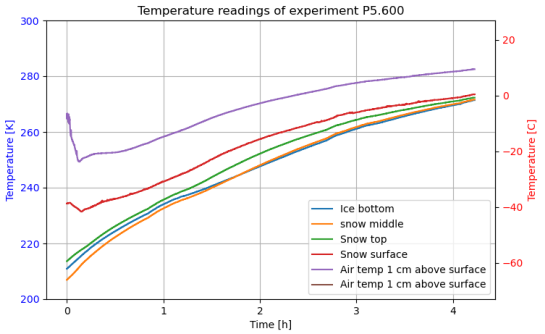


(c) Pressure

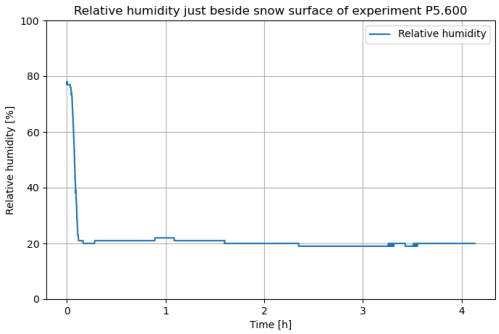
Figure A.14 Temperature, relative humidity and pressure readings of experiment P4.400

Experiment P5.600 measurements

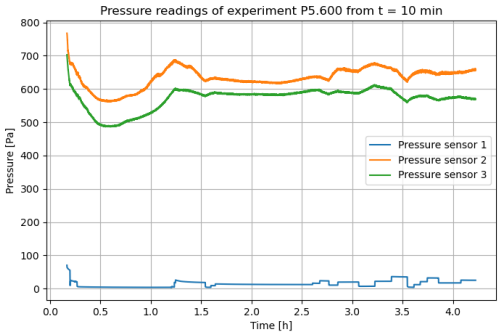
Figure A.15 shows the temperature, relative humidity and pressure during experiment P5.600. A similar drop in temperature and relative humidity as in experiment P4.400 can be seen at the beginning of the experiment. This was once again due to the vacuum pumps being turned on.



(a) Temperature



(b) Relative humidity

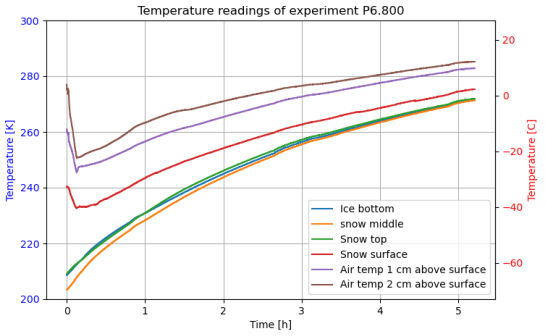


(c) Pressure

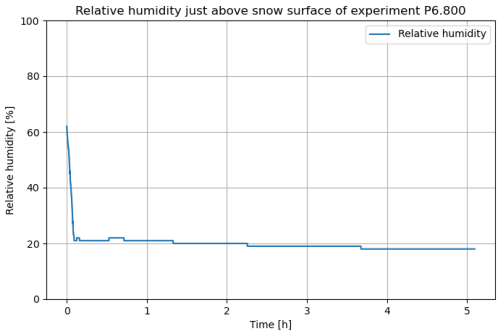
Figure A.15 Temperature, relative humidity and pressure readings of experiment P5.600

Experiment P6.800 measurements

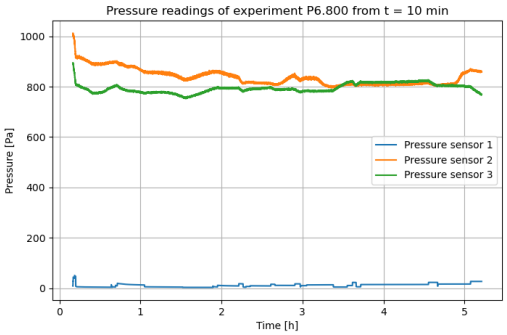
Figure A.16 shows the temperature, relative humidity and pressure during experiment P6.800. No unexpected decreases or increases in temperature, relative humidity or pressure occurred during this experiment.



(a) Temperature



(b) Relative humidity

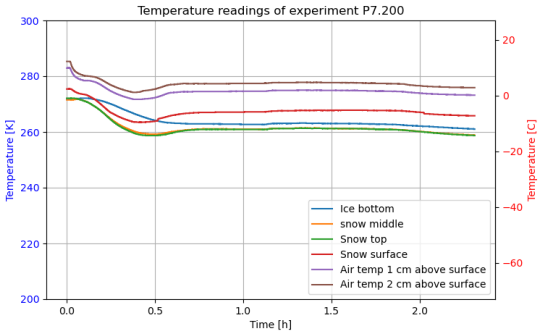


(c) Pressure

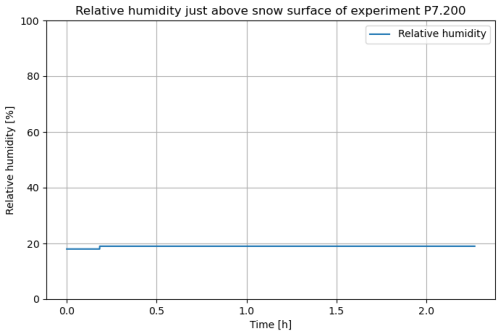
Figure A.16 Temperature, relative humidity and pressure readings of experiment P6.800

Experiment P7.200 measurements

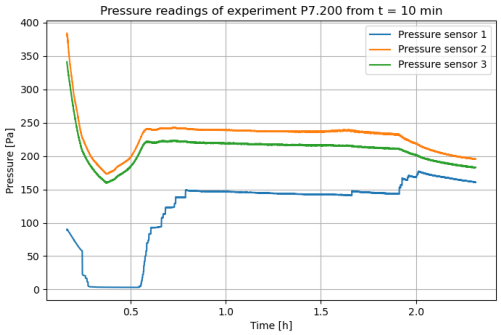
Figure A.17 shows the temperature, relative humidity and pressure during experiment P7.200. At the beginning of the temperature measurements a small decrease in temperature can be seen. This occurred due to the addition of extra LN2 before the conduction of this experiment when transitioning from a pressure of 800 Pa in the previous experiment to 200 Pa in this experiment. Due to this transition a drop in pressure in the beginning of the pressure measurements is also visible.



(a) Temperature



(b) Relative humidity



(c) Pressure

Figure A.17 Temperature, relative humidity and pressure readings of experiment P7.200

Experiment details

In this section all of the experiment details are presented. These details include experimental conditions aswell as which sensors are used and more information regarding the ice/snow samples used during each experiment. The details of all the experiments performed with the EPS setup can be found in Table A.1. The details of all the experiments performed to investigate the effect of temperature on penitente formation can be found in Table A.2. The details of all the experiments performed to investigate the effect of an added airflow on penitente formation can be found in Table A.3. Lastly the details of all the experiments performed to investigate the effect of pressure changes on penitente formation can be found in Tables A.4, A.5 and A.6.

Table A.1 Experimental setup details of experiments performed using EPS setup

Parameter	Experiment M1.CloudyIce	Experiment M2.ClearIce	Experiment M3.Snow
Set-up used	EPS setup	EPS setup	EPS setup
Insolation at surface [W/m^2]	$\sim$ 480	$\sim$ 480	$\sim$ 490
Relative humidity [%]	unknown	unknown	35 to 45
Pressure [Pa]	ambient	ambient	ambient
Experiment duration [h:min]	6:03	6:29	4:54
Bulk density ice/snow [kg/m^3]	unknown	unknown	unknown
Thermocouples used	6	6	4
RH sensor used	no	no	yes
Ventilator used	no	no	no
Freezer temperature used [°C]	-20	-20	-20
Ice thickness [cm]	15	12	5
Crushed ice thickness [cm]	0	0	9
Snow thickness [cm]	0	0	1
Cooling material used	5 kg crushed ice	2.5 kg crushed ice	2.5 kg crushed ice
Humidity absorbers used	no	yes	no

Table A.2 Experimental setup details of experiments performed to investigate the temperature effects on penitente formation

Parameter	Experiment T1.min25	Experiment T2.min25	Experiment T3.min80	Experiment T4.min80Coldfinger
Set-up used	PISCES setup	PISCES setup	PISCES setup	PISCES setup
Insolation at surface [W/m^2]	$\sim$ 245	$\sim$ 245	$\sim$ 288	$\sim$ 280
Relative humidity [%]	35 to 60	22 to 30	18 to 30	unknown
Pressure [Pa]	ambient	ambient	ambient	ambient
Experiment duration [h:min]	3:53	6:45	6:15	6:23
Bulk density ice/snow [kg/m^3]	425	465	465	463
Thermocouples used	6	6	6	6
RH sensor used	yes	yes	yes	yes but malfunctioned
Ventilator used	no	no	no	no
Freezer temperature used [°C]	-25	-25	-80	-80
Ice thickness [cm]	7	7	7	7
Crushed ice thickness [cm]	1.5	1.5	1.5	1.5
Snow thickness [cm]	6.5	5.5	6.5	6.5
Cooling material used	-25 °C aluminium pellets & 2 kg -20 °C crushed ice	-25 °C aluminium pellets & 4 l -20 °C crushed ice	-80 °C aluminium pellets & 4 l -20 °C crushed ice	-80 °C aluminium pellets & 4 l -20 °C crushed ice
Humidity absorbers used	90 g silicagel grains & 20 silicagel packets	90 g silicagel grains & 20 silicagel packets	90 g silicagel grains & 20 silicagel packets	90 g silicagel grains & 20 silicagel packets
coldfinger used	no	no	no	yes

Table A.3 Experimental setup details of experiments performed to investigate the airflow effects on penitente formation

Parameter	Experiment T4.min80Coldfinger	Experiment A1.BlownAir	Experiment A2.SuckedAir	Experiment A3.BlownAir
Set-up used	PISCES setup	PISCES	PISCES setup	PISCES setup
Insolation at surface $[W/m^2]$	~ 280	~ 265	~ 260	~ 300
Relative humidity [%]	unknown	18 to 22	18 to 21	17 to 22
Pressure [Pa]	ambient	ambient	ambient	ambient
Experiment duration [h:min]	6:23	4:45	6:06	3:01
Bulk density ice/snow $[kg/m^3]$	463	463	480	480
Thermocouples used	6	6	6	6
RH sensor used	yes but malfunctioned	yes	yes	yes
Ventilator used	no	yes (air blown to surface)	yes (air sucked from surface)	yes (air blown to surface)
Freezer temperature used [°C]	-80	-80	-80	-80
Ice thickness [cm]	7	7	7	7
Crushed ice thickness [cm]	1.5	1.5	1.5	1.5
Snow thickness [cm]	6.5	6.5	6.5	6.5
Cooling material used	-80 °C aluminium pellets & 4 l -20 °C crushed ice	-80 °C aluminium pellets & 4 l -20 °C crushed ice	-80 °C aluminium pellets & 4 l -20 °C crushed ice	-80 °C aluminium pellets & 4 l -20 °C crushed ice
Humidity absorbers used	90 g silicagel grains & 20 silicagel packets	90 g silicagel grains & 20 silicagel packets	90 g silicagel grains & 20 silicagel packets	90 g silicagel grains & 20 silicagel packets
Coldfinger used	no	no	no	no

Table A.4 Experimental setup details of experiments performed to investigate the pressure effects on penitente formation part 1

Parameter	Experiment P1.variable	Experiment P2.200	Experiment P3.ambient
Set-up used	PISCES setup	PISCES setup	PISCES setup
Insolation at surface [W/m^2]	$\sim$ 270	$\sim$ 260	$\sim$ 310
Relative humidity [%]	18 to 25	19 to 22	22 to 40
Pressure [Pa]	300 to 800	200	ambient
Experiment duration [h:min]	5:14	3:54	4:35
Bulk density ice/snow [kg/m^3]	unknown	492	501
Thermocouples used	5	6	6
RH sensor used	yes	yes	yes
Ventilator used	no	no	no
Freezer temperature used [°C]	-20	-80	-80
Ice thickness [cm]	5	7	7
Crushed ice thickness [cm]	6	1.5	1.5
Snow thickness [cm]	1	6.5	6.5
Cooling material used	none	-80 °C and -25 °C aluminium pellets	-80 °C aluminium pellets & 4 l -20 °C crushed ice
Humidity absorbers used	none	none	90 g silicagel grains & 20 silicagel packets
Coldfinger used	yes	yes	no

Table A.5 Experimental setup details of experiments performed to investigate the pressure effects on penitente formation part 2

Parameter	Experiment P4.400	Experiment P5.600	Experiment P6.800
Set-up used	PISCES setup	PISCES setup	PISCES setup
Insolation at surface [W/m^2]	$\sim$ 245	$\sim$ 230	$\sim$ 260
Relative humidity [%]	19 to 21	19 to 22	18 to 22
Pressure [Pa]	400	600	800
Experiment duration [h:min]	4:37	4:18	5:13
Bulk density ice/snow [kg/m^3]	508	509	513
Thermocouples used	6	6 (but one malfunctioned)	6
RH sensor used	yes	yes	yes
Ventilator used	no	no	no
Freezer temperature used [°C]	-80	-80	-80
Ice thickness [cm]	7	7	7
Crushed ice thickness [cm]	1.5	1.5	1.5
Snow thickness [cm]	6.5	6.5	6.5
Cooling material used	-80 °C and -25 °C aluminium pellets	-80 °C and -25 °C aluminium pellets	-80 °C and -25 °C aluminium pellets
Humidity absorbers used	none	none	none
Coldfinger used	yes	yes	yes

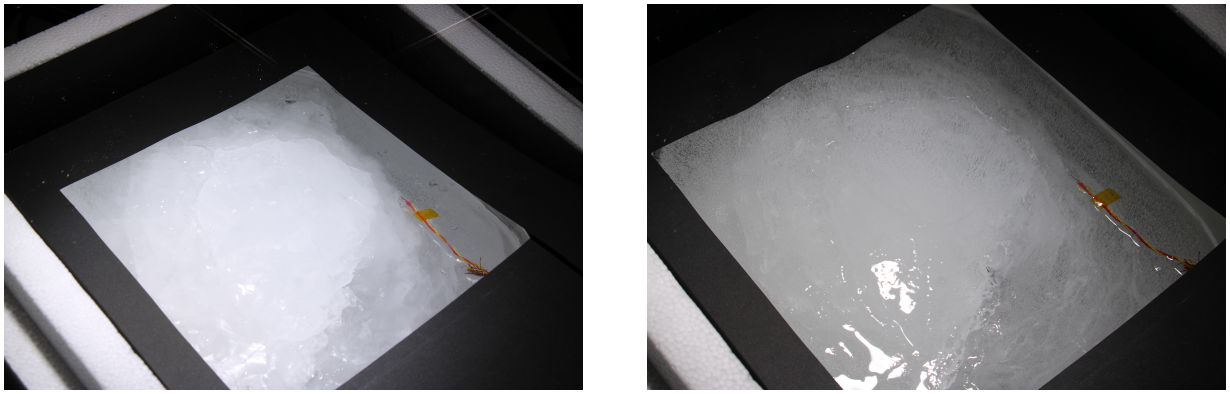
Table A.6 Experimental setup details of experiments performed to investigate the pressure effects on penitente formation part 3

Parameter	Experiment P7.200
Set-up used	PISCES setup
Insolation at surface [W/m^2]	$\sim$ 260
Relative humidity [%]	18 to 19
Pressure [Pa]	200
Experiment duration [h:min]	2:19
Bulk density ice/snow [kg/m^3]	513
Thermocouples used	6
RH sensor used	yes
Ventilator used	no
Freezer temperature used [°C]	-80
Ice thickness [cm]	7
Crushed ice thickness [cm]	1.5
Snow thickness [cm]	6.5
Cooling material used	-80 °C and -25 °C aluminium pellets
Humidity absorbers used	none
Coldfinger used	yes

Snow/ice surface pictures

In this section the snow/ice surface at the beginning and end of each experiment is presented.

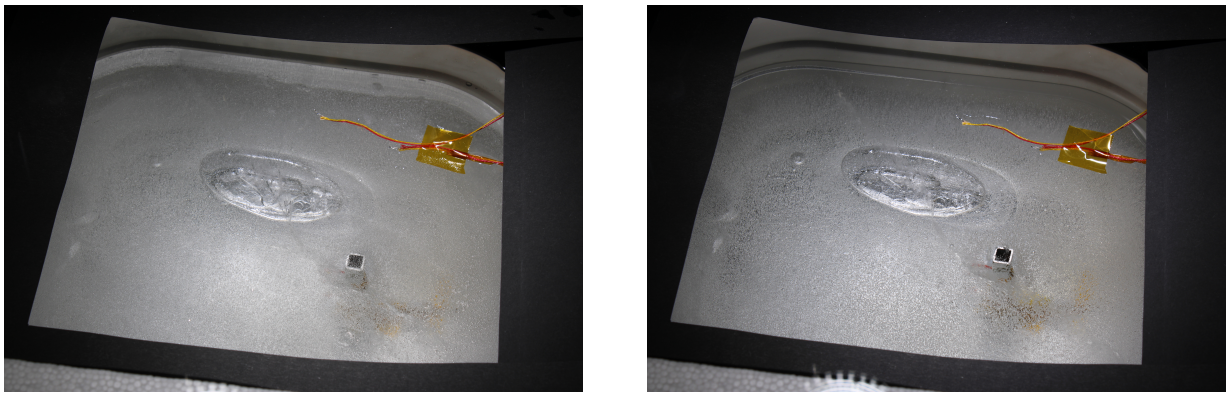
Experiment M1.CloudyIce



(a) Start experiment (b) End experiment

Figure A.18 Ice surface at start and end of experiment M1.CloudyIce

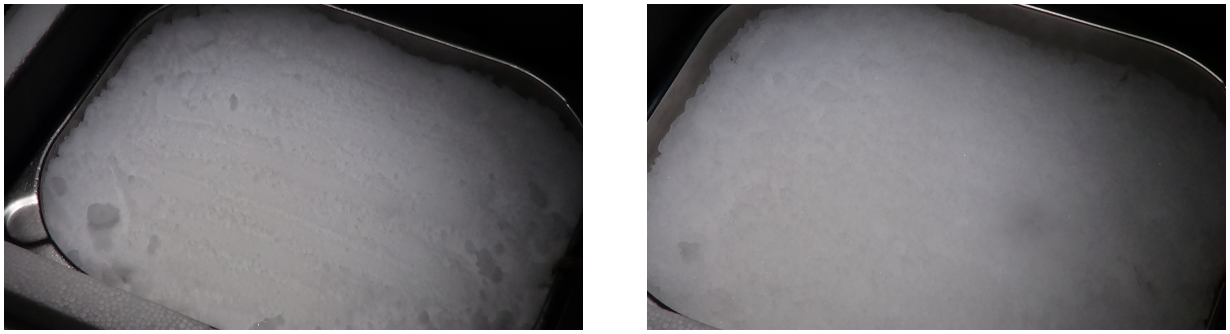
Experiment M2.ClearIce



(a) Start experiment (b) End experiment

Figure A.19 Ice surface at start and end of experiment M2.ClearIce

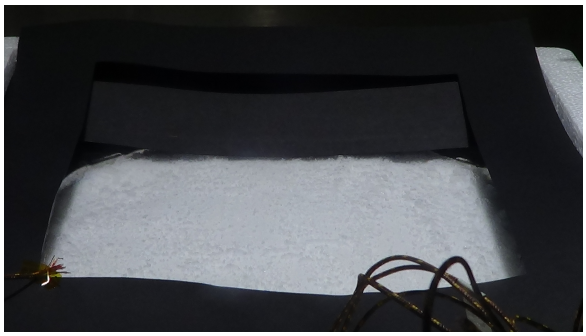
Experiment M3.Snow



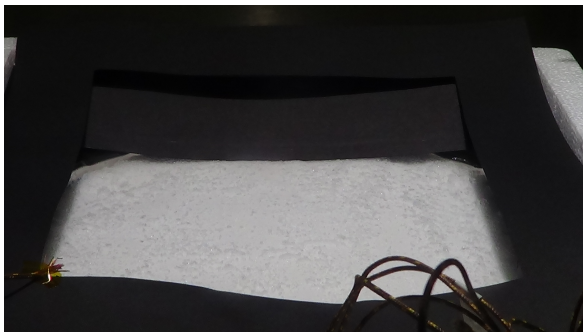
(a) Start experiment (b) End experiment

Figure A.20 Ice surface at start and end of experiment M3.Snow

Experiment T1.min25

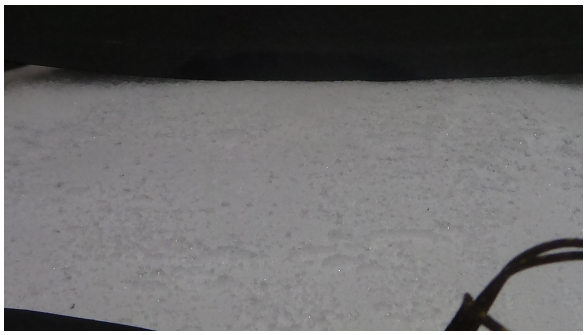


(a) At start of experiment (11:26)

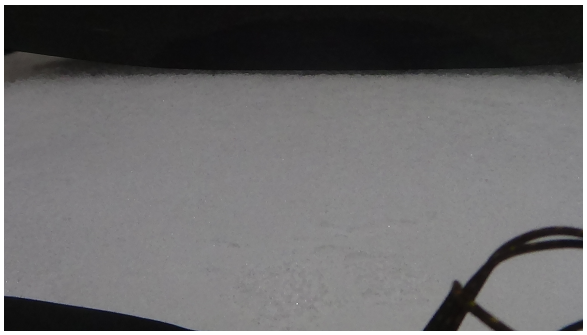


(b) 15 minutes before malfunction occurred (13:45)

Figure A.21 Snow surface of experiment T1.min25 at the start and just before the malfunction happened



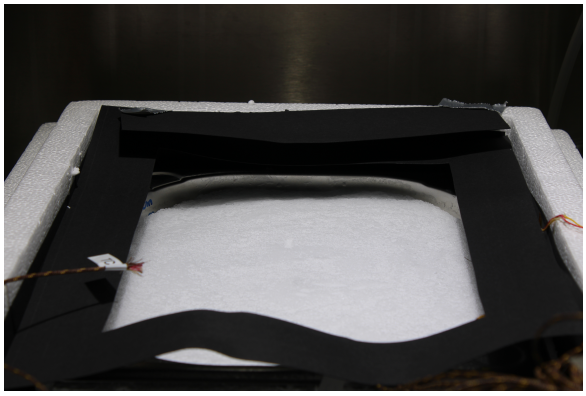
(a) 10 minutes after malfunction occurred (14:16)



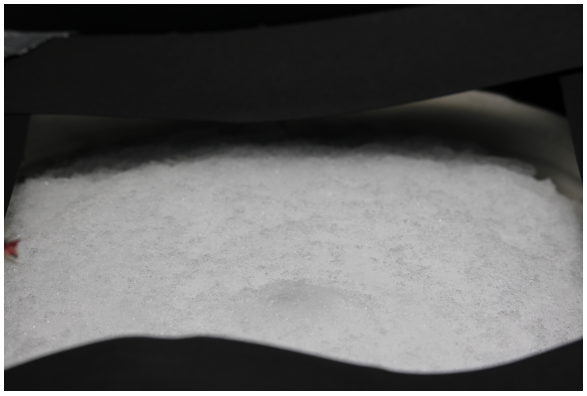
(b) At end of experiment (15:13)

Figure A.22 Snow surface of experiment T1.min25 just before the malfunction happened and at the end of the experiment

Experiment T2.min25



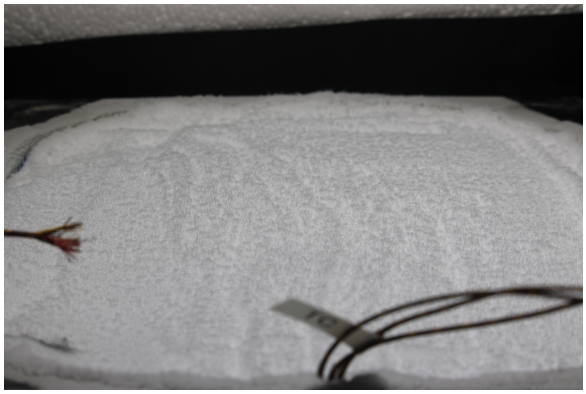
(a) Start experiment



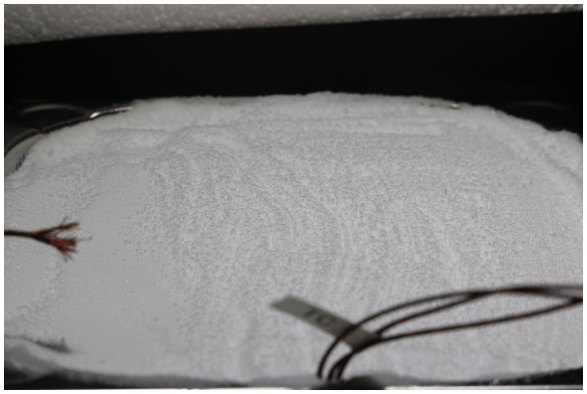
(b) End experiment

Figure A.23 Snow surface at start and end of experiment T2.min25

Experiment T3.min80



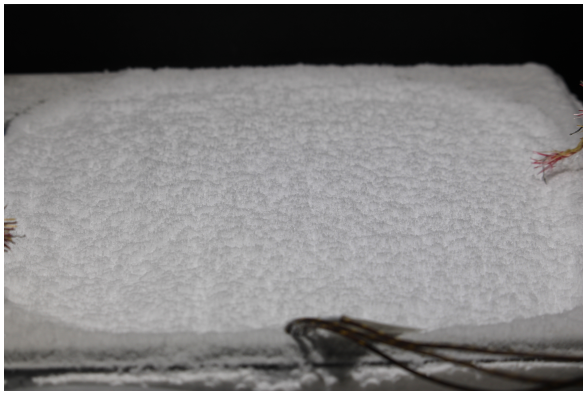
(a) Start experiment



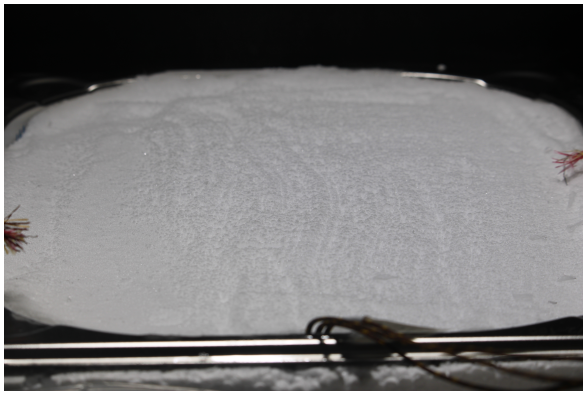
(b) End experiment

Figure A.24 Snow surface at the start and end of experiment T3.min80

Experiment T4.min80Coldfinger



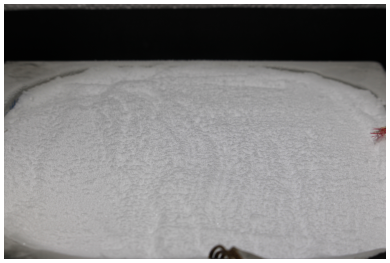
(a) Start experiment



(b) End experiment

Figure A.25 Snow surface at the start and end of experiment T4.min80Coldfinger

Experiment A1.BlownAir



(a) Start experiment



(b) Middle experiment



(c) End experiment

Figure A.26 Snow surface at start, middle and end of experiment A1.BlownAir

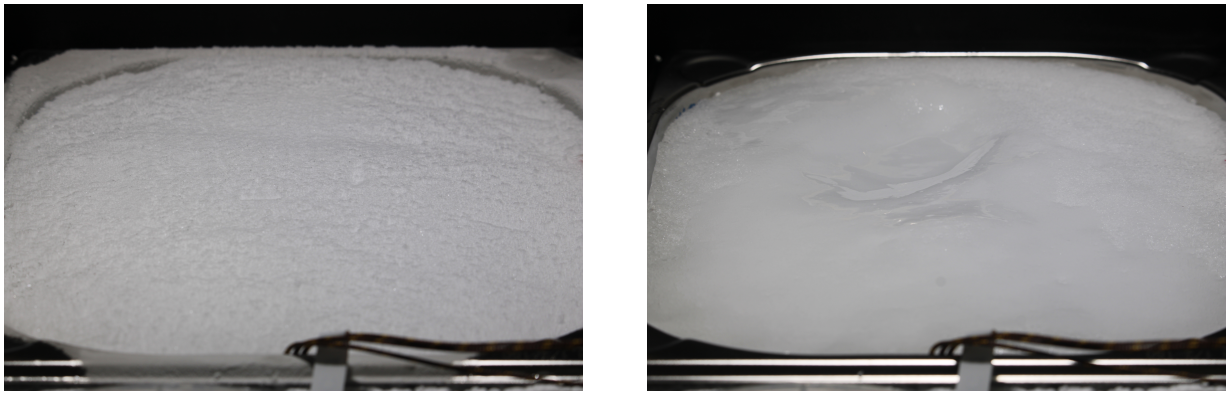
Experiment A2.SuckedAir



(a) Start experiment (b) End experiment

Figure A.27 Snow surface at the start and end of experiment A2.SuckedAir

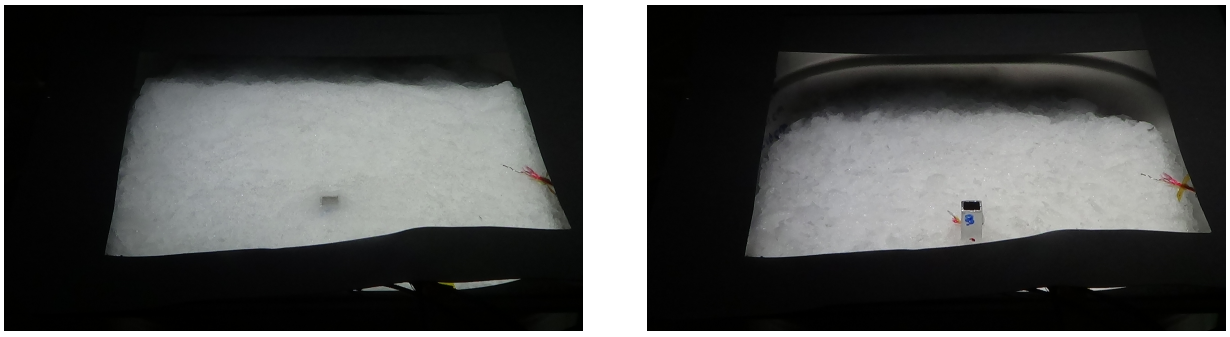
Experiment A3.BlownAir



(a) Start experiment (b) End experiment

Figure A.28 Snow surface at the start and end of experiment A3.BlownAir

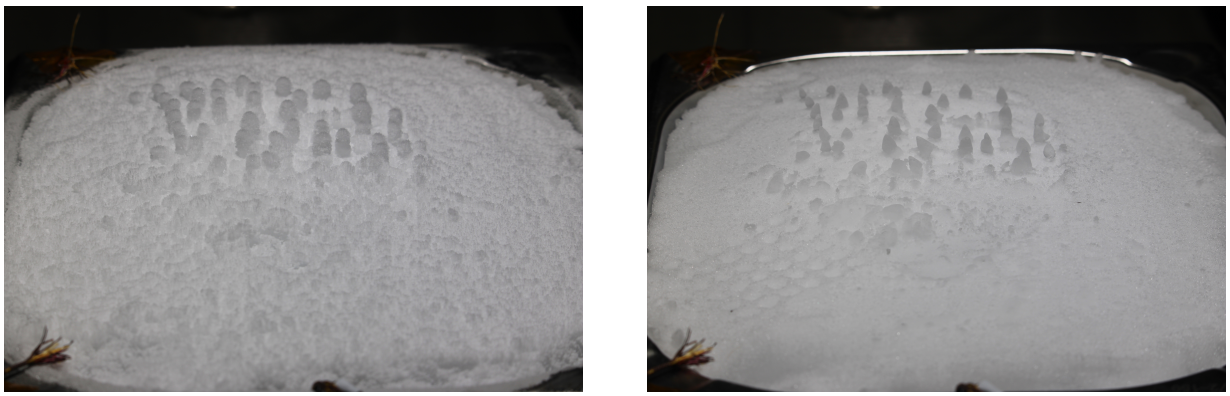
Experiment P1.variable



(a) Start experiment (b) End experiment

Figure A.29 Ice surface at start and end of experiment P1.variable

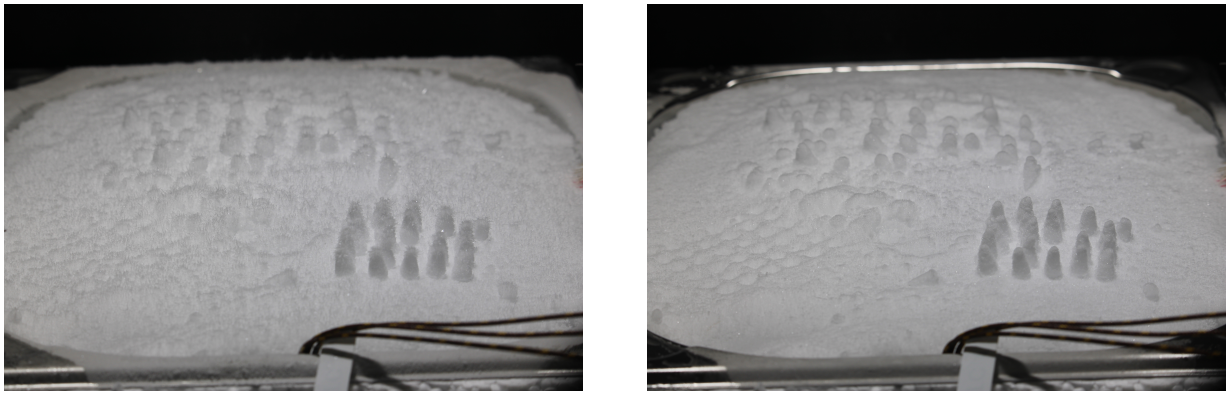
Experiment P2.200



(a) Start experiment (b) End experiment

Figure A.30 Snow surface at the start and end of experiment P2.200

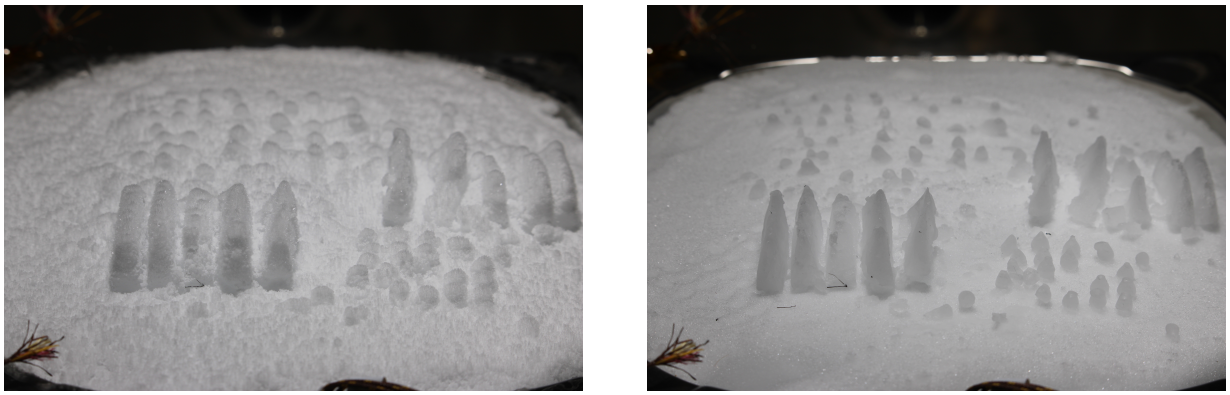
Experiment P3.ambient



(a) Start experiment (b) End experiment

Figure A.31 Snow surface at the start and end of experiment P3.ambient

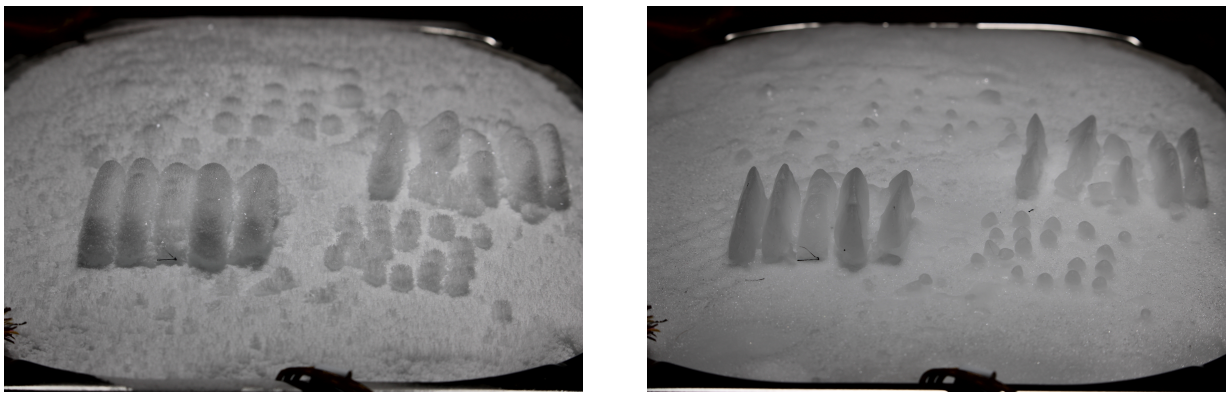
Experiment P4.400



(a) Start experiment (b) End experiment

Figure A.32 Snow surface at the start and end of experiment P4.400

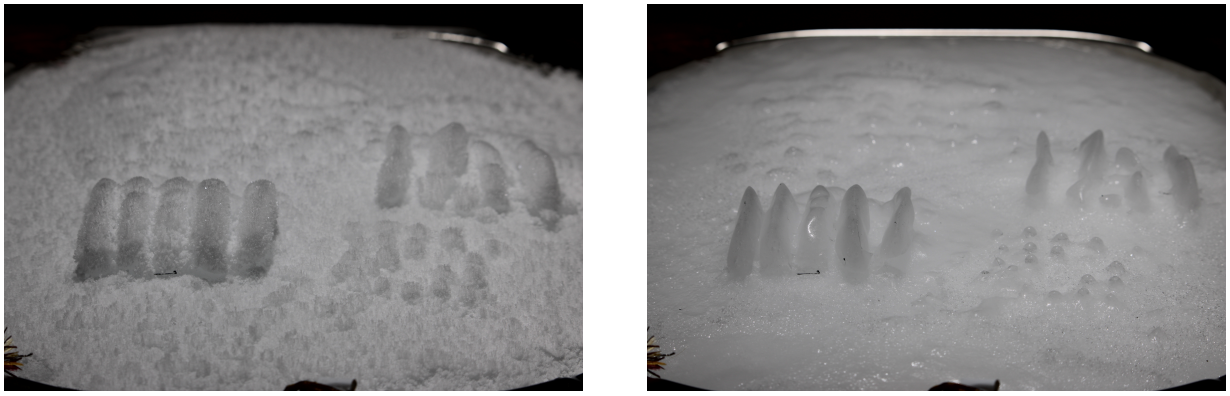
Experiment P5.600



(a) Start experiment (b) End experiment

Figure A.33 Snow surface at the start and end of experiment P5.600

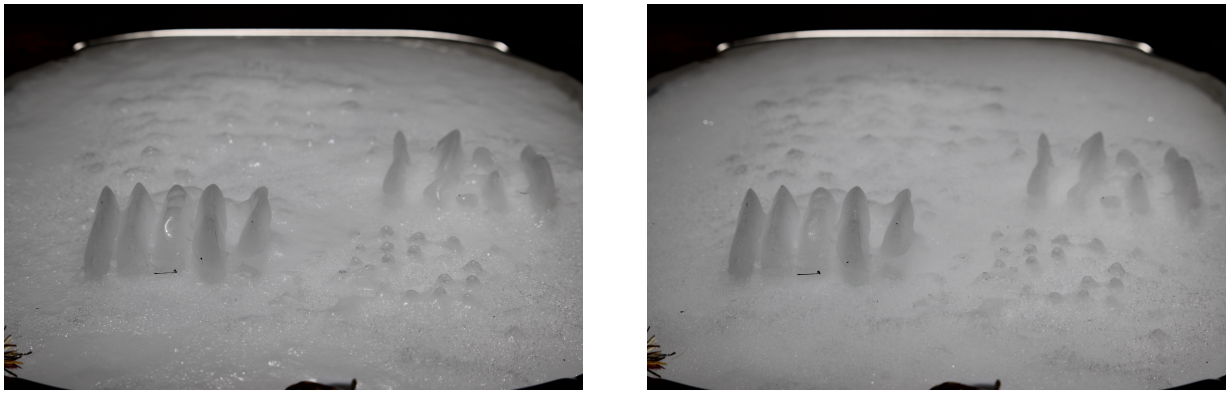
Experiment P6.800



(a) Start experiment (b) End experiment

Figure A.34 Snow surface at the start and end of experiment P6.800

Experiment P7.200



(a) Start experiment (b) End experiment

Figure A.35 Snow surface at the start and end of experiment P7.200

B Penitente Model Inputs and MCD graphs

In this appendix all the input conditions used to calculate the theoretical results using Claudin's penitente growth model will be presented. Moreover the temperature, pressure and insolation plots of Mars throughout the seasons simulated using the Mars Climate Database are presented. At the end of this appendix the python code used for this model is presented aswell.

Model inputs

The input conditions used in the penitente model to get the theoretical penitente growth rates and spacing for all experiments and Mars locations are presented in this section. The input conditions used for each experiment can be found in Table B.1. All these input conditions are based on values used by Claudin and Nguyen in their simulations aswell as the measurements performed during the experiments [18] [19]. The input conditions used for a first investigation into penitente formation on Mars can be found in Table B.2. These input conditions are based on values used by Claudin, Nguyen aswell as Martian conditions presented in Chapter 2. The conditions used for the Santiago Andes are based on pure ice, conditions presented by Lliboutry [20] and climatic conditions in the region [52] [53]. The input conditions used to calculate penitente growth rate and spacing at specific interesting locations where penitente formation is thought to be possible can be found in Table B.3. These input conditions are based on values used by Claudin and Nguyen aswell as values obtained using the Mars Climate Database [35] [36].

Table B.1 Input values used in Claudin's model. The temperature used is the temperature measurement of the snow/ice surface at time = 2 hours into the experiment

Experiment	**p [Pa]**	**T [K]**	$M_{s(atmos)}$ **[g/mol]**	D_ρ $[m^2/s]$	κ_s **[W/m/K]**	Λ **[m]**	ω **[-]**	ν $[m^2/s]$	u_* **[m/s]**	J_0^ψ $[W/m^2]$	ρ_s $[kg/m^3]$	**L** $[MJ/kg]$	α **[m/s]**	M_s **[g/-mol]**
M1.CloudyIce	101325	265	28.96	0.00003	2	0.016	0.5	0.00001	0.4	483.33	920	3	100	18
M2.ClearIce	101325	273	28.96	0.00003	2	0.016	0.5	0.00001	0.4	483.33	920	3	100	18
M3.Snow	101325	268	28.96	0.00003	0.32	0.016	0.7	0.00001	0.4	491.67	550	3	100	18
T1.min25	101325	272	28.96	0.00003	0.32	0.016	0.7	0.00001	0.4	243.33	425.43	3	100	18
T2.min25	101325	267	28.96	0.00003	0.32	0.016	0.7	0.00001	0.4	244.17	466.68	3	100	18
T3.min80	101325	258	28.96	0.00003	0.32	0.016	0.5	0.00001	0.4	300	550	3	100	18
T4.min80 Coldfinger	101325	262	28.96	0.00003	0.32	0.016	0.7	0.00001	0.4	281.67	462.58	3	100	18
A1.BlownAir	101325	273	28.96	0.00003	0.32	0.016	0.7	0.00001	0.4	265.83	462.58	3	100	18
A2.SuckerAir	101325	262	28.96	0.00003	0.32	0.016	0.7	0.00001	0.4	257.5	480.77	3	100	18
A3.BlownAir	101325	272	28.96	0.00003	0.32	0.016	0.7	0.00001	0.4	303.25	481.94	3	100	18
P1.variable	600	273	28.96	0.0004	0.32	0.016	0.7	0.00001	0.4	275	550	3	100	18
P2.200	200	260	28.96	0.0004	0.32	0.016	0.7	0.00001	0.4	262.5	492.31	3	100	18
P3.ambient	101325	243	28.96	0.00003	0.32	0.016	0.7	0.00001	0.4	310.83	511.66	3	100	18
P4.400	400	251	28.96	0.0004	0.32	0.016	0.7	0.00001	0.4	245.8	508.18	3	100	18
P5.600	600	258	28.96	0.0004	0.32	0.016	0.7	0.00001	0.4	231.7	508.95	3	100	18
P6.800	800	254	28.96	0.0004	0.32	0.016	0.7	0.00001	0.4	260	513.21	3	100	18
P7.200	200	267	28.96	0.0004	0.32	0.016	0.7	0.00001	0.4	260	513.21	3	100	18

Table B.2 Input values used in Claudin's model to simulate penitente formation on Mars [19]

Name	**p [Pa]**	**T [K]**	$M_{s(atmos)}$ **[g/mol]**	D_ρ $[m^2/s]$	κ_s **[W/m/K]**	Λ **[m]**	ω **[-]**	ν $[m^2/s]$	u_* **[m/s]**	J_0^ψ $[W/m^2]$	ρ_s $[kg/m^3]$	**L** $[MJ/kg]$	α **[m/s]**	M_s **[g/-mol]**
Nguyen	600	203	44.009	0.0004	2	0.016	0.5	0.00001	0.4	140	920	3	100	18
Updated Nguyen	600	203	44.009	0.0004	3	0.016	0.5	0.00001	0.4	140	920	3	100	18
Mars average	636	210	44.009	0.0004	0.55	0.016	0.8	0.00001	0.4	483.33	400	3	100	18
Phoenix	820	220	44.009	0.0004	1.5	0.016	0.7	0.00001	0.4	150	500	3	100	18
Mars North pole	800	250	44.009	0.0004	2.5	0.016	0.5	0.00001	0.4	150	500	3	100	18
Santiago Andes	60000	272	28.96	0.00003	2	0.016	0.4	0.00001	0.4	490	550	3	100	18

Table B.3 Input values used in Claudin's model to simulate penitente formation on potential locations where penitentes could form on Mars [19]

Name	**p [Pa]**	**T [K]**	$M_{s(atmos)}$ **[g/mol]**	D_ρ $[m^2/s]$	κ_s **[W/m/K]**	Λ **[m]**	ω **[-]**	ν $[m^2/s]$	u_* **[m/s]**	J_0^ψ $[W/m^2]$	ρ_s $[kg/m^3]$	**L** $[MJ/kg]$	α **[m/s]**	M_s **[g/-mol]**
Olympus Mons $L_s = 0°$ $t = 0h$	240	264	44.009	0.0004	0.55	0.016	0.8	0.00001	0.4	340	400	3	100	18
Olympus Mons $L_s = 0°$ $t = 18h$	180	252.5	44.009	0.0004	0.55	0.016	0.8	0.00001	0.4	380	400	3	100	18
Olympus Mons $L_s = 90°$ $t = 0h$	190	255	44.009	0.0004	0.55	0.016	0.8	0.00001	0.4	340	400	3	100	18
Olympus Mons $L_s = 90°$ $t = 18h$	190	255	44.009	0.0004	0.55	0.016	0.8	0.00001	0.4	380	400	3	100	18
Olympus Mons $L_s = 180°$ $t = 18h$	190	257.5	44.009	0.0004	0.55	0.016	0.8	0.00001	0.4	420	400	3	100	18
Olympus Mons $L_s = 270°$ $t = 0h$	240	259	44.009	0.0004	0.55	0.016	0.8	0.00001	0.4	300	400	3	100	18

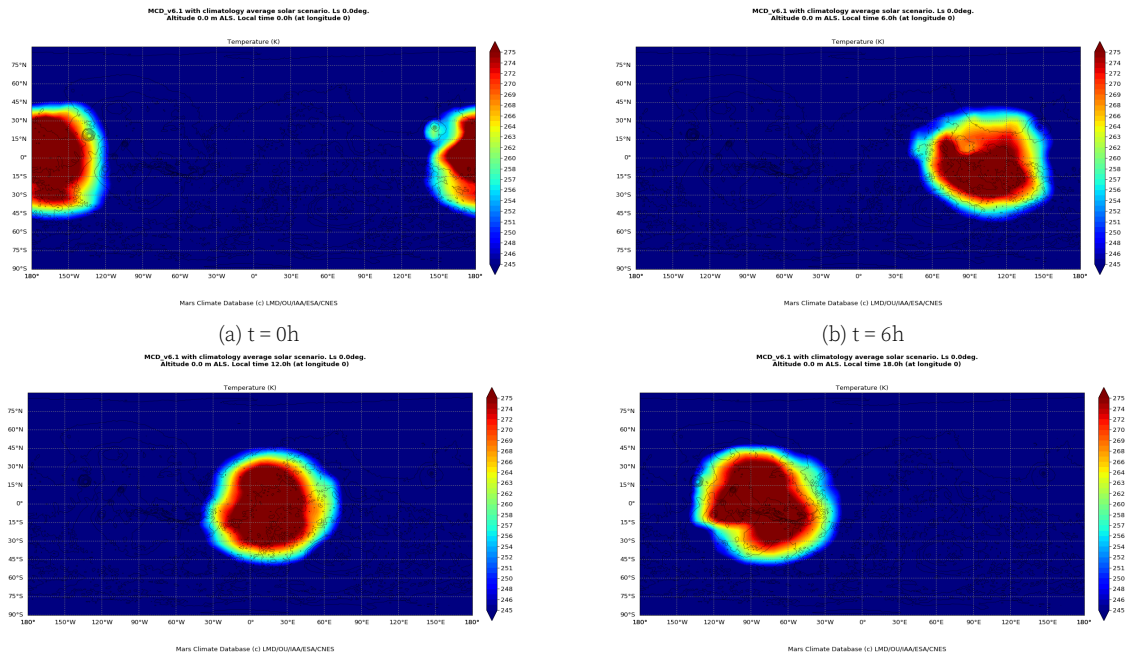
Elysium Mons $L_s = 90°$ $t = 0h$	400	265	44.009	0.0004	0.55	0.016	0.8	0.00001	0.4	400	400	3	100	18
Elysium Mons $L_s = 180°$ $t = 0h$	395	265	44.009	0.0004	0.55	0.016	0.8	0.00001	0.4	440	400	3	100	18
Arsia Mons $L_s = 180°$ $t = 0h$	275	260.5	44.009	0.0004	0.55	0.016	0.8	0.00001	0.4	300	400	3	100	18
Arsia Mons $L_s = 90°$ $t = 18h$	140	247.5	44.009	0.0004	0.55	0.016	0.8	0.00001	0.4	350	400	3	100	18
Alba Mons $L_s = 90°$ $t = 18h$	350	267	44.009	0.0004	0.55	0.016	0.8	0.00001	0.4	400	400	3	100	18
Alba Mons $L_s = 180°$ $t = 18h$	350	265	44.009	0.0004	0.55	0.016	0.8	0.00001	0.4	450	400	3	100	18

South polar region $L_s = 270°$ $t = 0h$	500	265	44.009	0.0004	0.55	0.016	0.8	0.00001	0.4	400	400	3	100	18

Mars Climate Database plots

This section presents the plots made using the Mars Climate Database general circulation model which have been used to simulate the temperature, pressure and solar insolation conditions on Mars throughout a Martian year at various times during the day. In order to get an overview of the seasonal and diurnal variations in these factors the plots have been made for Ls 0°, 90°, 180° and 270° at local times 0h, 6h, 12h, and 18h. These plots were then used to pinpoint locations on Mars were the temperature and pressure regime is within the penitente formation zone and thus penitente formation may be possible. The temperatures, pressures and solar insolation obtained using these plots have also been used in Claudin's penitente model to determine the growth rate and spacing of penitentes at the pinpointed locations.

Ls 0°



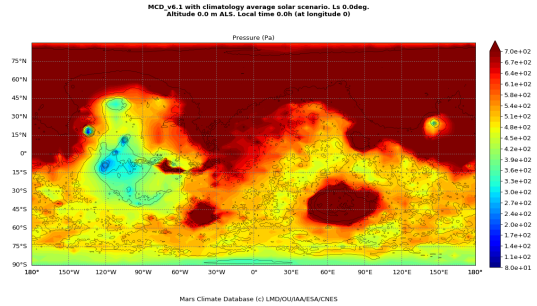
(a) t = 0h

(b) t = 6h

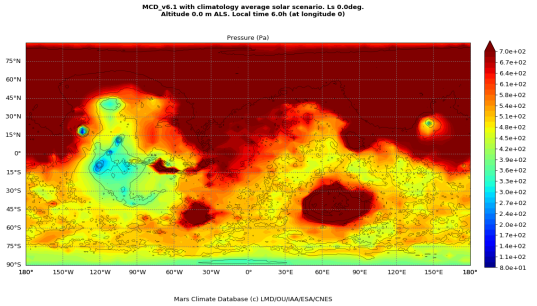
(c) t = 12h

(d) t = 18h

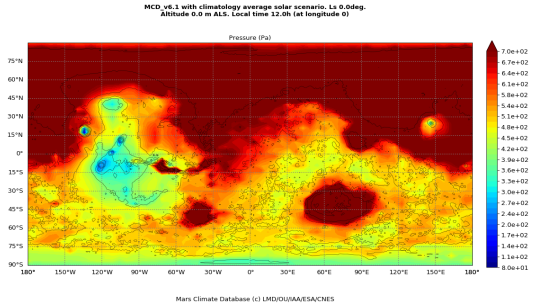
Figure B.1 Temperatures at Mars in range 245 to 275 K at $L_s = 0°$ at time 0h, 6h, 12h and 18h



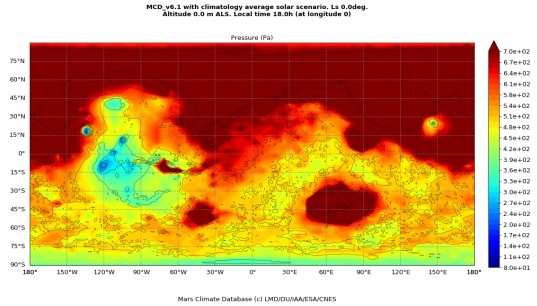
(a) t = 0h



(b) t = 6h

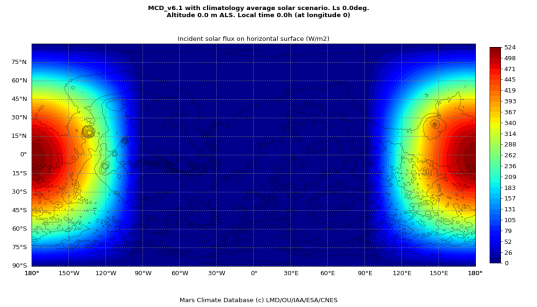


(c) t = 12h

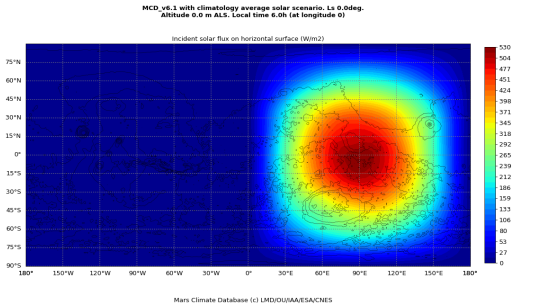


(d) t = 18h

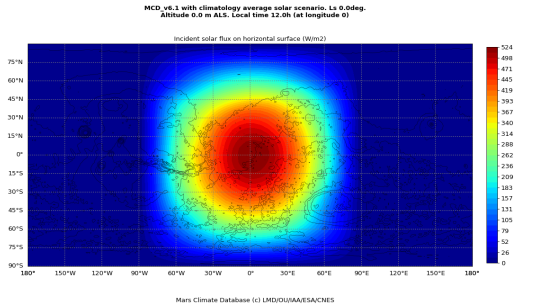
Figure B.2 Pressures at Mars in range 80 to 700 Pa at $L_s = 0°$ at time 0h, 6h, 12h and 18h



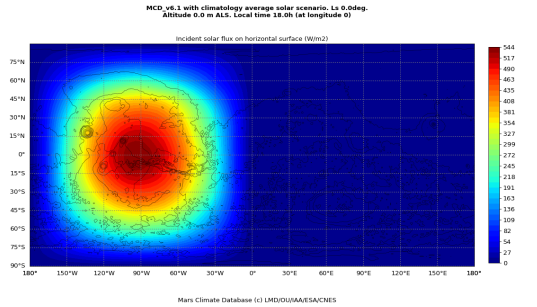
(a) t = 0h



(b) t = 6h



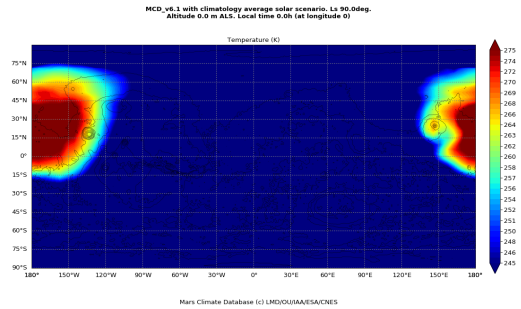
(c) t = 12h



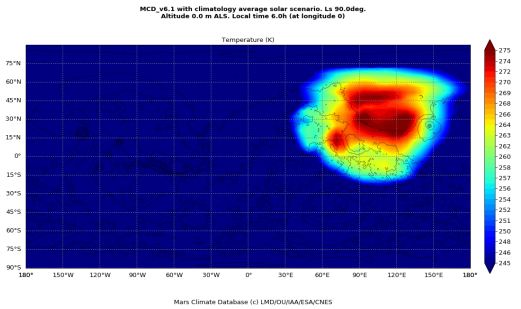
(d) t = 18h

Figure B.3 Solar insolation at Mars at $L_s = 0°$ at time 0h, 6h, 12h and 18h

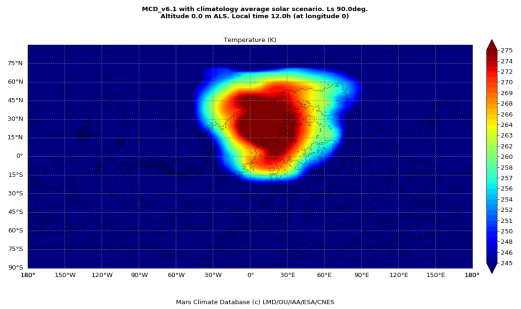
Ls 90°



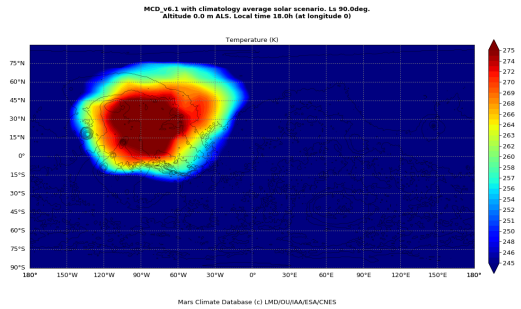
(a) t = 0h



(b) t = 6h

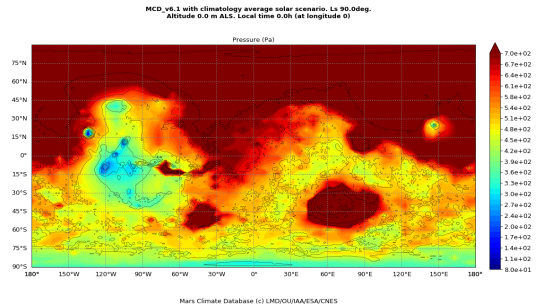


(c) t = 12h

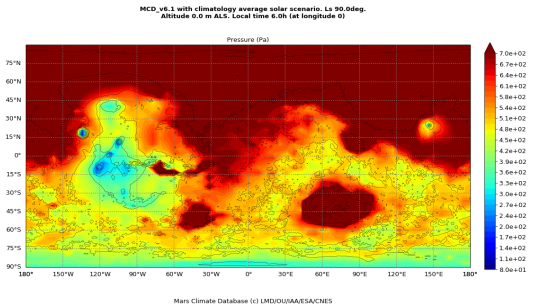


(d) t = 18h

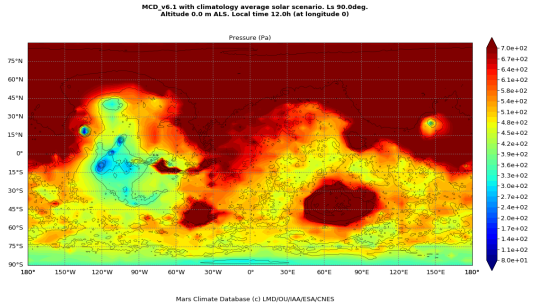
Figure B.4 Temperatures at Mars in range 245 to 275 K at $L_s = 90°$ at time 0h, 6h, 12h and 18h



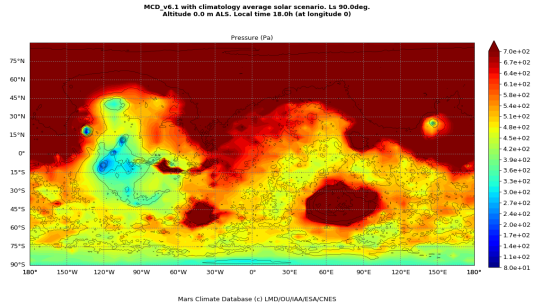
(a) t = 0h



(b) t = 6h

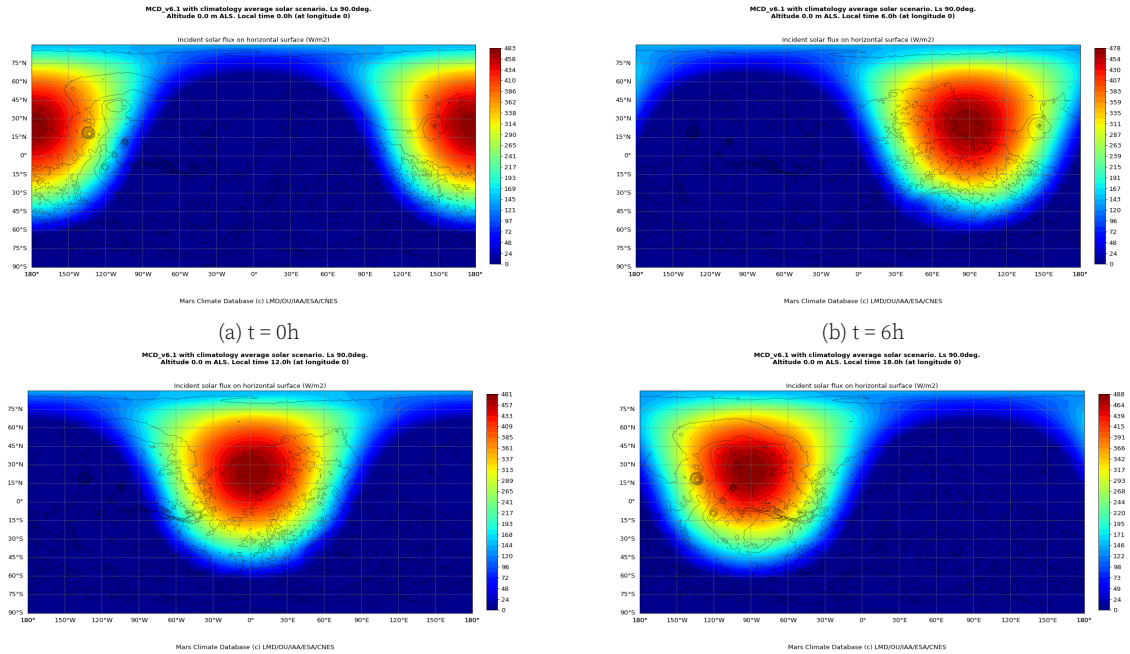


(c) t = 12h



(d) t = 18h

Figure B.5 Pressures at Mars in range 80 to 700 Pa at $L_s = 90°$ at time 0h, 6h, 12h and 18h

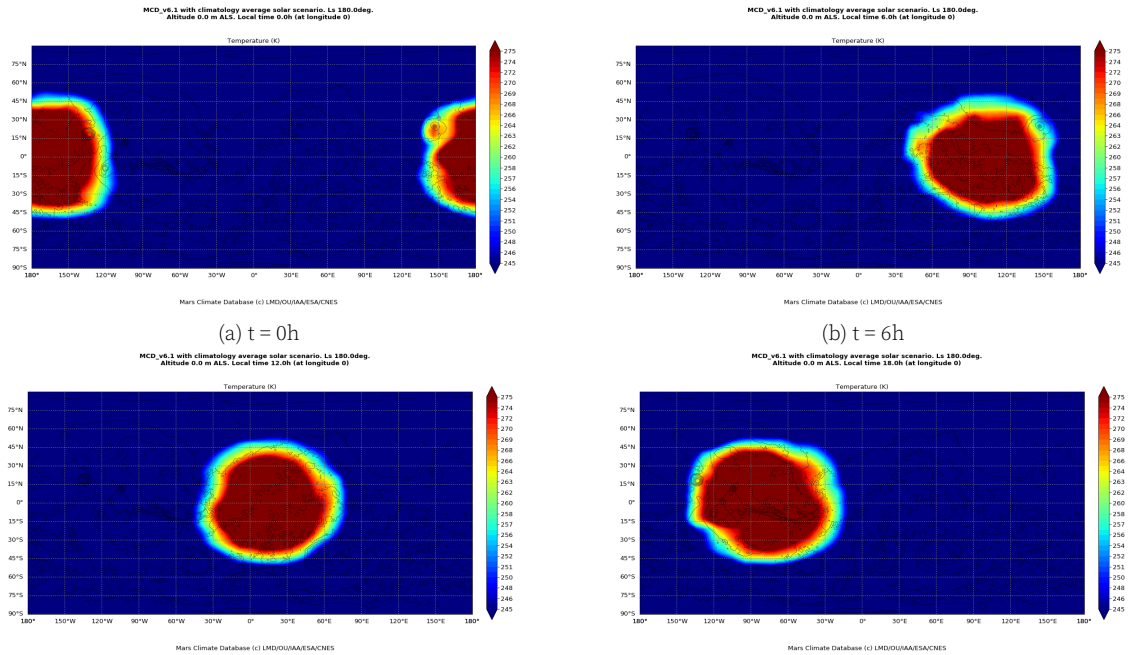


(a) t = 0h (b) t = 6h

(c) t = 12h (d) t = 18h

Figure B.6 Solar insolation at Mars at $L_s = 90°$ at time 0h, 6h, 12h and 18h

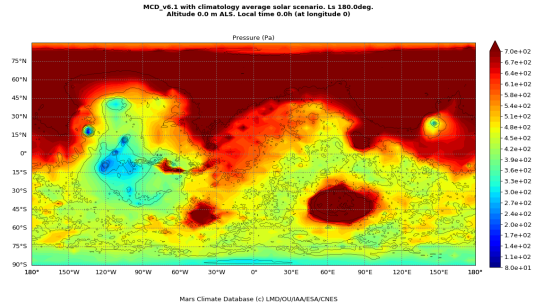
Ls 180°



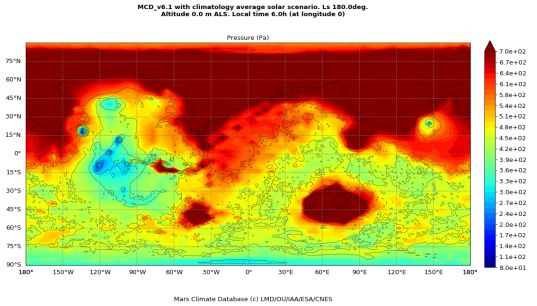
(a) t = 0h (b) t = 6h

(c) t = 12h (d) t = 18h

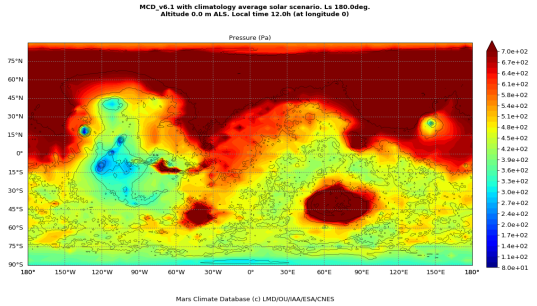
Figure B.7 Temperatures at Mars in range 245 to 275 K at $L_s = 180°$ at time 0h, 6h, 12h and 18h



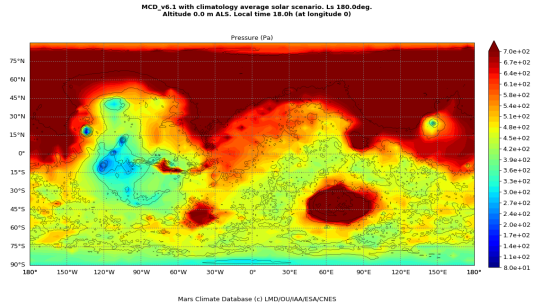
(a) t = 0h



(b) t = 6h

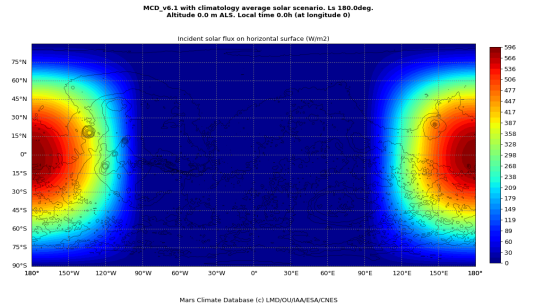


(c) t = 12h

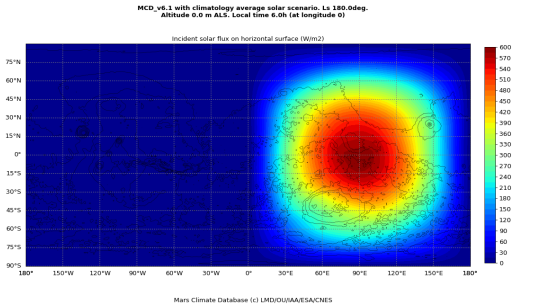


(d) t = 18h

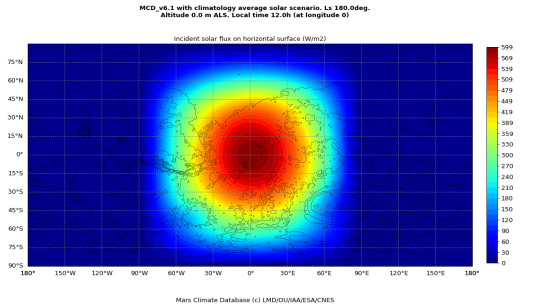
Figure B.8 Pressures at Mars in range 80 to 700 Pa at $L_s = 180°$ at time 0h, 6h, 12h and 18h



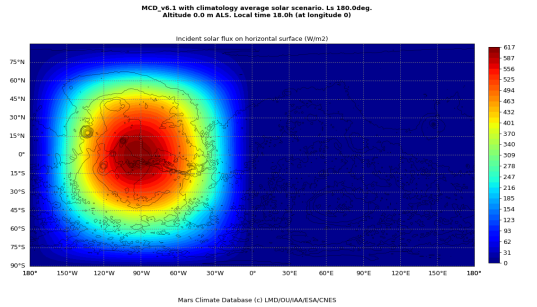
(a) t = 0h



(b) t = 6h



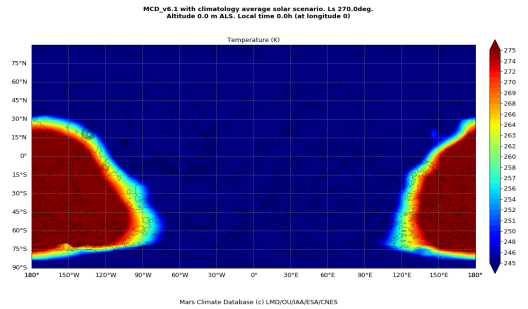
(c) t = 12h



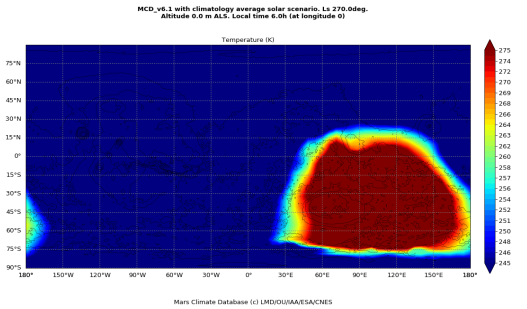
(d) t = 18h

Figure B.9 Solar insolation at Mars at $L_s = 180°$ at time 0h, 6h, 12h and 18h

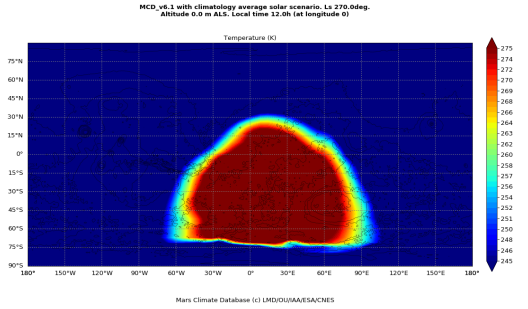
Ls 270°



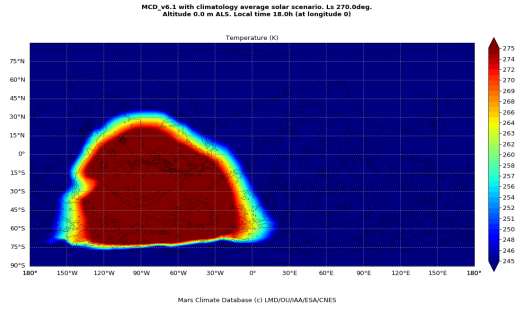
(a) t = 0h



(b) t = 6h

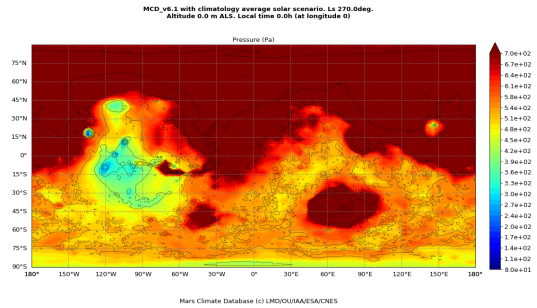


(c) t = 12h

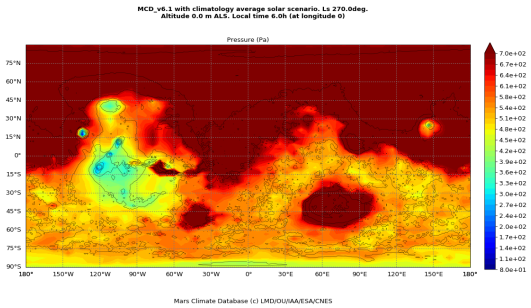


(d) t = 18h

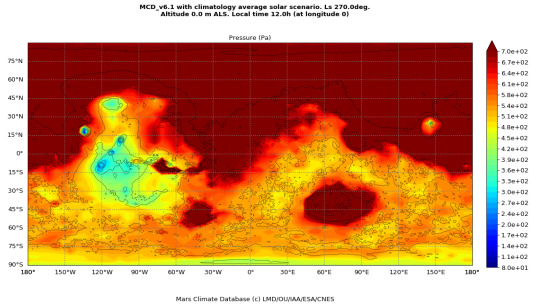
Figure B.10 Temperatures at Mars in range 245 to 275 K at $L_s = 270°$ at time 0h, 6h, 12h and 18h



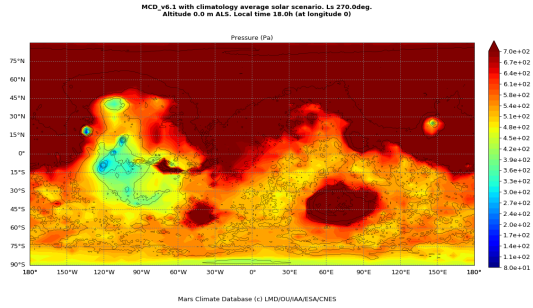
(a) t = 0h



(b) t = 6h

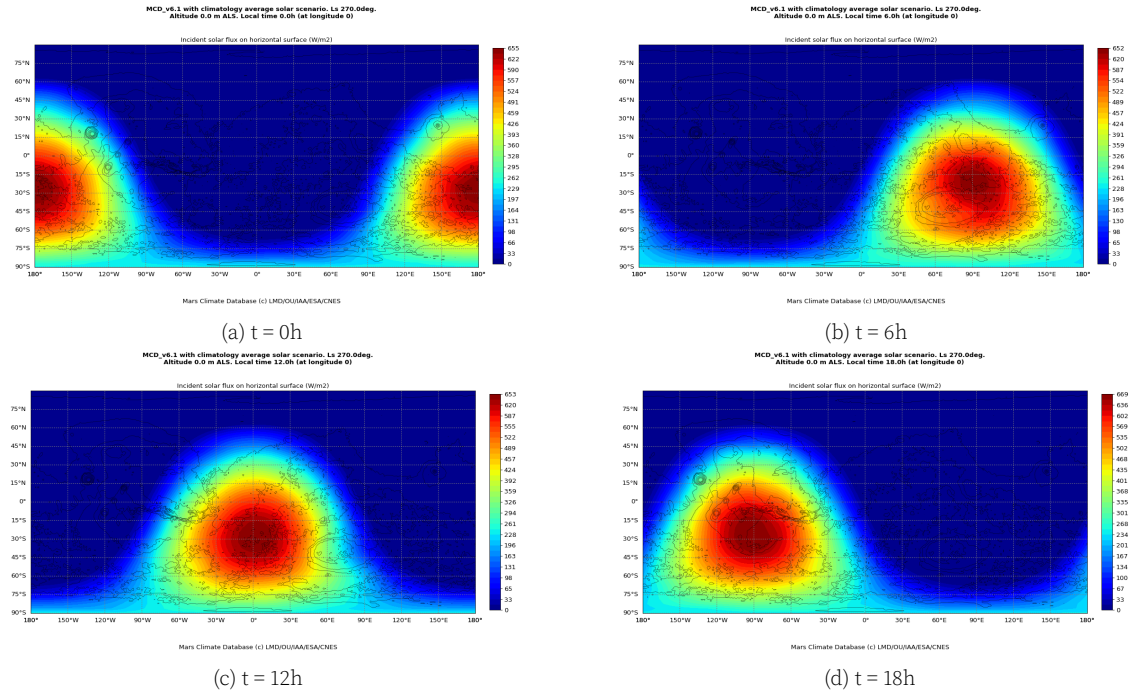


(c) t = 12h



(d) t = 18h

Figure B.11 Pressures at Mars in range 80 to 700 Pa at $L_s = 270°$ at time 0h, 6h, 12h and 18h



(a) t = 0h (b) t = 6h

(c) t = 12h (d) t = 18h

Figure B.12 Solar insolation at Mars at $L_s = 270°$ at time 0h, 6h, 12h and 18h

Model python code

```
import math
import numpy as np
import matplotlib.pyplot as plt
import pandas as pd
import Thesis_Functions as TF

#----------------------------------------IMPORT INPUT DATA FROM EXCELL-------------------
input_data = pd.read_excel('Model_inputs.xlsx')
#List of data sets in the excell
data_1 = "data_set"

#--- write down here below which data set you want to use---#

data_set = data_set #write down name of which data set you want to use

'Constants'
R = 8.314 #J/K/mol, perfect gas constant
M_s = input_data[data_set][20] #g/mol, molar mass (of water)
Alpha = input_data[data_set][15] #100 #m/s, sublimation kinetic constant
L_w = 2260 #J/g,  latent heat of vaporization of water

'Inputs'
p = input_data[data_set][0]
T = input_data[data_set][1]
M_s_atmos = input_data[data_set][2]
D_rho = input_data[data_set][3]
k_s = input_data[data_set][4]
Lamda = input_data[data_set][5]
Sigma = input_data[data_set][6]
mu = input_data[data_set][7]
u = input_data[data_set][8]
J_0 = input_data[data_set][9]
h_0 = input_data[data_set][10]
sol_duration = input_data[data_set][11]
```

```
rho_ice = input_data[data_set][12]
Earth_atmos = input_data[data_set][13]
L = input_data[data_set][14] #J/kg, Latent heat of sublimation for the ablation medium
water_ice = input_data[data_set][17]
RH = input_data[data_set][19]  #Relative humidity

if Earth_atmos == 1:
    Earth_atmosphere = True
elif Earth_atmos == 0:
    Earth_atmosphere = False

#Dew point calculation
A = L_w*M_s/(R*T)
T_d = T/(1-(1/A)*np.log(RH))  #K, dew point
if RH == 0.001:
    print('The dewpoint is unknown')
elif T_d > 273:
    print('The dewpoint is too high for sublimation to take place thus the given results'
          'are not a correct presentation of reality', T_d)
elif T_d < 273:
    print('The dewpoint is below zero, results give a good estimate of reality', T_d)


'Calculations'
rho_atmos = (p*M_s_atmos)/(R*1000*T)
if water_ice == 1:
    P_s = 100*10**(-9.09718*((273.16/T)-1)-3.56654*math.log10(273.16/T) +
                   0.876793*(1-(T/273.16)) + math.log10(6.1071))  #Pa, saturated vapor
                   #pressure at temperature K, this relation is only true for water,
                   #(Goff Gratch equation)
    rho_sat = (P_s*M_s)/(R*1000*T)  #kg/m^3, saturated vapour density
    rho_sat_dev = (rho_sat/T)*(((M_s*L)/(R*1000*T))-1)  #kg/m^3/K, first derivative of
    # saturated vapour density

elif water_ice == 0:
    rho_sat_dev = input_data[data_set][16]
elif water_ice == 2:
    P_s = (10**(6.81228 - (1301.679/(T-3.494))))*10**5  #Pa, Antione Equation for vapor
    # pressure for CO2 according to NIST
    rho_sat = (P_s * M_s) / (R * 1000 * T)  # kg/m^3, saturated vapour density
    rho_sat_dev = (rho_sat / T) * (
                ((M_s * L) / (R * 1000 * T)) - 1)  # kg/m^3/K, first derivative of
    # saturated vapour density



P = k_s/(rho_sat_dev*D_rho*L)
R_dimless = k_s/(rho_sat_dev*Alpha*Lamda*L)
if Earth_atmosphere == True:
    l = 5 * mu / u  # m, mixing length if Earth atmosphere is used.
    # Here mu is the air kinematic viscosity
elif Earth_atmosphere == False:
    l = 5*mu/(rho_atmos*u)  #m, mixing length if no Earth atmosphere is used.
    # Here mu is the dynamic viscosity of water vapour in the atmosphere


self_illum = Sigma/math.pi
w_a = ((1-Sigma)*J_0)/Lamda #W/m^3, interfacial value of absorbed light volumetric power

"Calculations for the penitente spacing"
wavelength = 0.001 #m, wavelength
wavelength_list = []
```

```
growth_list = []
growth_with_dim_list = []
wavelength_lamda_list = []
max_wavelength_range = input_data[data_set][18]
while 0 < wavelength <= max_wavelength_range:
    k = 2 * math.pi / wavelength  #wavenumber
    k_lamda = k*Lamda  #this is the wavelength times the exponential constant of
    # light penetration
    growth_rate_dimless =  ((k*Lamda/(1+P*math.tanh(k*l)+R_dimless*k*Lamda))*
                            ((1-(1/math.sqrt(1+(k**2*Lamda**2))))+
                             (self_illum*(1-((k*Lamda)/(math.sqrt(1+(k**2*Lamda**2))))))-
                             (P*(1-(1/math.cosh(k*l))))) #dimensionless growth rate
                             #of penitentes
    growth_rate_with_dim = w_a*growth_rate_dimless/(rho_ice*L)
    if growth_rate_dimless > 0:
        wavelength_list.append(wavelength)
        wavelength_lamda_list.append(k_lamda)
        growth_list.append(growth_rate_dimless)
        growth_with_dim_list.append(growth_rate_with_dim)
    wavelength = wavelength + 0.001

'plot of dimensionless growthrate vs wavelength times light penetration depth'
plt.figure(figsize=(10, 5))
plt.plot(wavelength_lamda_list, growth_list, marker="o",
         label="Dimensionless growth rate")
plt.ylabel('dimensionless growth rate of penitentes')
plt.xlabel('k Lamda [m^2]')
plt.title('dimensionless growth rate of penitentes vs wavelength times lamda')
plt.legend()
plt.show()


'print the results'
plt.figure(figsize=(10, 5))
plt.plot(wavelength_list, growth_list, marker="o", label="Dimensionless growth rate")
plt.ylabel('dimensionless growth rate of penitentes')
plt.xlabel('wavelength [m]')
plt.title('dimensionless growth rate of penitentes vs wavelength')
plt.legend()
plt.show()

plt.figure(figsize=(10, 5))
plt.plot(wavelength_list, growth_with_dim_list, marker="o", label="Growth rate")
plt.ylabel('growth rate of penitentes [1/s]')
plt.xlabel('wavelength [m]')
plt.title('growth rate of penitentes vs wavelength')
plt.legend()
plt.show()

"Make normalized plot of growth rate vs wavelength"
def normalize_list(values):
    min_val = min(values)
    max_val = max(values)
    if max_val == min_val:
        return [0.0 for _ in values]  # Avoid division by zero
    return [(x - min_val) / (max_val - min_val) for x in values]

normalized_growthrate = normalize_list(growth_with_dim_list)
plt.figure(figsize=(10, 5))
plt.plot(wavelength_list, normalized_growthrate, marker="o", label="Growth rate")
plt.yscale('log')  #makes a log scale of the plot
plt.xscale('log')
```

```
plt.ylabel('normalized growth rate of penitentes [1/s]')
plt.xlabel('wavelength [m]')
plt.title('normalized growth rate of penitentes vs wavelength')
plt.legend()
plt.show()

'Find the wavelength belonging to the max growth rate'
max_growth = max(growth_list)
max_growth_with_dim = max(growth_with_dim_list)
idx_max_growth = growth_list.index(max_growth)
wavelength_at_maxgrowth = wavelength_list[idx_max_growth]
k_m = 2*math.pi/wavelength_at_maxgrowth  #wave number related to the maximum growth rate

"Print results"
print('Penitente spacing =', wavelength_at_maxgrowth, 'm')
print('Dimensionless growth rate =', max_growth)
print('The penitente growth rate =', max_growth_with_dim, '[1/s]')
```